Orientation of the maximum horizontal stress (S_{Hmax}) in the Orange Basin and Outeniqua sub-Basins of South Africa: Neotectonic Implications

Andrew Selkirk Logue

Thesis presented for the degree of

Master of Science

Geological Sciences Department

University of Cape Town

February 2015

Supervisors:

Dr. Marco Andreoli (Necsa, University of the Witwatersrand)

Priv. Doz. Dr. Oliver Heidbach (GFZ Potsdam, University Karlsruhe)

Prof. Zvi Ben-Avraham (Tel Aviv University)

Prof. Anton le Roex (University of Cape Town)

Declaration

I, **Andrew Selkirk Logue**, declare that this research report is my own work. It is being submitted for the degree of **Master of Science** in the University of Cape Town. It has not been submitted before for any degree or examination at this or any other university.

_____ (signature)

The ____ day of _____, 2015

Corrections:

_____ (signature)

The ____ day of _____, 2015

Abstract

South Africa lies within an intraplate setting, characterised by sparse, scattered, low-magnitude seismicity not easily correlated with known neotectonic features. Recent seismicity has repeatedly been shown to result from the reactivation of pre-existing geological structures, typically large faults or shear zones, which are preferentially-aligned to the contemporary stress field. Expanding the catalogue of stress data for the region is therefore vital to better understand the regional stress field pattern and aid in identifying potentially seismogenic structures. In these intraplate regions, reliable high-quality indicators of maximum horizontal compressive stress (S_{Hmax}) are difficult to obtain in the absence of earthquake-derived focal mechanism solutions (so called "beach balls"). In South Africa however, extensive hydrocarbon exploration drilling in the Mesozoic offshore provide an opportunity to utilise the borehole breakout technique to derive quality S_{Hmax} orientation data.

In collaboration with the World Stress Map Project (WSM), and utilising borehole logs provided by the Petroleum Agency South Africa (PASA), training and software was provided to review, analyse and visualise borehole breakouts observed in 4-arm calliper logs from exploration areas in the Outeniqua and Orange basins.

A total of 131 borehole calliper logs were assessed and analysed which resulted in 29 usable S_{Hmax} orientations (22%): 9 for the Orange Basin, 19 for the Outeniqua Basin. Two calliper logs were provided in the dataset for the Durban Basin but with only 1 low-quality S_{Hmax} orientation produced. Of these results, 20 (15%) were of B- and C-quality (based on the WSM quality ranking criteria), and were suitable for both inclusion in the WSM catalogue and for use in generating a smoothed stress field map for South Africa. The remaining 9 D-quality S_{Hmax} orientations were consistent with the trends shown by the higher quality data. A total of 102 calliper logs were discarded due to missing parameters, printout errors, extensive washout or calliper-tool mechanical problems.

The individual data displays a regional trend of NNW-orientated S_{Hmax}, consistent with the limited WSM data previously available for the region. Average values for S_{Hmax}, based on B, C and D-quality data, are 163.6° (s.d. 12.15) in the Orange Basin, 185.9° (s.d. 48.89) in the Bredadorp sub-basin, 142.7° (s.d. 10.23) in the Pletmos sub-basin, 134.8° (s.d. 8.86) for the Gamtoos sub-basin and 149.8° (s.d. 2.65) for the Algoa sub-basin. Only 5 data, located in the fault-bounded eastern margin of the Bredasdorp sub-basin, reveal large variations in trend of

S_{Hmax}, oriented between WNW to ENE. These results impact the average S_{Hmax} orientation and suggest either local geological structures or lithology may be responsible for varying stress distribution over short distances (~100 km).

The S_{Hmax} results produced for the Orange Basin are consistent with other stress data for the western coastline including a high-quality focal mechanism solution from the Walvis Ridge, mud-volcano vent alignment, and recent indicators of fault-slip in the Namaqualand, South Africa and Hebron Fault, Namibia. The S_{Hmax} results for the Outeniqua Basin are also consistent with previous, albeit limited, borehole breakout analysis and limited results from recent Plio-Pleistocene geological indicators. This consistency with existing stress data suggest the borehole breakout results may indicate a real trend and also suggest a good coupling of basin deposits with the underlying continental and oceanic crust. This data can therefore be used not only to improve the understanding of the local stress fields affecting offshore basins but also contribute to mapping the region as a whole. The high variation seen in some results, such as in the western Bredasdorp Basin and seen in onshore Plio-Pleistocene indicators, do however indicate the risk of local variation that must be considered when utilising this data.

Attempts to create a regional stress map with limited stress data from the interior and clustered stress data for the offshore basins still reveals challenges. This results in the over-representation of data in some areas (which can lead to high-variance averages), and heavily-extrapolated, equally high-variance data in other areas. At the local basin scale, individual data is likely to provide a more reliable indication of the stress pattern. Overall the S_{Hmax} orientation for the country appears to trend NNW which reinforces the pattern described in previous studies.

Comparing the modelled data to the finite-element model created by Bird et al. (2006), the results generally supports the presence of a NNW-trending stress field established in the Outeniqua Basin and western interior of the country, however the new data (both real and modelled) disagrees with the finite-element model for the western offshore basins and indicates that this NNW-trending stress pattern persists into the offshore basins. The findings of this study also suggest the previously suggested NW-oriented "Wegener Stress Anomaly" ($S_1 > S_V > S_3$), initially assumed to affect only a narrow stretch of the western coastline of southern Africa, may instead be part of a broad region NNW-trending compressive stress.

Looking at the recent seismic data and the smoothed regional stress field data, little seismicity is seen in the offshore basins themselves. The data does however indicate 3 distinct clusters of seismic events in the western interior of the country, namely the Augrabies cluster, the Bushmanland Plateau cluster and western Cape Fold Belt cluster all of which display ongoing seismicity and are associated with structural lineaments typically oriented sub-parallel to S_{Hmax} in the modelled stress field.

Considering Anderson's classification scheme for relative stress magnitudes in the crust, the most likely environment in which these regions would experience reactivation of seismogenic structures is in a strike-slip setting where $S_{Hmax} > S_V > S_{hmin}$. The breakout technique in this project is not able to quantify forces, however these observations, previous compilations of mining data and recent updates to the limited regional motion tensors available for South Africa suggest there is a component of NW-oriented horizontal compression experienced at depth in the South African crust.

Acknowledgements

The author would like to acknowledge the continuous support of my supervisors, family, friends and colleagues over the course of this M.Sc. project. I would especially like to thank Dr. Marco Andreoli who has provided both guidance and supervision for both the M.Sc. project and work-related projects while I was employed at the South African Nuclear Energy Corporation (Necsa). I would also like to thank Priv. Doz. Dr. Oliver Heidbach for the training and support when I was given the opportunity to visit the GeoForschungsZentrum (GFZ), Potsdam to learn the theory behind the borehole breakouts technique and the software required to analyse and visualize the data. The partnership was formed as part the "Inkaba yeAfrica" joint research initiative between German and South African science communities.

Special mention must be given to the South African Nuclear Energy Corporation (Necsa), for the generous financial support in obtaining data used in this project and covering the travel/accommodation costs for training. Dr. Andreoli's NRF contributions also assisted greatly in covering tuition fees. I would also like to thank the Petroleum Agency SA for providing an extensive list of calliper logs for analysis, covering the majority of their exploration areas within the offshore sedimentary basins of South Africa.

Finally I would like to thank my wife for her seemingly limitless support and confidence in me, even in times when I doubt it was deserved.

Table of Contents

LIST OF FIGURES

CHAPTER 1: INTRODUCTION

Understanding current tectonic activity (or "neotectonics") in South Africa has become increasingly important as the country expands critical infrastructure such as vital municipal services and specifically nuclear-related projects. Neotectonics can be described as the study of recent crustal deformation, detectable either by geological or geomorphological processes that are considered Plio-Pleistocene in age (<5 MA). It can also be considered a study of any current or ongoing geological processes - plate motion, orogeny, rifting and seismicity.

Most seismicity is directly related to the response of pre-existing geological structures (such as faults and shear zones) interacting with the contemporary stress field (Zoback, 2010). This "stress field" can be broadly defined as a representation of the change of stress state through space. The stress data is typically presented in a form of gridded data, each point displaying an averaged orientation for the maximum horizontal compressive stress (S_{Hmax}) based on the statistical smoothing of available real data. This data represents an approximation of the internal distribution of force at a point, balanced against external forces such as plate tectonics, mantle geodynamics and topographic effects (Zang & Stephansson, 2010).

Previous studies have shown that pre-existing lineaments are more prone to reactivation if they are favourably orientated to the contemporary stress field, so knowledge of the orientation of maximum horizontal stress in a region can provide a means for identifying potential seismogenic structures, even in areas of infrequent seismicity or limited seismic network coverage (White *et al.*, 1986; Andreoli *et al.*, 1996; Zoback, 2010). This is especially true in an intraplate setting in which geological structures can remain inactive and unrecognised by human observation due to long periods of quiescence. McCalpin and Nelson (2009) note these geologic structures can continue to propagate in intraplate regions and the potential for sudden release, in the form of earthquake rupture, still present a considerable hazard.

Intraplate regions, such as southern Africa, Australia and the central to eastern United States, are often regarded as relatively aseismic but are characterised by sparse, scattered, low-intensity seismic events which are not easily correlated with known neotectonic features (Andreoli *et al*., 1996). Historical records also show these regions can still experience

potentially devastating earthquakes such as the "New Madrid" earthquakes in the central United States which had magnitudes estimated between M7.0 to M8.1 (Stover and Coffman, 1993). Since earthquake monitoring by seismograph began in 1910, there have been several earthquakes exceeding M_W 5 in the western half of South Africa, not associated with regions of more frequent events attributed to gold and platinum mining activities in the northeast of the country [http://www.geoscience.org.za/index.php/component/content/article?id=1612: historical-earthquakes – last accessed 15/02/2015]. The most famous of which is the series of primary earthquakes and aftershocks in Ceres, between 1969 and 1970, the largest recorded as M_W 6.2 (Midzi *et al*., 2013). The western half of South Africa, while typically characterised by low-frequency and low-magnitude seismicity, appears to display an incredibly complex history of stress field changes over the last 500 Ma (Viola *et al.*, 2012).

As of late 2010, the South African government has tabled plans to increase the nuclear fleet in South Africa, increasing energy production to a potential 9,600 MW (IRP 2010-2030). This increase, up from the 1,800 MW currently produced by the Koeberg nuclear power plant (NPP), will include the construction of new NPPs and an increase in radioactive waste which would have to be safely stored. Low- to intermediate-level waste is currently handled by the Vaalputs Radioactive Waste Disposal Facility in the Northern Cape Province, situated in the Bushmanland plateau region. While the stable interiors of continents are typically considered ideal for siting long-term radioactive waste disposal sites, low rates of deformation in these regions make it difficult to characterise long-term seismic activity (Pusch, 2008). This uncertainty can result in hazard assessments that are unsuitable to the strict requirements for a nuclear site (Fenton *et al.*, 2006). A better understanding of the contemporary stress field in South Africa is therefore required to ensure future NPPs are well-sited and long-lived radioactive waste disposal sites continue to function safely over the extended periods of time required.

Earthquakes currently present the single greatest threat to nuclear infrastructure and waste repositories. Sudden displacement of new or pre-existing geological structures can drastically strain structures, foundations or excavations and also alter the hydraulic performance of a rock unit or engineered barrier (Pusch, 2008). The hydraulic behaviour of a geological unit is a vital parameter in predicting and modelling the behaviour of radioisotopes movement in the geosphere when dealing with accidental releases (Pusch, 2008). In nuclear-related sites located on the coastline, offshore earthquakes can both directly impact structural

stability and potentially trigger devastating tsunamis, as seen with the 2011 Fukushima incident in which the tsunami far exceeded design parameters. In South Africa, water requirements for cooling NPPs and the need to provide electricity to regions distant from the coal fields and coal-burning power plants in the east and north-eastern parts of the country have resulted in both current and proposed nuclear developments to be clustered in western half of the country, primarily along the western and southern coastline which are also in close proximity to the major offshore sedimentary basins (Figure 1).

Purpose and scope of project

Against this background we note that South Africa has recently experienced a string of earthquakes, primarily tectonic in nature as seen in the Augrabies region [http://www.geoscience.org.za/latest-news/1455-seismicity-in-the-augrabies-area - last accessed 15/02/2015], and most recently with the M5.5 Orkney earthquake in August, 2014 which caused extensive damage to the nearby community and claimed one life [http://www.geoscience.org.za/latest-news/2090-media-release-5-5-magnitude-earthquake-tremors-continue - last accessed 15/02/2015] (Figure 2). The nature of the Orkney earthquake is still currently under debate with proposed causes ranging from pure mining to pure tectonics, as a possible response to far-field stresses generated by the continued extension of the East African Rift system (Bird *et al.*, 2006).

Figure 1: The location of both current and proposed nuclear infrastructure in South Africa visualised using Google Earth. The areas highlighted in grey roughly indicate the extent of offshore basins and sub-basins, currently explored or exploited for petroleum products. Exploration boreholes in these regions provide a potential source of data on crustal stress if suitable calliper logs records are kept.

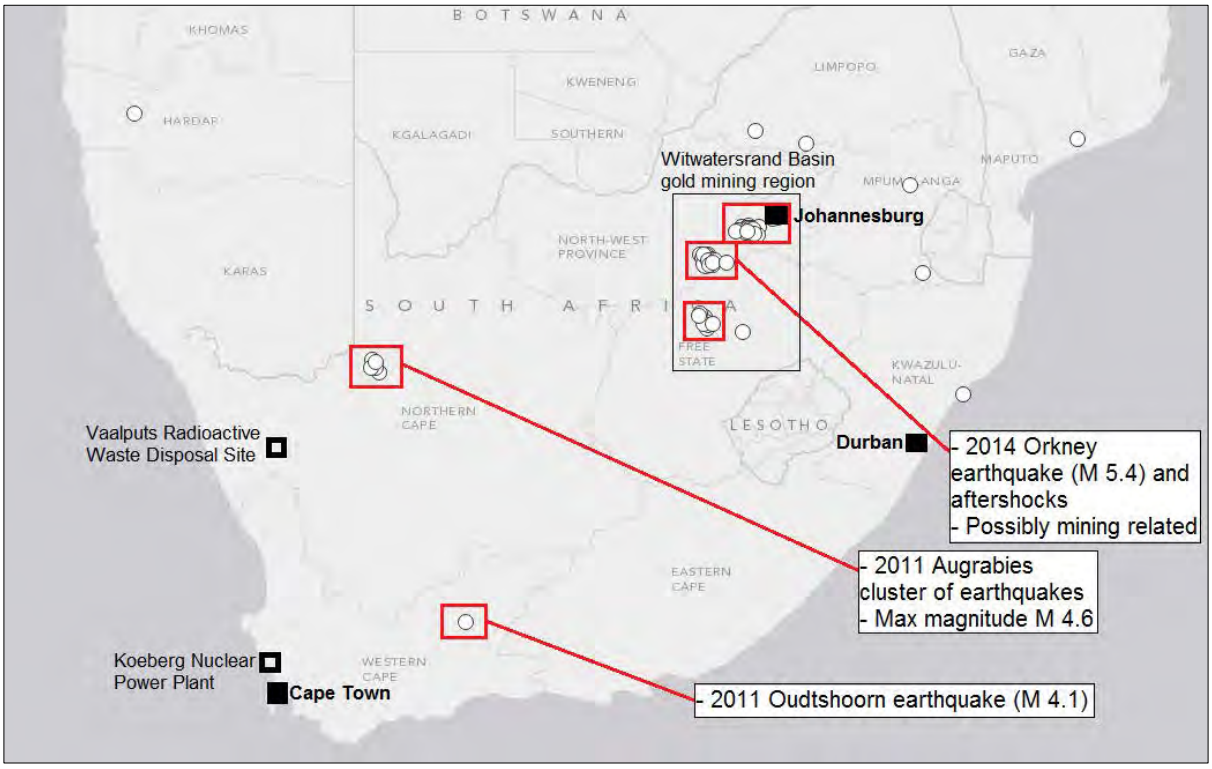

Figure 2: Large earthquakes in South Africa from 2010 to 2015 (events obtained online from the USGS Earthquake Archives)

In looking to establish a greater understanding of the regional stress field in South Africa, the author was introduced to the WSM project, an initiative established to provide a global database for contemporary tectonic stress information for the Earth's crust. As the database grows with contribution from around the world, stress data coverage increases in density, and the project aims to allow researchers to look at the mechanisms controlling stress ranging from 1st order plate boundary forces, through 2nd order intraplate forces (such as mountain belts and regions affected by glacial rebound), and finally 3rd order forces such as the influence of local faults (Heidbach *et al.*, 2007). The WSM project also provides an internationally-accepted ranking scheme to guarantee reliability and global comparability based up on the work done started by Zoback and Zoback (1989, 1991) and expanded by Sperner *at al.* (2003). The WSM project compiles global stress orientations derived from a range of sources however almost 80% of the WSM orientation data is derived from focal mechanism solutions from earthquake events (Heidbach *et al.*, 2010).

The next largest source of stress indicators in the WSM database are derived from borehole breakouts (~19%), which are concentrated in off- and onshore sedimentary basins in regions previously or currently associated with hydrocarbon exploration (e.g. the North Sea) and regions of intense exploration drilling (e.g. Athabasca Basin, Canada) (Heidbach *et al.*, 2010). The remaining 1% of the WSM database typically comes onshore industry measurements, such as over-coring, hyrdofracturing tests, as well as young geological indicators such as fault-slip indicators and volcanic alignment (Heidbach *et al.*, 2010). These data form the bulk of the existing South African compiled by Stacey and Wesseloo (1998). In South Africa, infrequent and low-magnitude seismicity results in a scarcity of FMS calculations resulting in a limited catalogue of earthquake events and poor identification of seismogenic structures, which in turn would introduce great uncertainty into any attempt at constructing a probable seismic hazard assessment for the region (England and Jackson, 2011). This information vital for the nuclear industry and any other critical infrastructure.

As seen in the most recent 2008 release of the WSM data (Figure 3), the African plate has a considerable amount of data but this is primarily FMS data generated from seismic events along the plate boundaries and clustered within the active East African Rift system. South Africa however has very few data which can be used to create a reliable regional model of the stress field. This presented an opportunity to collaborate with the World Stress Map team, based within the GFZ Potsdam, to expand the current WSM database for South Africa and to produce a more detailed stress field map by considering other methods of determining the S_{Hmax} orientations within the region.

In similar intraplate, seismically-quiescent regions, the borehole breakout technique has been successfully used for determining the orientation of maximum horizontal stress (S_{Hmax}) (Zoback, 2010). Borehole breakouts observed in the exploration wells in the offshore sedimentary basins provide an opportunity to expand on the sparse stress orientation data for South Africa. The current WSM data for South Africa is derived from limited FMS data, previous borehole breakout analyses of only a few boreholes, and *in situ* measurements from mining operations such as hydraulic fracturing, rock slotting and over-coring data (Stacey and Wesseloo, 1998) which is often unreliable and sensitive to the impact of the surrounding excavations (Zoback, 2010). As current and future nuclear-related projects in South Africa will be located along the west and southern coastline, borehole breakout analysis in these offshore basins can provide valuable stress orientation data very close to proposed sites.

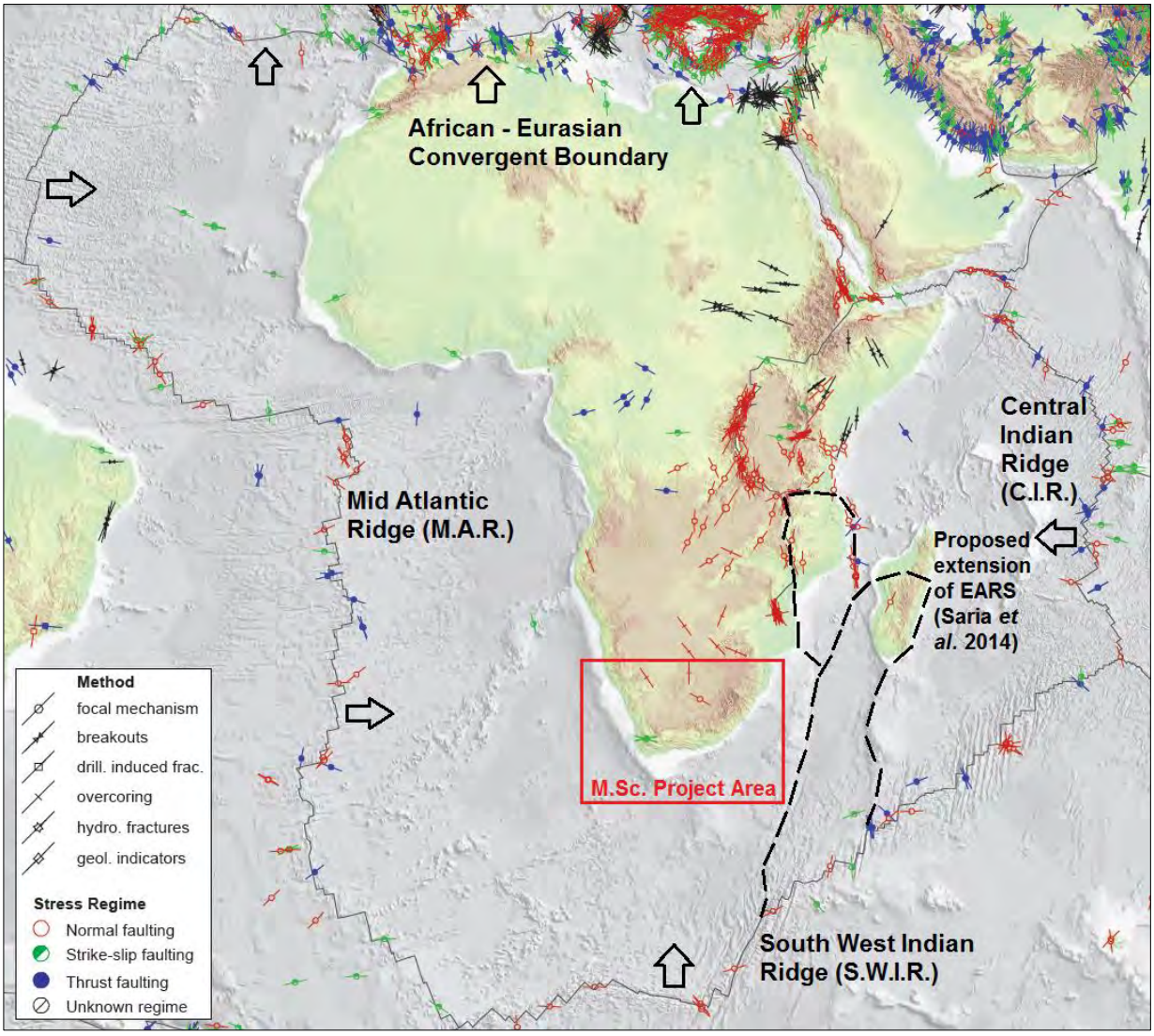

Figure 3: Stress orientation data for the African plate from the 2008 release of the World Stress Map (A to C quality based on standardised ranking systems). While the African-Eurasian collision zone and East African Rift System are well represented, other parts of the African plate have little to no data (modified after Heidbach, O., Tingay, M., Barth, A., Reinecker, J., Kurfeß, D., and Müller, B., The World Stress Map database release 2008 doi:10.1594/GFZ.WSM.Rel2008, 2008). The project study area and major tectonic features are indicated.

For this project the Petroleum Agency South Africa (PASA) provided 131 borehole calliper logs from the major offshore sedimentary basins for analysis (Figure 4). These calliper logs came primarily from the extensive exploration drilling done between 1980 and 1992 when the company was operating under the name "Soekor".

Combined with existing onshore data from the WSM release, any S_{Hmax} orientations derived from borehole breakout analysis in these basins can be used to bolster the current regional stress map which has a limited density real data which results in unreliable statistically-smoothed results. As European studies have previously indicated a good correlation between onshore and offshore orientation data suggesting a good coupling of the overlying sediments with the underlying continental and oceanic crust (Zoback, 1992), it was decided this project would be worthwhile in contributing to the understanding of the regional stress field acting in both coastal basins and to support existing data for inland regions derived from earthquake-derived FMS and fault-joint analysis in young geological structures.

The author was given the opportunity to spend six weeks under the supervision of Priv. Doz. Dr. Oliver Heidbach at the GFZ Helmholtz Centre in Potsdam, during which both software and training was provided for the author to analyse for breakouts, determine S_{Hmax} orientations and finally attempt to generate a higher-quality smoothed, gridded-map of the regional stress field for South Africa.

Over the course of this project, the boreholes were assessed using the software provided and, where sufficient parameters are available for producing breakout data (Figure 5), they were analysed for borehole breakout orientations and the resultant S_{Hmax} orientation. Where WSM-quality standards have been met, these S_{Hmax} orientations are incorporated into the WSM database. This new stress data was then processed using smoothing scripts to generate an updated stress field maps for the coastal basins and South Africa as a whole. Both real breakout data and smoothed gridded data were visualised using GIS software to aid in the discussion of the results with regard to other datasets including basin structure and seismicity.

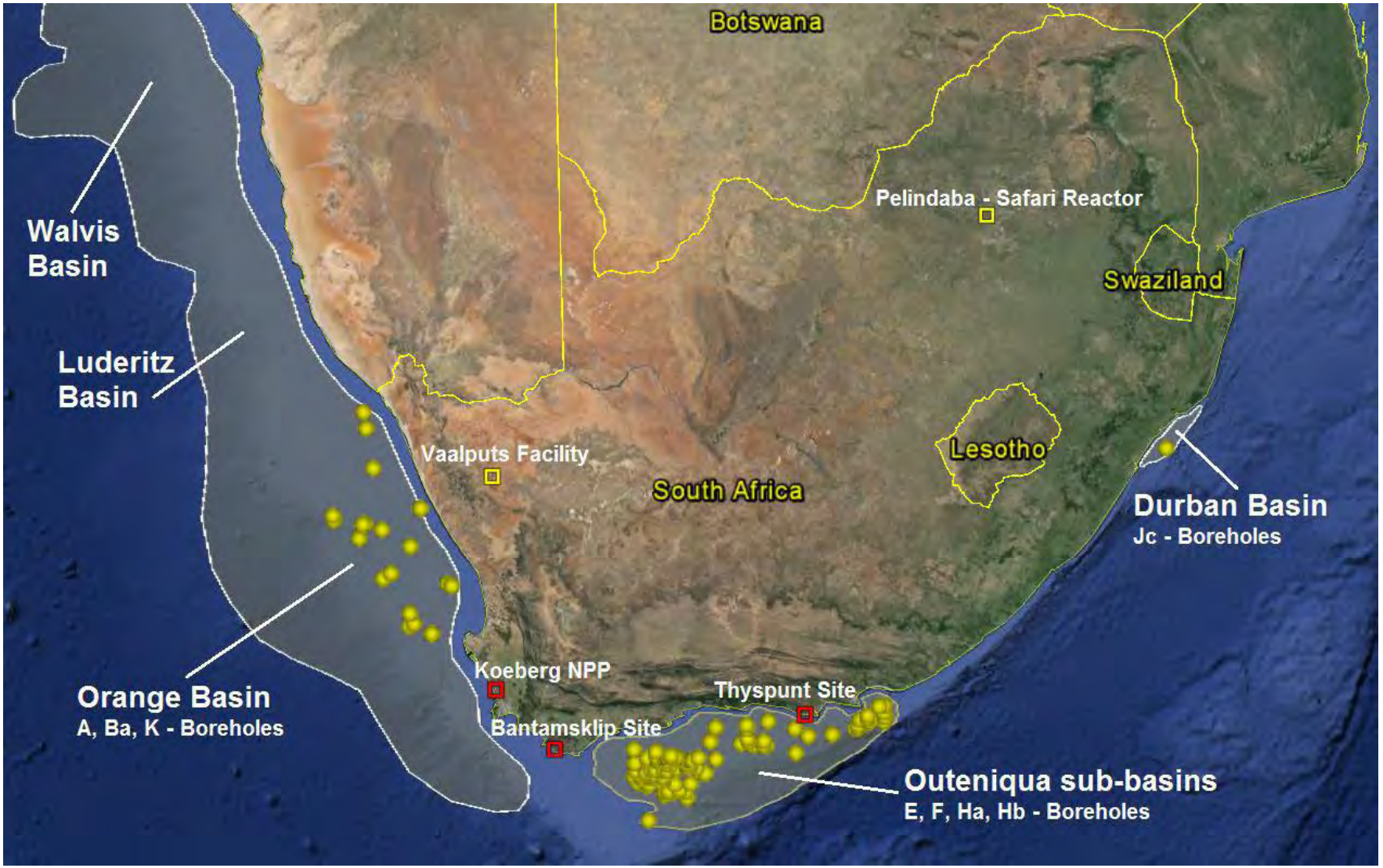

Figure 4: The location of all available borehole data provided by the Petroleum Agency SA visualised using Google Earth. The major offshore basins and well-field names are also indicated.

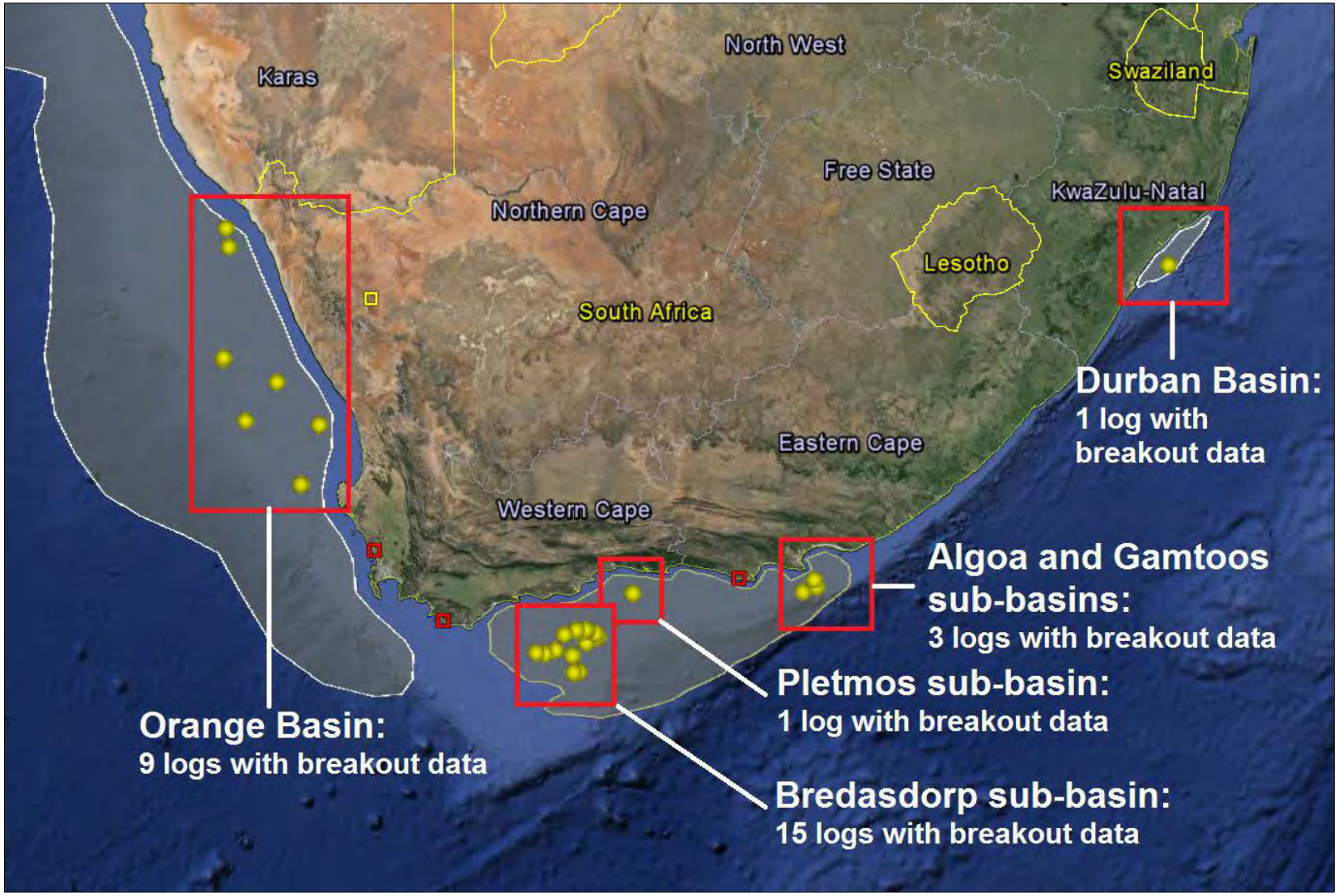

Figure 5: The location of all data-producing boreholes is considerably lower than the total sample size but still provides good coverage off the regions of interest. Boreholes in close proximity may not visible due to overlapping symbols. Data visualised using Google Earth.

CHAPTER 2: GEOLOGICAL SETTING

Regional geology

South Africa is located in an intraplate setting, geographically occupying the southernmost continental crust of the African plate. Its location is unique in that it surrounded almost entirely by spreading margins with the only convergent margin, the African/Eurasian collision zone, located over 8,000 km to the north (Figure 3) (Viola *et al*., 2005).

Located at considerable distance from spreading margins and extremely distant from the nearest convergent margin (typically associated with high earthquake frequency and large magnitudes), the mechanisms of seismicity in South Africa are poorly understood and current models for the stress field of southern Africa are constructed using relatively few data. These modelled results do not always to conform to the expected stress field pattern observed in the field (Andreoli *et* al., 1996; Bird *et al.*, 2006). Numerous driving forces have been considered for the region which include: the propagation of far-field stresses from divergent (ridge-push) and even distant convergent (slab-pull) margins (Andreoli *et al*., 1996; Viola *et al*., 2005), local topographic features, and the possible impact of mantle geodynamics associated with the large low-velocity province identified below southern and east Africa (described as the African Superplume or African Superswell, based on shear-wave velocities and geochemical signal) (Nyblade and Robinson, 1994; Behn *et al.*, 2004). The "ridge-push" forces generated by the closest plate boundaries, stress orientation data from the rift margins of well-studied EARS and geodetic data for the drift direction of the African plate suggest a broad NW – SE to W – E orientated maximum horizontal stress (S_{Hmax}) would be present across most of southern Africa. However the currently available on- and offshore orientation data (Andreoli *et al*., 1996; Stacey and Wesseloo, 1998; Viola *et* al., 2005; Bird *et al*., 2006, Heidbach *et al*., 2010) have consistently shown a broad regional trend of NW – SE orientated S_{Hmax}.

The boreholes analysed in this study fall within three offshore sedimentary basins along the western and southern coastal shelf of South Africa, the Orange, Outeniqua and Durban basin. Defining the coastal shelf as extending from the shoreline out to 200 m depth (below average sea level), these Mesozoic to Quaternary sedimentary basins cover an area of 165,000km^2. Taking into account the full extent of the sedimentary basins, extending out to 2,000 m depth, these cover an area of 400,000km^2 before the appearance of oceanic gabbro (Figure 6) (Broad *et al.*, 2006).

Basins description: generalities

The Orange, Outeniqua and Durban basins form part of two passive margins, formed in an extensional environment related to the breakup of the West Gondwana supercontinent in the early Mesozoic, a process continuing into the present. The western coastline is an example of a purely divergent passive margin, whereas the south and eastern coastlines are closer to transform margins (Broad *et al.*, 2006) due to the presence of the prominent **A**gulhas-**F**alkland **F**racture **Z**one (**AFFZ**), a palaeo-transform zone of dextral slip (right-lateral), which records over 1,200 km of movement related to accommodating spreading ridges during the breakup of Gondwana (Watkeys, 2006). This structure forms the outermost limit of the Outeniqua sub-basins and stretches along the eastern coastline, terminating south of the Durban Basin.

These sedimentary basins are coupled to the African plate, deposited above both oceanic crust and rifted continental margin, and are surrounded by well-defined spreading ridges to the east, south and west (Broad *et al.*, 2006). These spreading ridges are the Mid-Atlantic Ridge to the west, the Central Indian Ridge to the east and the Southwest Indian Ridge to the south and south-east. The Southwest Indian Ridge is the closest divergent plate boundary to the present continental shelf at >1,500 km from the Outeniqua Basin. The underlying crystalline basement is varied and not always precisely known due to the limit of drilling. For the Orange basin, the basement may comprise of rocks from the Karoo Supergroup, the Cape Supergroup or the Malmesbury Group. In places, the basement may also be rocks of the Namaqua-Natal Metamorphic Province (Broad *et al.*, 2006). The Outeniqua sub-basins are typically underlain by metamorphosed and heavily-deformed rocks of the Cape Supergroup (Broad *et al.*, 2006). The Durban Basin is the least explored basin however the basement geology is likely rocks of the Namaqua-Natal Metamorphic Province and oceanic gabbro (Broad *et al.*, 2006).

The closest active tectonic boundary which may affect the region investigated in this project is the southern extent of the East African Rift system, a >5,000 km long divergent margin between the African and Somalian plates (and other minor plates), propagating southwards through African continent originating from the Afar depression (Figure 3). The southernmost recognised extent of the EARs, based on seismicity and volcanism, is in northern Mozambique, > 2,000 km from the Outeniqua and Orange Basins (Saria *et al.*, 2014).

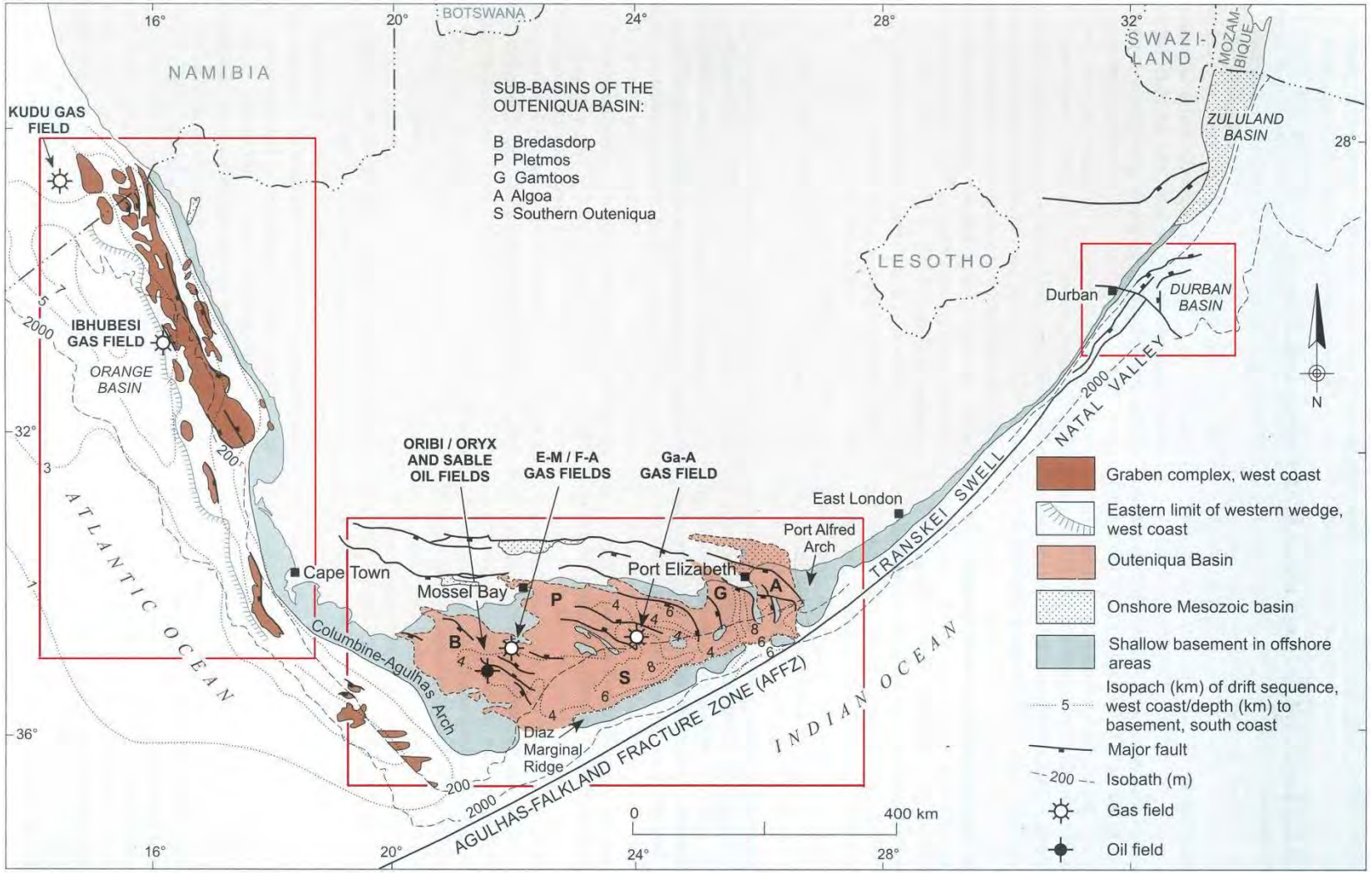

Figure 6: The location, general geology and major geological structures associated with South Africa's offshore basins which are considered in this study (modified after Broad et al., 2006). Both the Orange and Outeniqua Basins have been extensively investigated for hydrocarbon reservoirs, with most exploration and production concentrated in the Outeniqua sub-basins which as a result provide the majority of the borehole logs analyses in this project.

The nearest convergent boundary is the African - Eurasian collision zone which runs roughly east-west across the northern coastline of Morocco, Algeria and Tunisia, continuing to the Hellenic and Cyprean arcs in the eastern Mediterranean Sea (Ben-Avraham and Tibor, 1993). This convergent margin is still over 7,500 km from the study area (Figure 2). With respect to surrounding tectonic plates, geodetic data indicates the African plate is drifting towards the NE (Nocquets *et al.*, 2006; Saria *et al.*, 2014).

When considering the geological setting of southern Africa, the possible impact of the African Superswell, as first comprehensively described by Nyblade and Robinson (1994), must also be mentioned. This large low-velocity province has been suggested as the possible cause for the dynamic topography of the region which has resulted in a broad region of uplift spreading from Southern to East Africa. It has been suggested mantle flow beneath the African Plate may result in "mantle drag" on the overlying crust, affecting stress patterns (Nyblade &Robinson, 1994; Lithgow-Bertelloni & Silver, 1998).

The Outeniqua Basin

The Outeniqua Basin encompasses a series of fault-bounded sub-basins. From west to east these are: the Bredasdorp, Pletmos, Gamtoos and Algoa sub-basins. To the south, below the 300 m isobaths is a distal basin known as the Southern Outeniqua sub-basin which terminates against the AFFZ (Figure 6). The arcuate trend of the sub-basins appear to be inherited from the complex structure of the basement which is primarily rocks of the metamorphosed and deformed Cape Supergroup (Figure 7) (De Swardt and McLachlan, 1982). The Outeniqua basin lacks extensive carbonate and evaporite units when compared to many European sedimentary basins. This is a positive aspect when considering the reliability of borehole breakout data as the presence of low-strength evaporates units within a sedimentary basin can result in the stresses propagated through the crystalline basement decoupling from the overlying sediments. This can result in inconsistent stress orientations calculated over depth (Heidbach *et al.*, 2007).

The two major sedimentary basins, the Bredasdorp and Pletmos, share a similar depositional history consisting of 5 main phases (Brown *et al.*, 1996; Broad *et al.*, 2006):

1. Mid-Jurassic to Early-Cretaceous syn-rift sedimentation 1: These deposits associated with active rifting and half-graben formation are typically fluvial and lacustrine

sediments grading into deltaic and shallow-marine deposits and are also associated with volcanics or volvanoclastics.

2. Early Cretaceous syn-rift phase 2: Deep water deposits, primarily marine claystones and turbidites, formed in rapidly developing basins due to increased subsidence and formation of sub-basins separated by structural highs. This sequence represents the target rock for most exploration drilling in the basin.
3. Early to Mid-Cretaceous transitional (early drift) phase: Deposits from this sequence area associated with higher energy environments and shelf progradation from the northern margins. Interbedded claystones and shelf sandstones are found to the north whereas fan sandstones dominate the deeper southern part of the basin.
4. Mid to Late-Cretaceous drift phase: Further subsidence occurred due to thermal cooling and sediment loading.
5. Paleogene to Present upper drift phase: Further deposition of deep marines sediments including shales targeted for potential hydrocarbon reserves. Shelf deposits comprise of calcareous sandstones and marls.

Both the Gamtoos and Algoa sub-basins consist of both onshore and offshore sequences (Broad *et al*., 2006):

1. The Early Cretaceous syn-rift depositional phase consists of continental conglomerates and sandstones overlain by brackish shales, siltstone and sandstones representing near-shore deposits. Late syn-rift deposits include marine shales and sandstones.
2. The Early to Middle Cretaceous transitional and drift phases, primarily marine claystones and turbidites transitioning to shelf sandstones, were formed during a period of uplift, erosion and canyon formation.
3. Late Cretaceous and Tertiary depositional phase is consistent with deposits seen in the Bredasdorp and Pletmos sub-basins to the south.

The calliper logs for boreholes intersecting the available geological profile indicate that most are targeting organic-rich source rocks at the late syn-rift/transitional boundary. The average breakout depths in these boreholes indicate the majority of breakouts are found in drift sediments consisting of marine claystones and prograding shelf deposits well above the faulted basin and syn-rift deposits (Figure 7).

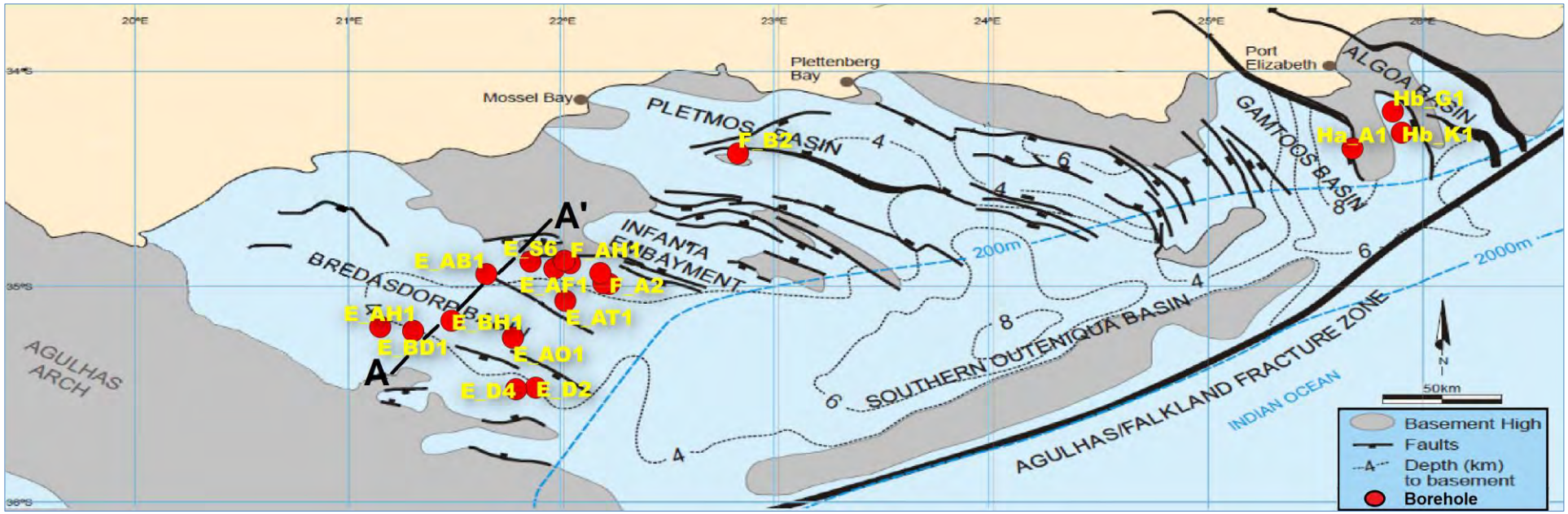

Figure 7: The Outeniqua Basin is structurally complex and subdivided into numerous fault-bounded sub-basins separated by basement highs (modified from map in Petroleum Agency SA report - http://www.petroleumagencysa.com/images/pdfs/Western_Bredasdorp_Basin.pdf). The Agulhas-Falkland Fracture Zone is a palaeo-transform zone related to the Gondwana breakup and not a currently active seismogenic fault. The apparent N - S compression of the map is due to the re-projection of the map into the GIS software to match the projection used for other datasets.

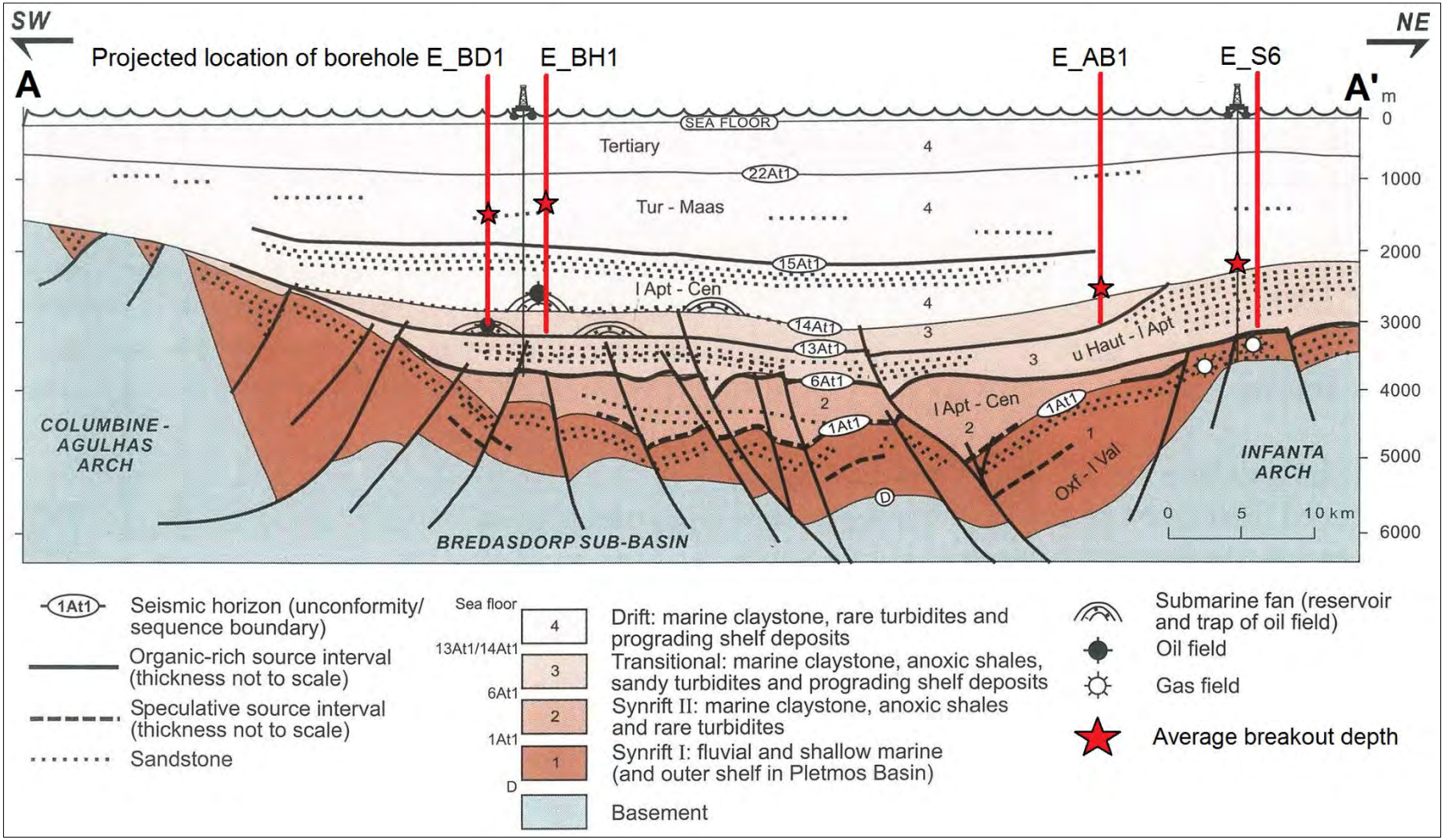

Figure 8: A cross section indicating the structure and general stratigraphy of the Bredasdorp sub-basin. This sub-basin provides the majority of boreholes analysed in this study and displays the greatest variation in S_{Hmax} orientation over short distances (Broad et al., 2006).

The Orange basin

The Orange basin forms part of the greater Southwest African Coastal basin stretching from the Walvis Ridge in the north to the Agulhas Fracture Zone in the south (Figure 9). The Orange Basin is the largest offshore basin in South Africa covering 145,000km^2 (down to the 2000m isobath) and including a thin sliver of sediments running south past the Cape Peninsula along the margin of the Columbine-Agulhas Arch (Figure 9). This margin has been described as a purely passive volcanic margin (Gerrard and Smith, 1982; Broad *et al.*, 2006). The Orange Basin is structurally less complex than the Outeniqua Basin. Structural subdivisions seen in the Orange Basin are typically subparallel to the coastline whereas east-west orientated highs separating the segments correlate with transform zones formed to accommodate differential movement during the Gondwana super-continent breakup. The western-most margin is a continuous linear high known as the Marginal Ridge (Figure 9) (Gerrard and Smith, 1982; Broad *et al.*, 2006). As with the Outeniqua Basin, the Orange Basin does not have any major carbonate or evaporite units.

The depositional history of the Orange Basin consists of 4 main phases (Brown *et al.*, 1996; Broad *et al.*, 2006):

1. Mid to Late-Jurassic syn-rift phase: The onset of rifting generated a series of coast-parallel grabens. The sediments grade from coarse continental clastics, through fluvial and lacustrine sediments with volcanics and volcanoclastics present in places.
2. Late-Jurassic to Early-Cretaceous post-rift transitional phase: These sediments were deposited in a shallow and restricted to the proto-Atlantic and comprise of coastal, deltaic and limited marine deposits.
3. Early-Cretaceous to Tertiary drift phase: Deposits comprise primarily of marine sediments with shelf turbidites.
4. Late-Cretaceous to Present late drift phase: Reduced subsidence rates and the establishment of a stable shelf environment led to the deposition of calcareous sandstones and marls.

The two boreholes closest to the available profile appear to be wells targeting structural traps in slump deposits above organic-rich source rocks. Steep lystric faults are common near the shelf edge and also in near-shore sections of the basin which inherit the steep fault pattern of the underlying rifted continental margin. The average breakout depth occurs in Late Cretaceous drift deposits which consist of marine shales and sandstones (Figure 10).

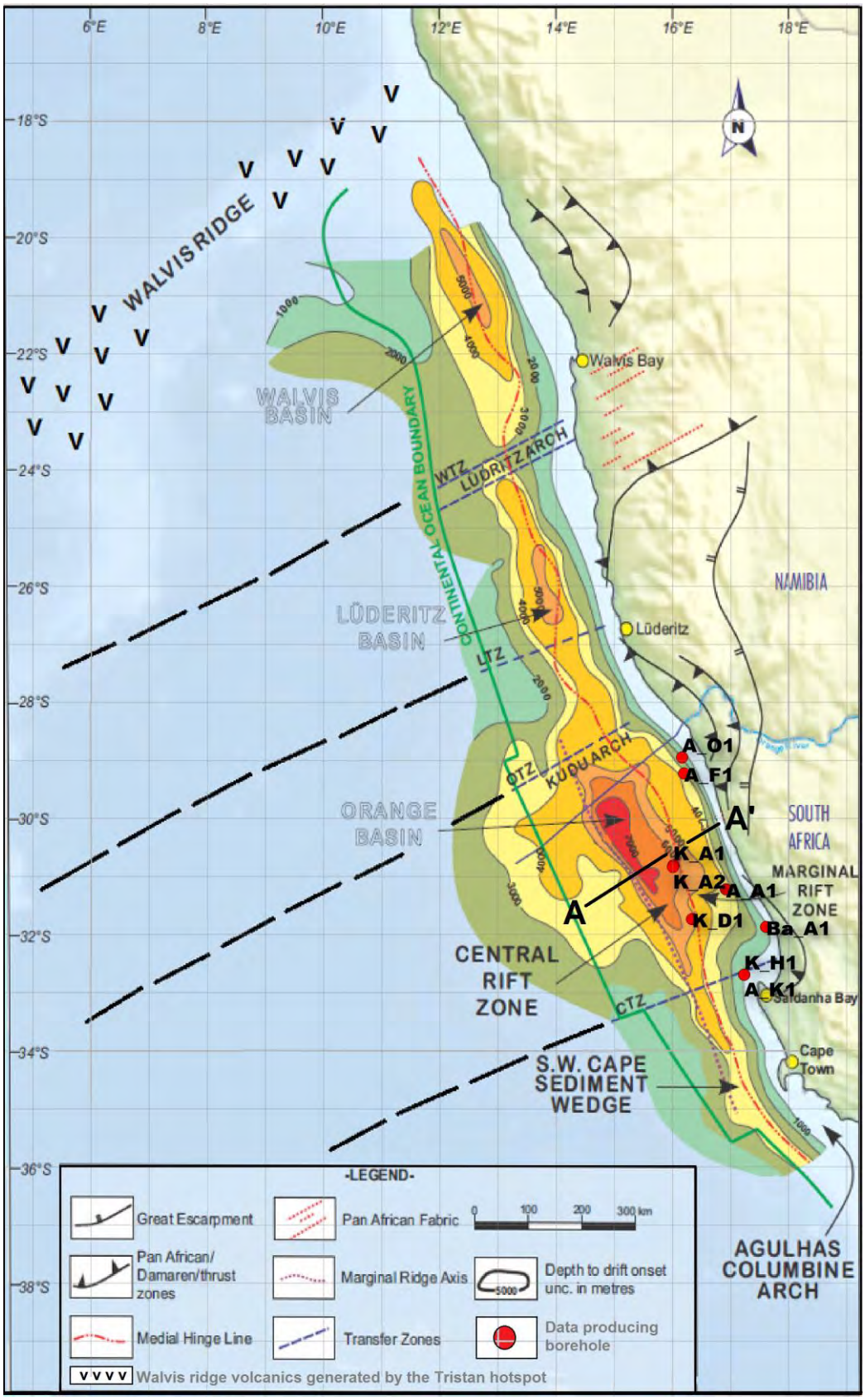

Figure 9: The Orange Basin is a purely divergent margin with a relatively simple structural geology. Major basin faults is coast-parallel and structural highs separating basins are associated with transform zones (modified after map in Petroleum Agency SA report - http://www.petroleumagencysa.com/images/pdfs/Orange_Basin_Brochure_web1.pdf)

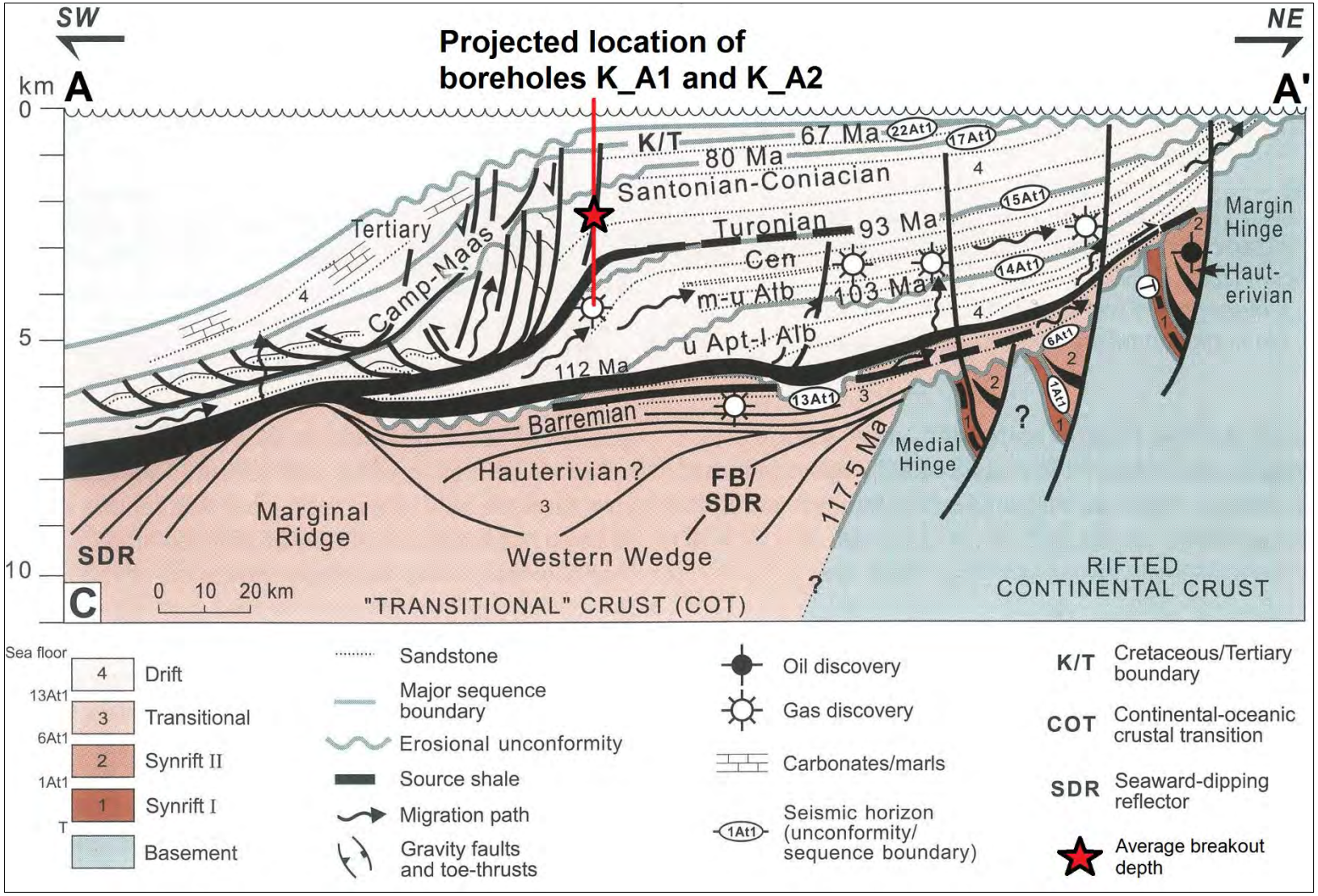

Figure 10: General structure and stratigraphy of the Orange Basin (modified after Broad *et al.*, 2006). Coast-parallel faults dominate this purely divergent margin with transform zones forming highs between basins.

The Durban Basin

The Durban Basin is a small Mesozoic offshore basin encompassing roughly 10,000 km^2 and is situated between the structural high of the Transkei Swell in the south and the Zululand Basin to the north (Figure 11). The sediments range from Late Jurassic deep-water syn-rift deposits to Tertiary shelf-sediments with evidence of Tertiary-age intrusives. The total basin thickness can reach 4000 m (Broad *et al.*, 2006) and syn-rift deposits have been correlated with red continental sediments at the base of the onshore Zululand Basin. The basin forms the northern termination point of the Agulhas Falkland Fracture.

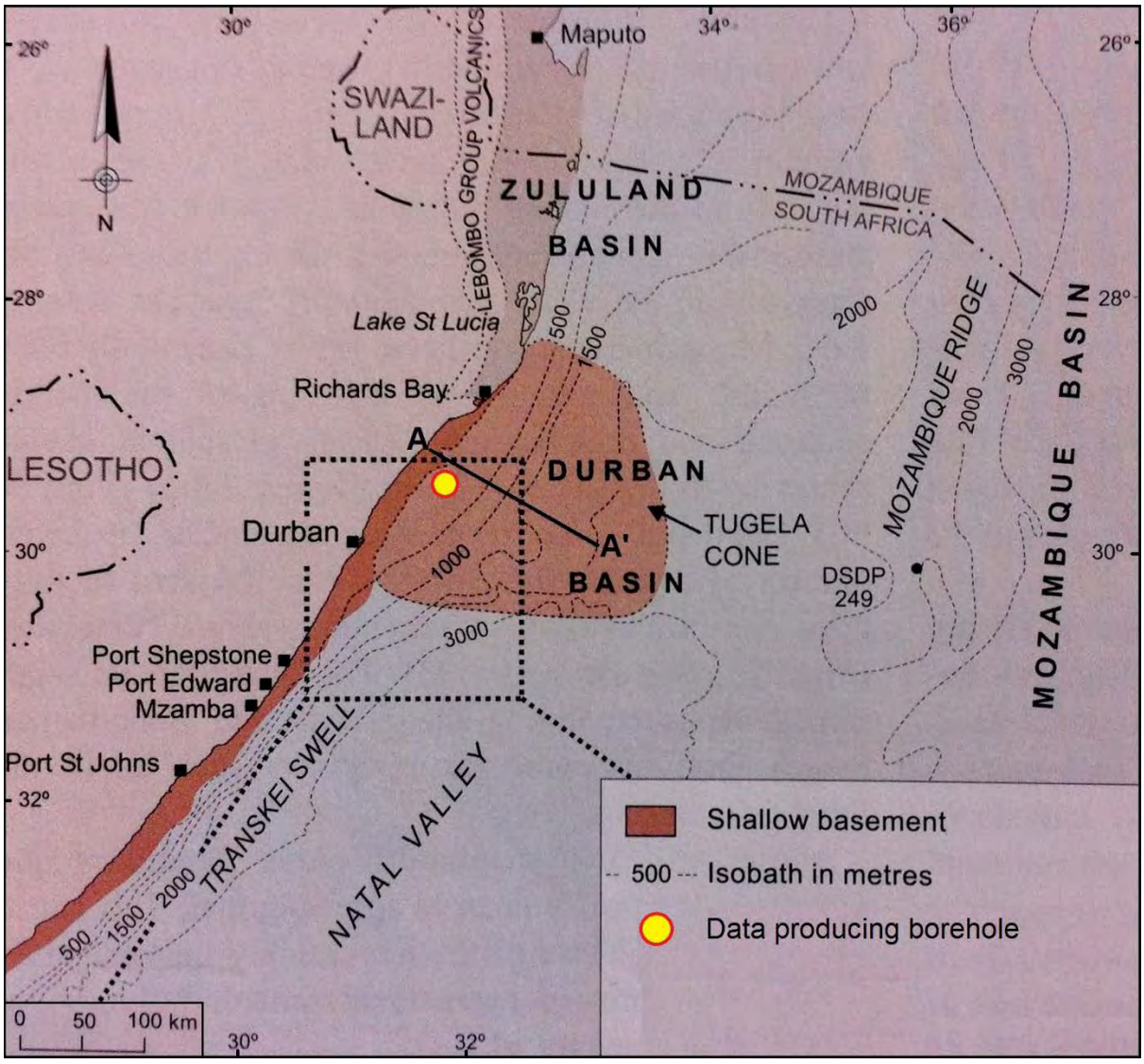

Figure 11: Overview of the Durban Basin structure (modified after Broad *et al.*, 2006).

The single borehole which produced breakout data is located in the shallow near-shore part of the basin, targeting organic-rich shales in the syn-rift deposits (Figure 12). The short zone of breakouts occurs on the boundary of the syn-rift/late-drift unconformity in shelf sediments consisting primarily of shale.

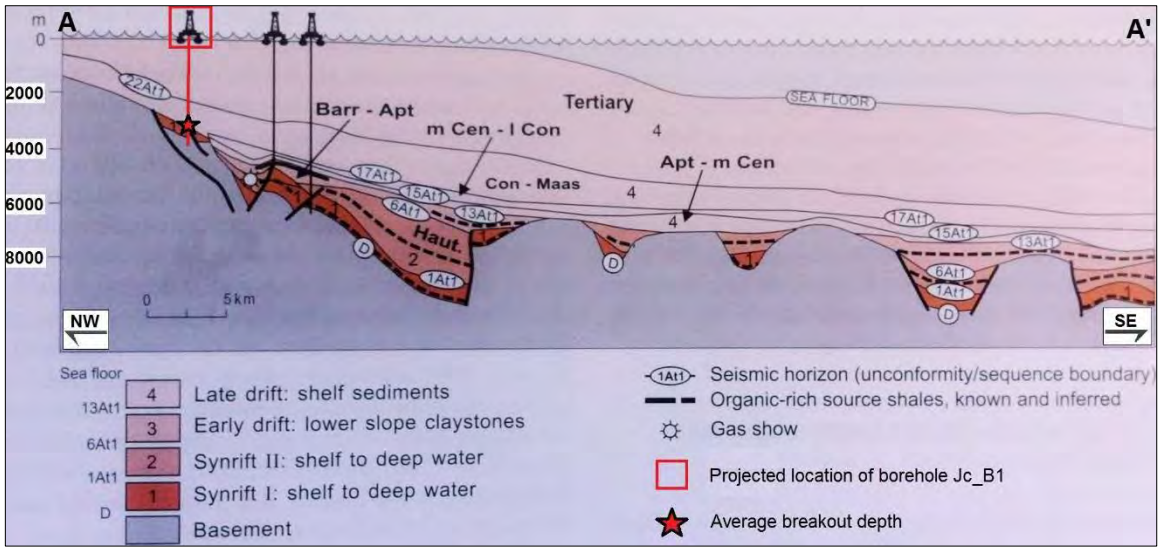

Figure 12: Generalised cross section through the Durban Basin (modified after Broad *et al.*, 2006)

CHAPTER 3: BOREHOLE BREAKOUT ANALYSIS

Borehole breakout generation

A myriad of geological processes associated with plate tectonics continuously generates stress in the Earth's crust. These stresses can never be directly measured but are rather inferred from disturbed samples and excavations (Zang & Stephansson, 2010). Force applied to a rock will vary from point to point and idealised concepts using a localised point are not sufficient to describe real behaviour. As a result, it is more efficient to introduce the concept of **traction** (force acting on a unit area) represented by a **stress tensor**. This tensor consists of three stress components - the principal stresses (S_1, S_2, S_3) and three associated stress directions – the principle stress axes (n_1, n_2, n_3). As seen in Figure 13, these six quantities are used to describe the state of stress at a point with respect to a global coordinate system (Jaeger *et al.*, 2007; Zang & Stephansson, 2010).

Considering stress within the Earth's crust, it is intuitive that the Earth's gravity field is a dominant force at depth and generates a principle stress axis, orientated vertically towards the surface. This principle component of crustal stress is referred to as the **vertical stress** (S_v). The two other components required to define the crustal stress field are both perpendicular to S_v and are referred to as the **maximum horizontal stress** (S_{Hmax}) and **minimum horizontal stress** (S_{hmin}). Near surface in the Earth's crust, S_v is the dominant force with $S_v >> S_h \neq S_H$. As depth increases, a more lithostatic stress state, $S_v = S_h = S_H$, is expected (Figure 13) (Zang & Stephansson, 2010).

When a sample is removed from its native stress state, or an excavation is made into stressed rock, stress accumulation around the excavation can result in **strain** - a change in volume of the material (Jaeger *et al.*, 2007). This deformation is vital in the generation of borehole breakouts used to determine the orientation of the horizontal stresses at depth. Experimental work and in-field observations describe a predictable concentration of stress generated around a cylindrical opening and the resultant deformation and failure (Figure 14) (Zoback, 2010).

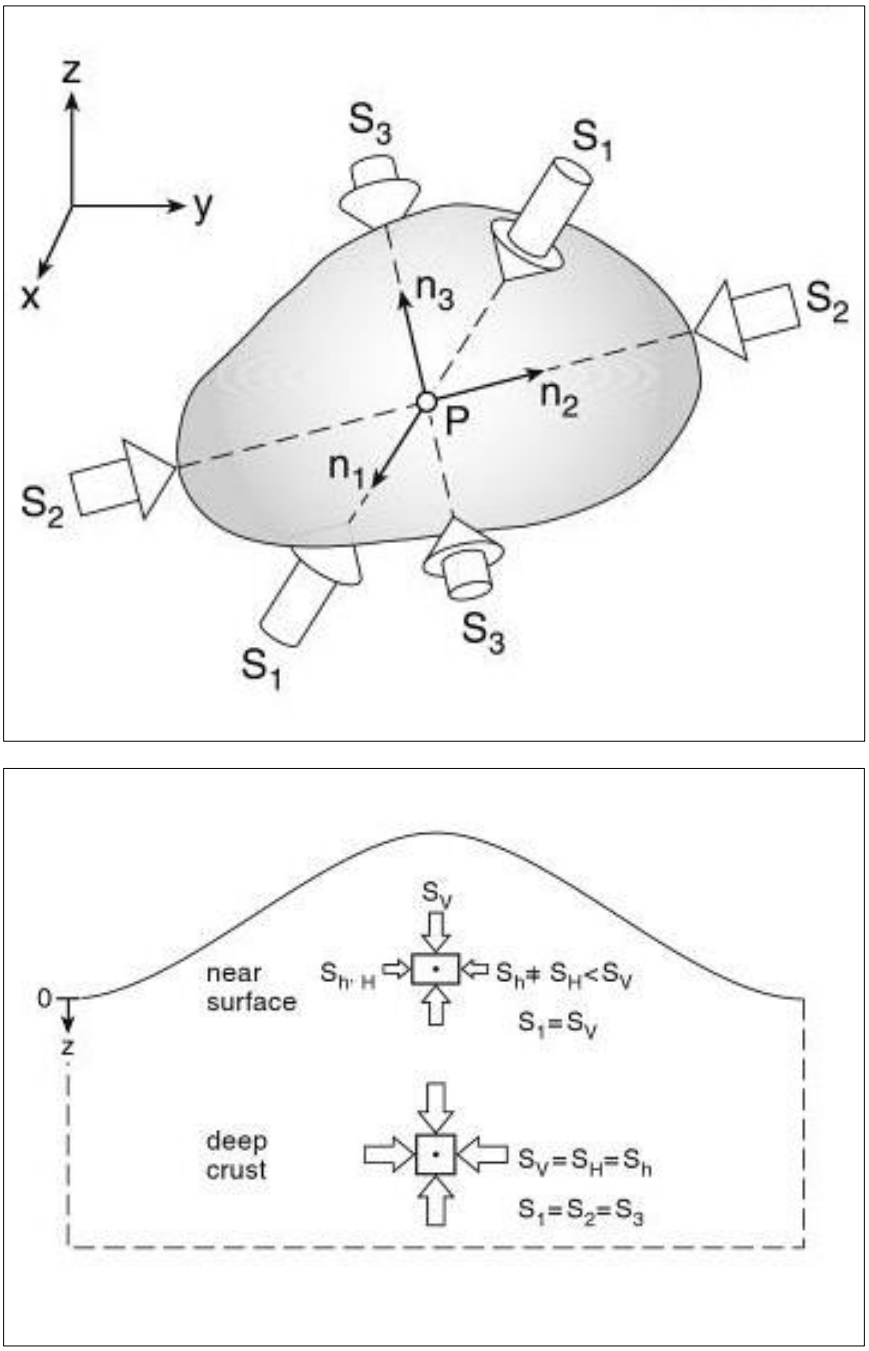

Figure 13: Top - a simplified example of the 6 components required to construct a stress tensor in an arbitrary body. Bottom - Heim's rule proposes that at shallow depths in the crust, S_v is considerably greater than S_{Hmin} and S_{Hmax}. S_v is also vertically aligned with the force of gravity, whereas the other principle axes are located on the horizontal plane (Zang and Stephansson, 2010). It is within this horizontal plane S_{Hmax} and S_{hmin} are defined for the crustal stresses.

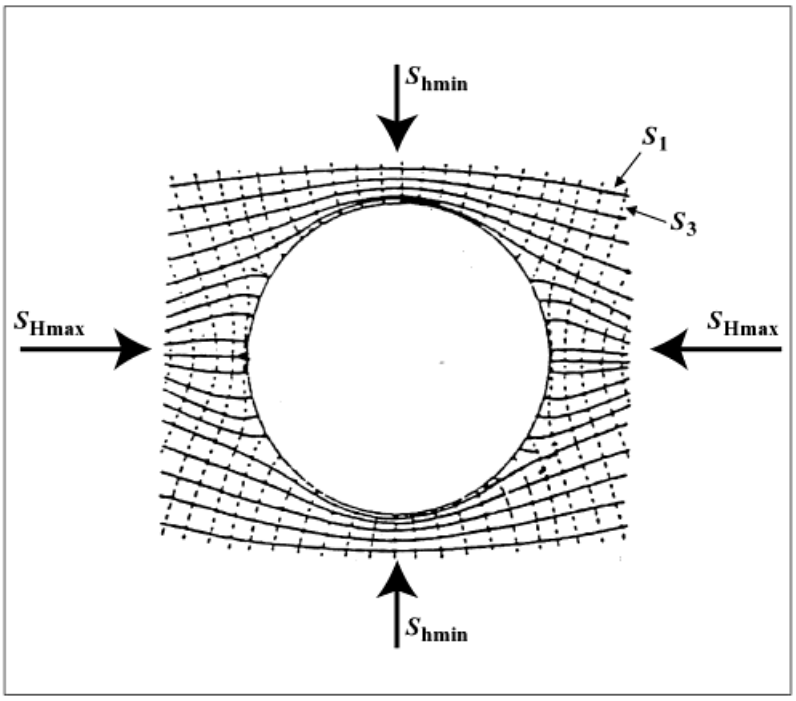

Figure 14: The concentration of stresses around a cylindrical opening, similar to what would be experienced in an exploration borehole at depth (Zoback, 2010). The concentration of stress around the S_{hmin} axis can exceed the maximum compressive strength of the material resulting in failure.

“

The theory behind borehole breakout formation is well understood and was first described, although without the current application, over a hundred years ago by the German engineer Ernst Kirsch in 1898. The current application of using borehole breakouts to determine S_{Hmax} orientation was first applied in the Athabasca sedimentary basin in western Canada (Zobach *et al.*, 1985). Measurement techniques have been well established and hypotheses verified in field observations (Bell *et al.*, 1993, 1994).

As seen in Figure 15, the removal of material in the borehole results in a concentration of stress parallel to the minimum horizontal stress axis (S_{hmin}). This leads to eventual failure of as accumulated stress exceeds the material strength. The method of failure has been described as due to shear failure (mode II cracks) by Zoback *et al.* (1985) or as a result of extensional failure (mode I cracks) by Zheng *et al.* (1989). The eventual failure and spalling of material from the borehole wall typically results in a bimodal increase in area which is detectible during logging by 4 or 6-arm callipers (Figure 15).

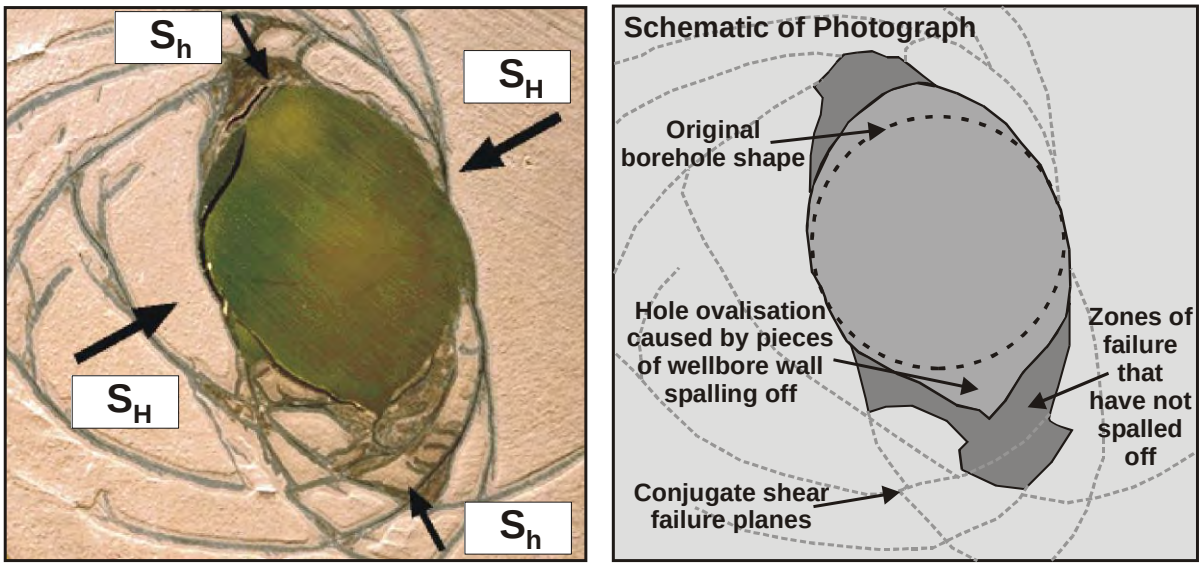

Figure 15: Experimental work demonstrates the accumulation of stress and generation of interconnected fractures sub-parallel to Sh. This leads to spalling of material and bimodal enlargement of the borehole which can be detected during calliper logging (Plumb and Hickman, 1985).

The stress concentration and subsequent deformation is not always consistent however and this can result in a variety of deformation features within the borehole: A complete 360° collapse of the borehole wall results in a **washout** and general enlargement of the borehole beyond drill-bit specifications. A **key seat** feature occurs when only one side of the borehole is elongated, normally due to mechanical notching. Both features need to be considered when analysing for borehole breakouts (Plumb and Hickman, 1985; Zoback, 2010).

Borehole log data

The petroleum industry routinely runs calliper logs down newly drilled exploration boreholes in order to assess the cross-sectional area of the borehole over depth in order to estimate the total volume of concrete needed to case the well. A calliper tool is inserted down to the base of the most recently drilled section and winched up slowly while rotating through 360° to produce a log of depth vs. calliper diameter. This process is automatically logged and the output is a file containing depth measurements with the associated calliper diameters. Numerous other essential parameters for breakout analysis are also recorded including the azimuth of the primary calliper pad, the relative bearing of the borehole if it is not exactly vertical, and the deviation from vertical at any given depth.

When this calliper diameter and orientation data is stacked over depth, it provides a reliable estimation of the cross-sectional area of the borehole over a chosen length. Combined with depth measurements, this can provide a reliable estimation of the volume required for borehole casing, however for the purposes of this project, the variation in cross-sectional area is key to identifying borehole breakouts. Both 4-arm and 6-arm calliper logs are used by the petroleum industry however this study utilises the common 4-arm calliper logs provided.

Compiling depth, calliper-diameter and calliper-orientation readings over a selected section of borehole allows for a reasonable pseudo cross-section to be visualised for sections of interest. With the **F**our **A**rm **C**aliper **T**ool (**FACT**) software provided by the WSM team, this dataset can be analysed and allow the user to identify changes in the cross-sectional area of the borehole and identify potential zones of borehole breakout.

Figure 16 is an idealised example of a calliper logging tool and indicates the five key parameters required for visualising potential breakouts using the **FACT** software:

1. Depth (**DEPT**): This value is used to define any calliper measurement in space and also to calculate the distance between the top and bottom of major breakouts zones. This also allows for the user to determine total length of all breakout zones throughout the borehole and calculate the average depth of the breakouts (**z**).
2. Calliper 1 and calliper 2 diameters (**CAL1** and **CAL2**): These callipers are perpendicular in the 4-arm logs used for this project. When these data are compiled in a cross-section over chosen depth, it allows the user to visualise the enlargement or collapse of the borehole circumference relative to the known bit-size utilized for drilling. The typical bit-sizes used for the wells are 8.5 inch (deep drilling), 12.25 inch (intermediate depths) and 17.5 inch (shallow drilling).
3. The azimuth of the primary calliper pad (**P1AZ**): This value, coupled with the relative bearing of the borehole itself, is vital in defining the true azimuth of the lead calliper arm. It allows the FACT software to accurately determine the orientation of the other calliper arms and place the data within a standard coordinate system (**x**,**y**).
4. Relative bearing (**RB**) represents the dip-bearing of borehole in the event the well is not completely vertical. This angle, coupled with well deviation, is used to correct calliper orientation values to the horizontal plane in which S_{Hmax} and S_{hmin} are described.

5. The deviation (**DEVI**) of the borehole from vertical: This value, in addition to the relative bearing, allows for the software to correct the P1AZ value to the horizontal plane. It also factors strongly into the exclusion criteria as extreme deviation from vertical (typically beyond 15°) results in spalling that may be a response to hanging-wall collapse rather than stress accumulation (Zoback, 2010).

Another value that may be used in preparing calliper log data is the azimuth of borehole drift **(HAZI).** It is typically unused in the FACT analysis however it may be used to calculate a missing parameter in the calliper logs using the equation:

Using any basic spreadsheet software, the calliper logs are checked to ensure sufficient parameters are present, and then edited and merged to create a file suitable for analysis by FACT (a tab-separated *.DAT is used). During this first review step, any file with insufficient parameters or clearly erroneous data is discarded. Common erroneous values include unchanging calliper diameter values (indicating the tool failed to open), no rotation of P1AZ (unable to determine real orientations) and log output issues such as depth and calliper diameter readings with additional digits which far exceed real drilling limits.

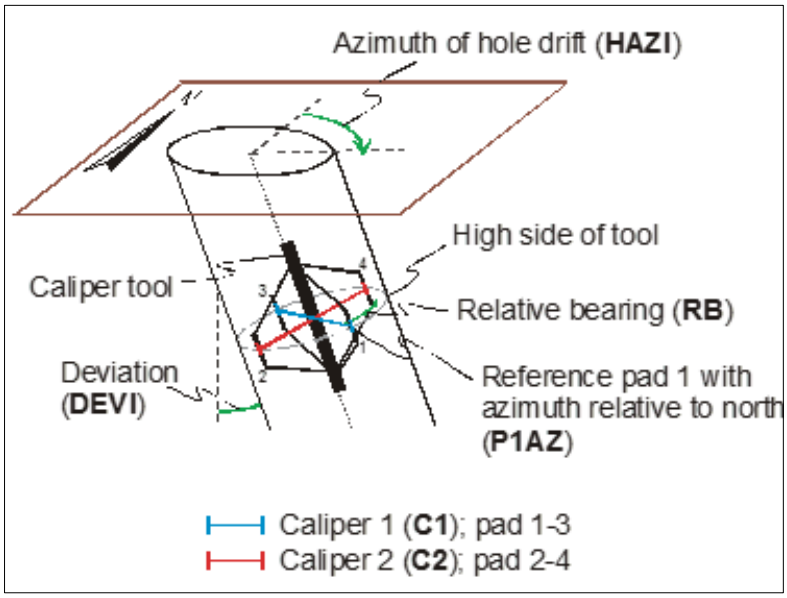

Figure 16: A diagrammatic representation of the 4-arm calliper tool and the values required for input into the FACT software.

When a file possesses sufficient parameters, these columns (sometimes merged from multiple files if necessary) are compiled into a single spreadsheet and filtered to include only the required data. For input into FACT, the data must be presented, from left to right, as: DEPTH, CAL1, CAL2, PAZ1, RB and DEVI. The depth data is inverted so the column runs from the deepest values to shallow. Figure 17 demonstrates the stages of refining the original log file down to usable data for analysis.

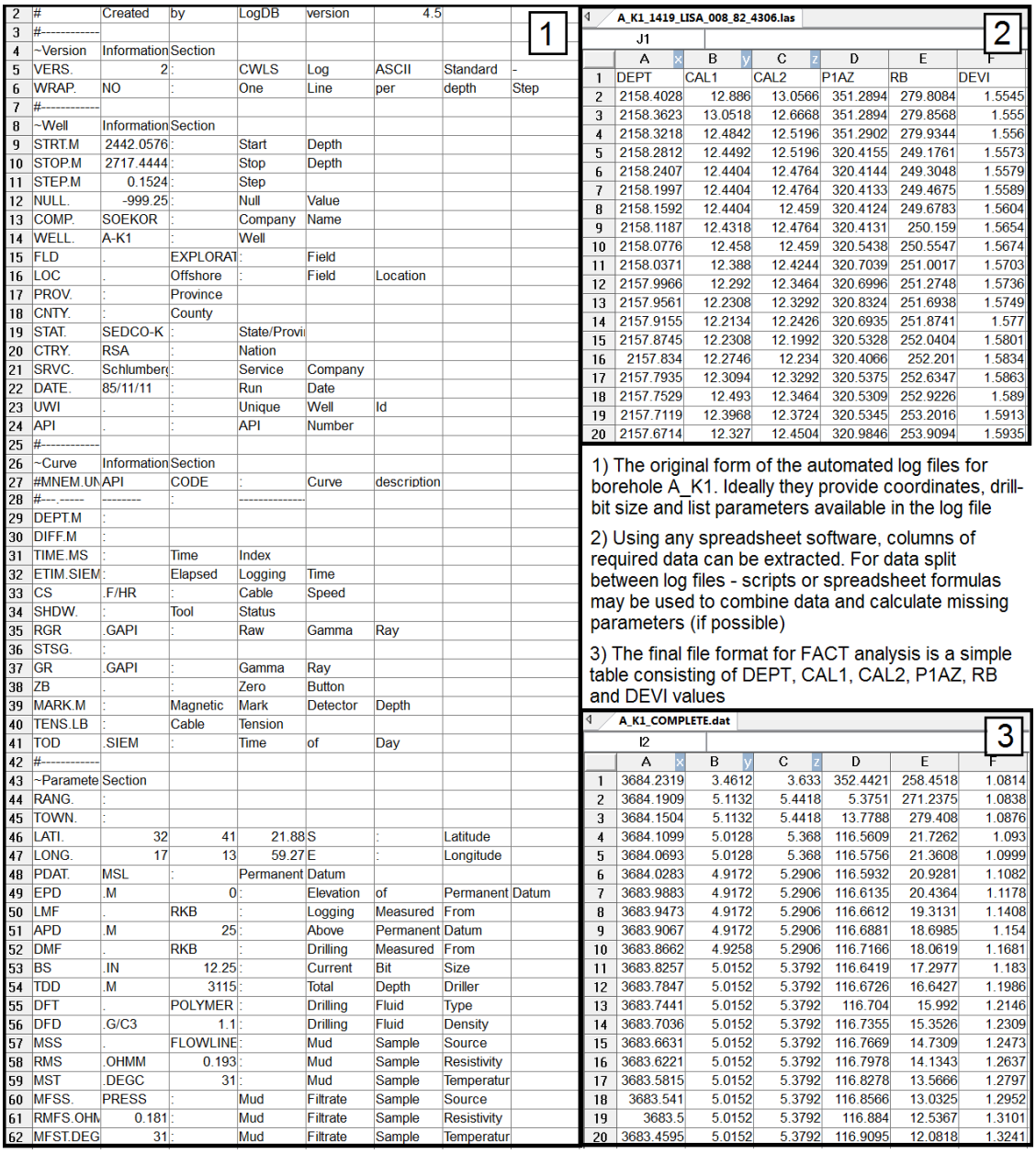

2	#	Created	by	LogDB	version	4.5		
3	#----------							
4	~Version	Information	Section					
5	VERS.	2	:	CWLS	Log	ASCII	Standard	-
6	WRAP.	NO	:	One	Line	per	depth	Step
7	#----------							
8	~Well	Information	Section					
9	STRT.M	2442.0576	:	Start	Depth			
10	STOP.M	2717.4444	:	Stop	Depth			
11	STEP.M	0.1524	:	Step				
12	NULL.	-999.25	:	Null	Value			
13	COMP.	SOEKOR	:	Company	Name			
14	WELL.	A-K1	:	Well				
15	FLD	.	EXPLORAT	:	Field			
16	LOC	.	Offshore	:	Field	Location		
17	PROV.	:	Province					
18	CNTY.	:	County					
19	STAT.	SEDCO-K	:	State/Provi				
20	CTRY.	RSA	:	Nation				
21	SRVC.	Schlumber	:	Service	Company			
22	DATE.	85/11/11	:	Run	Date			
23	UWI	.	:	Unique	Well	Id		
24	API	.	:	API	Number			
25	#----------							
26	~Curve	Information	Section					
27	#MNEM.UN	API	CODE	:	Curve	description		
28	#---.-----	--------	:	----------				
29	DEPT.M	:						
30	DIFF.M	:						
31	TIME.MS	:	Time	Index				
32	ETIM.SIEM	:	Elapsed	Logging	Time			
33	CS	.F/HR	:	Cable	Speed			
34	SHDW.	:	Tool	Status				
35	RGR	.GAPI	:	Raw	Gamma	Ray		
36	STSG.	:						
37	GR	.GAPI	:	Gamma	Ray			
38	ZB	.	:	Zero	Button			
39	MARK.M	:	Magnetic	Mark	Detector	Depth		
40	TENS.LB	:	Cable	Tension				
41	TOD	.SIEM	:	Time	of	Day		
42	#----------							
43	~Paramete	Section						
44	RANG.	:						
45	TOWN.	:						
46	LATI.	32	41	21.88	S	:	Latitude	
47	LONG.	17	13	59.27	E	:	Longitude	
48	PDAT.	MSL	:	Permanent	Datum			
49	EPD	.M	0	:	Elevation	of	Permanent	Datum
50	LMF	.	RKB	:	Logging	Measured	From	
51	APD	.M	25	:	Above	Permanent	Datum	
52	DMF	.	RKB	:	Drilling	Measured	From	
53	BS	.IN	12.25	:	Current	Bit	Size	
54	TDD	.M	3115	:	Total	Depth	Driller	
55	DFT	.	POLYMER	:	Drilling	Fluid	Type	
56	DFD	.G/C3	1.1	:	Drilling	Fluid	Density	
57	MSS	.	FLOWLINE	:	Mud	Sample	Source	
58	RMS	.OHMM	0.193	:	Mud	Sample	Resistivity	
59	MST	.DEGC	31	:	Mud	Sample	Temperatur	
60	MFSS.	PRESS	:	Mud	Filtrate	Sample	Source	
61	RMFS.OHM	0.181	:	Mud	Filtrate	Sample	Resistivity	
62	MFST.DEG	31	:	Mud	Filtrate	Sample	Temperatur	

	A	B	C	D	E	F
1	DEPT	CAL1	CAL2	P1AZ	RB	DEVI
2	2158.4028	12.886	13.0566	351.2894	279.8084	1.5545
3	2158.3623	13.0518	12.6668	351.2894	279.8568	1.555
4	2158.3218	12.4842	12.5196	351.2902	279.9344	1.556
5	2158.2812	12.4492	12.5196	320.4155	249.1761	1.5573
6	2158.2407	12.4404	12.4764	320.4144	249.3048	1.5579
7	2158.1997	12.4404	12.4764	320.4133	249.4675	1.5589
8	2158.1592	12.4404	12.459	320.4124	249.6783	1.5604
9	2158.1187	12.4318	12.4764	320.4131	250.159	1.5654
10	2158.0776	12.458	12.459	320.5438	250.5547	1.5674
11	2158.0371	12.388	12.4244	320.7039	251.0017	1.5703
12	2157.9966	12.292	12.3464	320.6996	251.2748	1.5736
13	2157.9561	12.2308	12.3292	320.8324	251.6938	1.5749
14	2157.9155	12.2134	12.2426	320.6935	251.8741	1.577
15	2157.8745	12.2308	12.1992	320.5328	252.0404	1.5801
16	2157.834	12.2746	12.234	320.4066	252.201	1.5834
17	2157.7935	12.3094	12.3292	320.5375	252.6347	1.5863
18	2157.7529	12.493	12.3464	320.5309	252.9226	1.589
19	2157.7119	12.3968	12.3724	320.5345	253.2016	1.5913
20	2157.6714	12.327	12.4504	320.9846	253.9094	1.5935

	A	B	C	D	E	F
1	3684.2319	3.4612	3.633	352.4421	258.4518	1.0814
2	3684.1909	5.1132	5.4418	5.3751	271.2375	1.0838
3	3684.1504	5.1132	5.4418	13.7788	279.408	1.0876
4	3684.1099	5.0128	5.368	116.5609	21.7262	1.093
5	3684.0693	5.0128	5.368	116.5756	21.3608	1.0999
6	3684.0283	4.9172	5.2906	116.5932	20.9281	1.1082
7	3683.9883	4.9172	5.2906	116.6135	20.4364	1.1178
8	3683.9473	4.9172	5.2906	116.6612	19.3131	1.1408
9	3683.9067	4.9172	5.2906	116.6881	18.6985	1.154
10	3683.8662	4.9258	5.2906	116.7166	18.0619	1.1681
11	3683.8257	5.0152	5.3792	116.6419	17.2977	1.183
12	3683.7847	5.0152	5.3792	116.6726	16.6427	1.1986
13	3683.7441	5.0152	5.3792	116.704	15.992	1.2146
14	3683.7036	5.0152	5.3792	116.7355	15.3526	1.2309
15	3683.6631	5.0152	5.3792	116.7669	14.7309	1.2473
16	3683.6221	5.0152	5.3792	116.7978	14.1343	1.2637
17	3683.5815	5.0152	5.3792	116.8278	13.5666	1.2797
18	3683.541	5.0152	5.3792	116.8566	13.0325	1.2952
19	3683.5	5.0152	5.3792	116.884	12.5367	1.3101
20	3683.4595	5.0152	5.3792	116.9095	12.0818	1.3241

Figure 17: The basic process of converting an automated calliper log file into usable data for FACT analysis. The raw file contains a header with most borehole data and a list of parameters. This header information is noted and then the log file is simplified and rearranged for input to the FACT software.

Breakout analysis software - FACT

Prepared calliper log files are analysed, breakout rose-diagrams are generated using the "Four Arm Caliper Tool" (FACT) software provided by the WSM team and S_{hmin} orientations are picked and averaged. The FACT analysis tool presents the compiled calliper log data as a 2D profile, down-borehole, on the initial start-up screen (Figure 18). The most important information displayed to the user is the depth reading (DEPT), calliper diameter values (CAL1 and CAL2), the bearing of the primary pad (P1AZ) and deviation from vertical (DEVI).

Before analysis begins, the Header file is edited to input the log parameters for the section of interest and error limits (Figure 19). Inputting the correct borehole parameters and acceptable error limits is essential before beginning analysis as the software will automatically apply them for the user during manual picking of borehole breakout data.

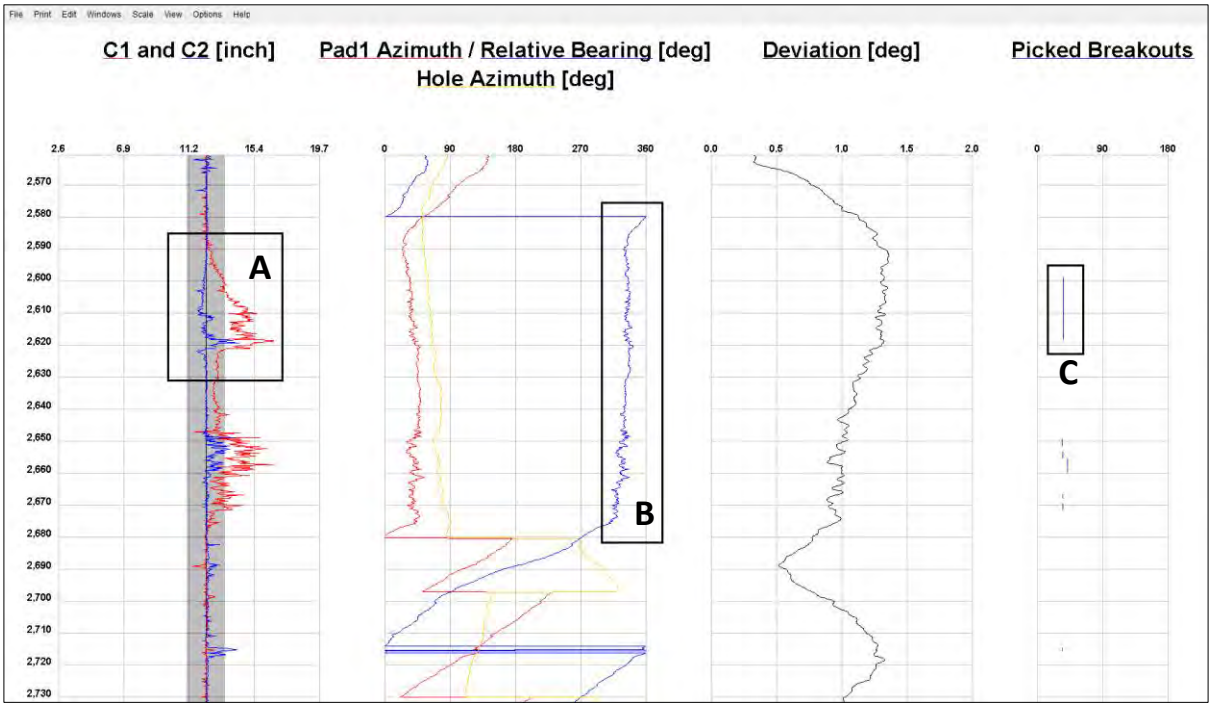

Figure 18: The basic user interface for the FACT software. The main details presented are the depth reading, calliper pad diameter/azimuth, the P1AZ azimuth and also the deviation of the borehole from vertical. The borehole used for this example is A_K1

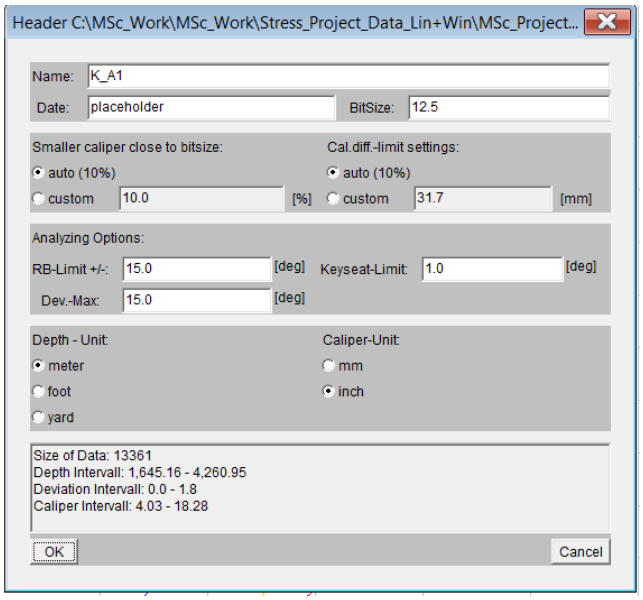

Figure 19: The FACT header file for borehole A_K1. This displays information on the dataset and allows the user to enter parameters for the borehole and set exclusion parameters which the software enforces when the user is manually picking potential borehole breakouts.

When selecting what appears to be a borehole breakout (Figure 18 - **A**), it is important to see a break in rotation of the calliper (Figure 18 - **B**) indicating the calliper arms have rotated into, become lodged, and then rotated out of a breakout zone. Only a single calliper arm should show a large deviation from the drill-bit size, indicating a bimodal increase in cross-sectional area as expected in Figure 15. Table 1 below summarises the basic criteria which should be satisfied in order to correctly identify an acceptable breakout zone. Additional information presented in the software includes the minimum deviation from the drill-bit size (the grey zone in Figure 18 - **A**), the deviation of the borehole from vertical and zones which have already been picked for breakout analysis (Figure 18 - **C**). This visual feedback allows the user to quickly assess potential breakout zones and easily find previous picks in a calliper log file for review.

Table 1: Basic criteria to satisfy when selecting an appropriate borehole breakout for analysis.

1. Tool rotation must cease in the zone of enlargement.
2. There must be clear tool rotation into and out of the enlargement zone.
3. The smaller calliper reading is close to bit size. Top and bottom of the breakout should be well marked.
4. Calliper difference has to exceed bit size by 10 %.
5. The enlargement orientation should not coincide with the high side of the borehole in wells deviated by more than 5°.
6. The length of the enlargement zone must be greater than 1 m.

A depth range is selected from the overview screen (Figure 18) and can then be viewed as a 2D cross-section (showing the overall borehole calliper locations over a range of depth values) in the "Detail" screen (Figure 20). A more detailed log is provided to refine the breakout zone (Figure 20 - **A**) from which breakout orientation is extracted. In this more detailed log, green data indicates regions excluded from analysis based on parameters entered into the header file and this also allows the user to more accurately assess if the feature is a breakout or washout/key-seat feature (Figure 21). Selecting a breakout zone results in the cross-sectional display seen above the log (Figure 20 - **B**), which allows the user to best define the range of visible breakouts orientations by manually selecting the spread of data points and adding it to the breakout log (Figure 22). Ideally numerous zones in a calliper log should be analysed for breakout orientation to ensure a sufficient total length of breakouts and a reasonable standard deviation for average breakout orientation. The overall number of breakout zones, total breakout picks and standard deviation are used to define the quality of the orientation data as on WSM quality ranking criteria (Table 2).

Table 2: WSM quality ranking criteria for borehole breakout data (s.d. standard deviation) (Sperner *et al.*, 2003)

A-Quality	B-Quality	C-Quality	D-Quality	E-Quality
Wells that have ten or more distinct breakout zones with a combined length > 300 m; and with s.d. ≤ 12°	Wells that have at least six distinct breakout zones with a combined length > 100 m; and with s.d. ≤ 20°	Wells that have at least four distinct breakouts zones with a combined length > 30 m; and with s.d. ≤ 25°	Wells that have less than four breakouts zones or a combined length < 30 m or with s.d. > 25°	Wells with no reliable breakouts detected or with extreme scatter of breakout orientations (s.d. > 40°)

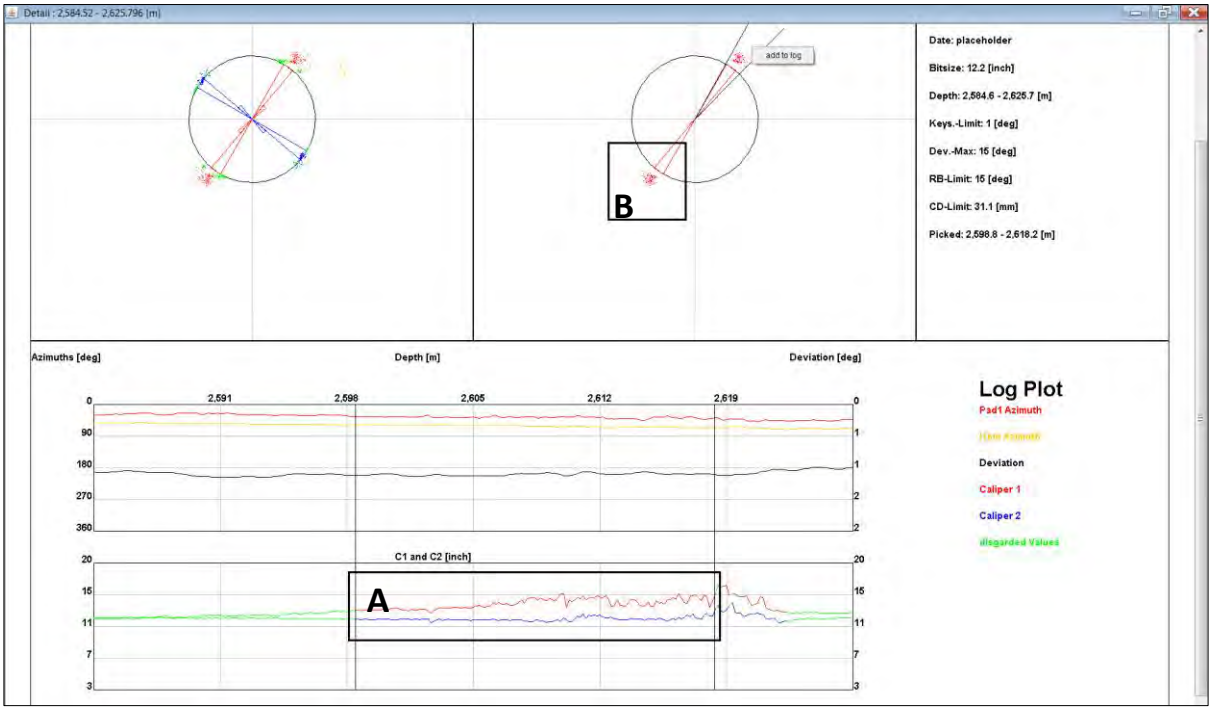

Figure 20: In this example from borehole A_K1, the manual picking process relies on the user identifying borehole breakouts in the log profile and then selecting the range of angles determined for each breakout length.

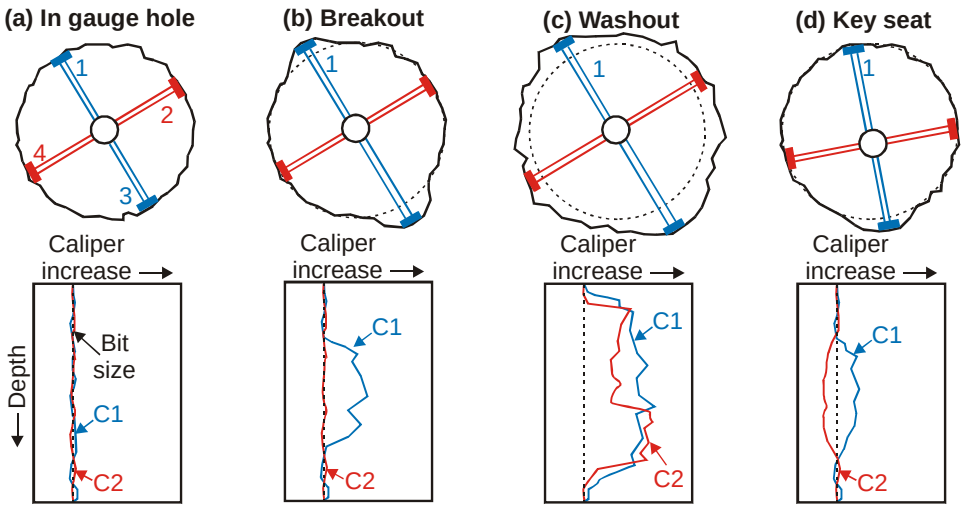

Figure 21: A representation of possible borehole conditions and the resultant calliper representation of these features in the FACT software.

The final step of analysing a calliper log is the "Breakout Log" screen (Figure 22) which compiles user-picked breakout data and produces a mean breakout orientation, indicating the orientation of S_{hmin}. Two S_{hmin} azimuths (and standard deviations) are presented for the data, one with the length-weighted average, giving higher weighting to larger breakout zones, and the other average based on the total number of picks for each orientation. Only the length-weighted data is presented and utilised for further analysis and mapping.

Once the mean breakout orientation is calculated, the mean S_{Hmax} value can be determined by adding or subtracting 90° from the breakout orientation given it operates perpendicular to S_{hmin} on a horizontal plane. This value is then corrected for the magnetic declination at the time of the drilling to give an accurate orientation for S_{Hmax}.

1) Calculation for mean breakout (S_{hmin}) orientation based on the length-weighted azimuth:

$$L = \sum_{i=1}^{n} l_i$$

$$C = \frac{1}{L} \sum_{i=1}^{n} l_i \cos\theta_i^*$$

$$S = \frac{1}{L} \sum_{i=1}^{n} l_i \sin\theta_i^*$$

2) Calculation for number-weighted azimuth:

$$C = \frac{1}{n} \sum_{i=1}^{n} \cos\theta_i^*$$

$$S = \frac{1}{n} \sum_{i=1}^{n} \sin\theta_i^*$$

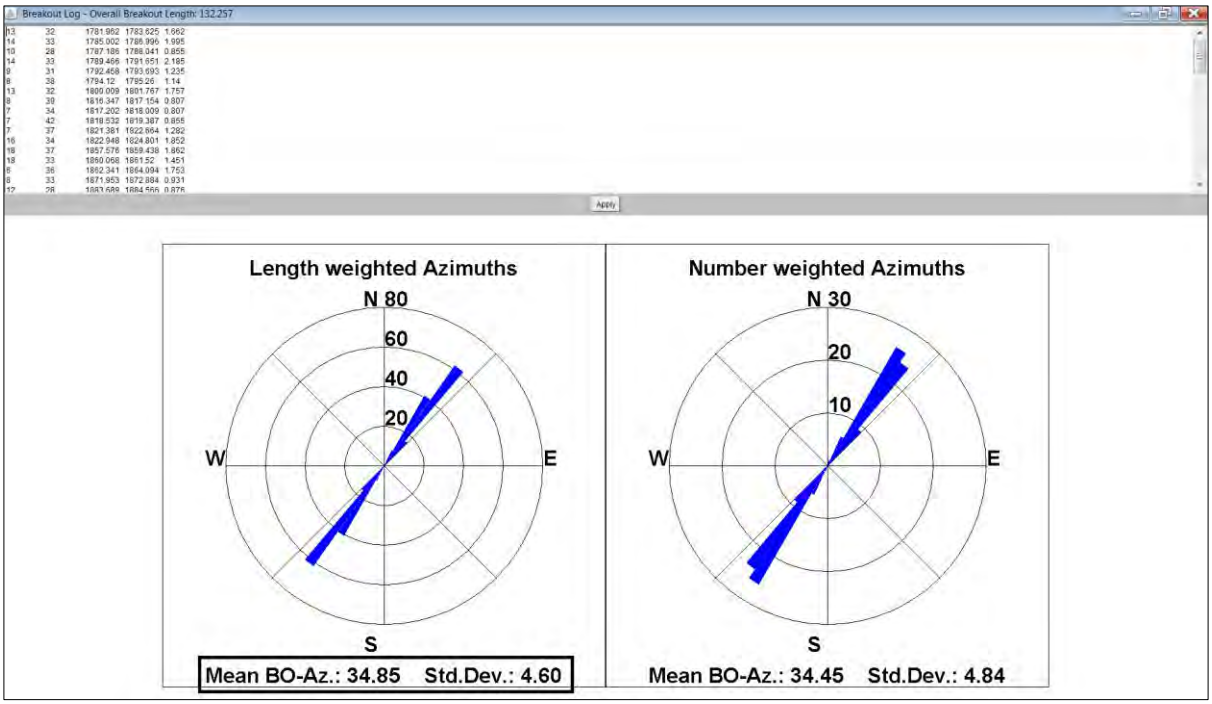

Figure 22: The final output from the FACT software for borehole A_K1 gives the total number of breakout picks, total breakout length, length- and number-weighted mean orientations (and standard deviation). The total number of breakout zones, total breakout length and standard deviation determines the quality of the data.

Smoothing of stress data

Modifiable scripts provided by the WSM team were used to smooth orientation data derived from FACT breakout analyses. The first script (Figure 23) calculates:

1. The mean S_{Hmax} orientation for a user-defined grid size.
2. The variance of the mean orientation.
3. The number of orientation data within the user defined search radius.
4. The mean distance to the data records used for determining the average.
5. The quadrants in which data points are located around the averaged grid point.

The mean orientation is calculated using the Mardia (1972) method for directional statistics (to accommodate for data spread across a spherical surface) using both distance and quality weighting.

The second script (Figure 24), filters the gridded average S_{Hmax} produced from the first script. This script allows the user to:

1. Filter the data based on minimum number of real data average per grid point.
2. Filter results based on the maximum variance for each averaged S_{Hmax}.
3. Determine the wavelength of the stress pattern – indicating the minimum search radius in which the "minimum number of data" and "maximum variance" is satisfied.

The final data is output in the form of the "mean_azi.dat" and "variance.dat" files which can be converted into simple comma-separated file for further visualisation in either the WSM or standard GIS software. The parameters chosen for data smoothing are discussed further in Chapter 4.

```
# USER SETTINGS:
#-----------------------------------------------------------------
---------------
qual_range = ['A', 'B', 'C']                                    #
used qualities
qual_weight = {'A': 1./15, 'B': 1./20, 'C': 1./25, 'D': 1./40} #
quality weight
pbe_flag = 'NO'                                                 #
exclude PBEs
srad_range = [50., 100., 200., 300., 400., 500., 600., 700.,
800., 900., 1000.]    # search radii
#srad_range = [100., 150., 250., 500., 1000.]                   #
search radii
#srad_range = [1000.]                                           #
TEST search
dist_weight_treshold = 30
delta_g = 0.30                      # grid spacing in degrees
                                    # IMPORTANT: 180/delta_g must
be integer

#-----------------------------------------------------------------
```

Figure 23: The first smoothing script utilised to generate global mean SHmax for a given grid size and search radius.

```
---------------
# USER SETTINGS
#-----------------------------------------------------------------
---------------
num_thres = 5      # DATA NUMBER THRESHOLD
var_thres = 25     # VARIANCE THRESHOLD
rad_min = 50      # smallest search radius as defined in script
meanSH2grid_1.py
qs_min = 1         # if qs=1 at least two diagonal quadrants must
contain data,
                   # for qs_min=0 if loop has no meaning as
minimum one
                   # quadrant must have data anyway
dr_max = 0.95      # maximum ratio of mean distance and search
radius
scale  = 0.15
#-----------------------------------------------------------------
```

Figure 24: The second smoothing script filters the results from the global grid created by the first script.

Presenting the data

Once all boreholes were reviewed and analysed, orientation data is tabulated and the tabulated data is formatted for entry into the WSM2008 release file for use with the smoothing scripts. Breakout rose-diagrams (S_{hmin}), produced by the FACT software, were stored and modified to indicate the S_{Hmax} orientation for each analysed borehole.

Data was also prepared as "user data" for the browser-based **C**reate **A** **S**tress **M**ap **O**nline (CASMO) software, accessible the WSM website (http://dc-app3-14.gfz-potsdam.de/pub/introduction/introduction_frame.html - last accessed: 15/02/2015), which allows the user to quickly display data in the correct WSM format and compare it with the existing catalogue.

A KML-script, also provided by the WSM project, was utilised to convert S_{Hmax} orientation data into a format for display with the widely-used Google Earth software. The orientation data can again be presented displaying the WSM-defined symbology and additional datasets can be easily overlain using basic Google Earth features.

Smoothing was done using the editable scripts described above (using the "Python" programming language) and the resultant gridded mean orientation data was visualised using the open-source QGIS software (www.qgis.com – last accessed: 15/02/2015). This allowed for additional datasets to be incorporated with the smoothed stress map for analysis and effective presentation.

CHAPTER 4: RESULTS

Data recovery, analysis and quality

Of the 131 boreholes provided by the Petroleum Agency South Africa, one borehole possessed no coordinate data, 10 boreholes had logs with insufficient parameters for FACT analysis, and 2 boreholes displayed obvious errors with the values for DEPT and P1AZ which far exceeded logical limits. These 13 logs were discarded. When plotted, the remaining 118 boreholes indicated a good spread of potential breakout data that could be obtained throughout the Orange Basin and Outeniqua sub-basins (see Figure 3 in Chapter 1). Two calliper logs provided fell within the Durban Basin on the eastern coastline and were also reviewed for completeness.

The 118 potential borehole calliper logs were processed and loaded into the FACT software to determine if they contained clear borehole breakouts. After analysis and review, only 29 boreholes were found to have breakout data of sufficient quality to be used for this project, however the available data still provided a good spatial distribution across the offshore basins of interest (Figure 25). Only the large Pletmos Sub-Basin was poorly represented with one isolated orientation data that could be used.

Using the WSM quality rankings (Table 2): the data-producing boreholes generated 9 D-quality, 14 C-quality and 6 B-quality mean breakout, and subsequently, S_{Hmax} orientations. In order to ensure robust, easily comparable results, the author followed the WSM guidelines established in Table 1 during analyses of the calliper log files. One exception was made when small breakouts between 0.5 - 1 m were present as part of a large breakout zone. Rather than select a broad zone that may contain narrow zones of excluded data, the author individually picked and recorded each segment of the breakout zone. Isolated breakouts < 1.0 m in length were not picked for analysis. Additionally, no breakout orientations were used for analysis if they occurred at less than 500 m depth (as was observed in borehole F_A2).

Conservative error limits were also retained as per WSM guidelines which reduced the overall user-picked breakout length but ensured more consistent orientation data and lower standard deviation for mean breakout orientations in most boreholes:

- **Bit-size** was set the value given in the calliper log files (if provided) or calculated from average calliper values and industry drilling standards.
- **Smaller calliper to close to bit-size** was set to 10%. This ensures that if the smaller of two calliper arms was not within range of the bit-size, the data is disregarded as this likely represents a washout feature.
- **Calliper difference limit** was set to 10% which is conservative for larger shallow-depth bit-sizes, but ensures small degrees of collapse or tool marks are not analysed as breakouts in large diameter boreholes.
- **Relative bearing +/-** was set to 15° to ensure any breakouts with an orientation within the specified range of **RB** are disregarded as this likely represents a key-seat feature.
- **Key-seat Limit** was set to 1% to ensure the above restriction was applied as soon as the well deviates from vertical.
- **Dev. Max** was set to 15% based on WSM guidelines as any further deviation from vertical is unlikely to produce breakouts generated only by horizontal compressive forces and may be influenced by "hanging wall" collapse under the influence of the vertical stress component.

The mean S_{Hmax} results were then tabulated and include all the required parameters for ranking (Table 3). The 20 breakout orientations of B- and C-quality which suitable to contribute to the current WSM catalogue are used for generating a smoothed, gridded stress map for the regions of interest. The remaining 9 D-quality S_{hmax} data are presented with the individual breakout data as they support the overall trends indicated by the higher quality data.

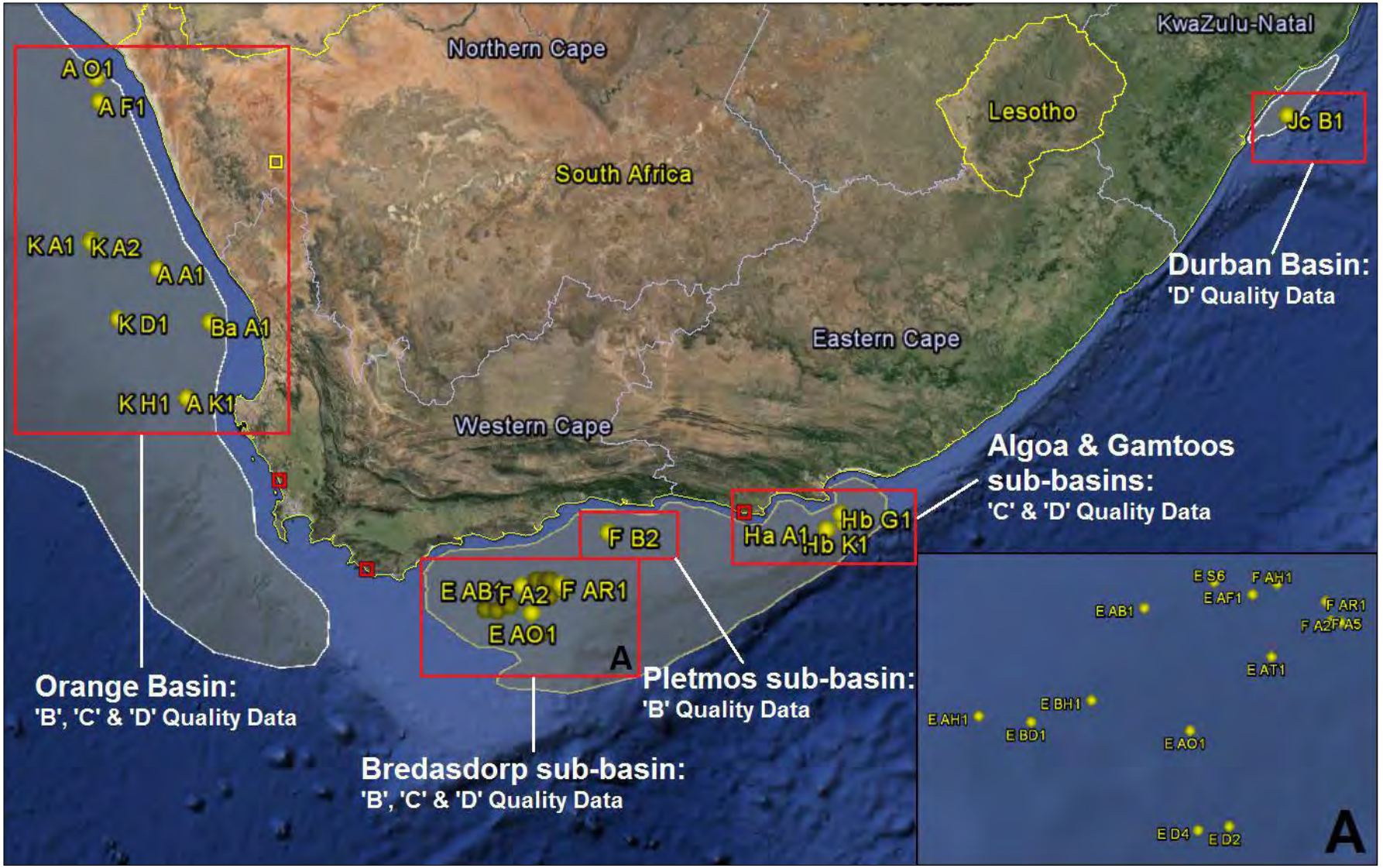

Figure 25: The location of all data producing boreholes the range of data quality obtained. Visualised in Google Earth.

Table 3: All borehole data - corrected for magnetic declination

Borehole ID	Location (Decimal Latitude	Longitude)	S_{Hmax} (length-weighted	Standard Deviation	Average Magnetic Declination	Corrected S_{Hmax}	S_{Hmax} (number-weighted	Standard Deviation	Average Magnetic Declination	Corrected S_{Hmax}	WSM Quality	Total breakout length (m)	Depth Range	Avg. Breakout Depth (m)	Picks
A_A1	-31.2195	16.92035	141.3	10.03	22	163.3	141.6	10.78	22	163.6	B	129	2,578.35 - 3,806.97	2904	89
A_F1	-29.2244	16.19956	149.2	3.4	22	171.2	149.4	3.12	22	171.4	C	33	2,231.61 - 2,846.74	2415	20
A_K1	-32.6894	17.23313	138.8	3.97	22	160.8	139.9	5.4	22	161.9	C	47	2,090.61 - 3,121.87	3348	22
A_O1	-28.9485	16.16566	157.5	1.76	22	179.5	157.6	2.06	22	179.6	D	13	1,808.23 - 4,569.52	4291	5
Ba_A1	-31.8671	17.60955	117.4	12.51	22	139.4	119.5	17.06	22	141.5	D	18	217.68 - 1,374.94	660	8
E_AB1	-34.9414	21.63773	123.5	18.04	24	147.5	116.6	26.99	24	140.6	D	53	1,846.27 - 2,957.37	2493	4
E_AF1	-34.9161	21.95487	112.6	11.57	24	136.6	107.6	11.46	24	131.6	C	83	1,392.02 - 2,883.1	1770	24
E_AH1	-35.1871	21.14363	138.7	31.02	24	162.7	129.4	25.87	24	153.4	D	44	2,706.3 - 3,728.92	3309	20
E_AO1	-35.2377	21.76164	138.3	2.12	24	162.3	137.3	2.06	24	161.3	D	27	1,394.61 - 3,356.61	3133	3
E_AT1	-35.0661	22.00594	258.1	5.95	24	282.1	263	4.64	24	287	C	94	1,498.4 - 3,381.91	1867	21
E_BD1	-35.2057	21.29701	138.7	2.36	24	162.7	138.9	5.53	24	162.9	C	76	1,494.28 - 3,247.03	1640	4
E_BH1	-35.1582	21.47533	200	2.78	24	224	199.4	2.76	24	223.4	C	53	1,291.44 - 3,357.68	1442	10
E_D2	-35.4696	21.86854	146.9	2.94	24	170.9	145.2	3.91	24	169.2	C	37	1,521.74 - 3,370.9	1706	11
E_D4	-35.477	21.77673	129.1	12.2	24	153.1	137.1	18.47	24	161.1	B	380	1,766.9 - 3,630.86	2329	13
E_S6	-34.8837	21.84366	115.2	16.86	24	139.2	110.7	19.33	24	134.7	C	80	1,694.6 - 2,901.86	2129	6
F_A2	-34.9873	22.21024	118.1	9.46	24	142.1	115.6	10.01	24	139.6	C	50	356.91 - 2,903.8	1800	9
F_A5	-34.9838	22.18312	181.7	22.16	24	205.7	190.3	15.14	24	214.3	C	192	427.65 - 2,989.91	1932	8
F_AH1	-34.8912	22.02797	142.5	33.74	24	166.5	142.5	31.61	24	166.5	D	20	1,588.78 - 2,688.33	2158	6
F_AH2	-34.8794	22.001	257.9	21.95	24	281.9	250.8	18.68	24	274.8	C	51	1,578.05 - 2,673.46	1825	11
F_AR1	-34.9367	22.16896	226.8	14.2	24	250.8	229.2	12.61	24	253.2	C	97	1,899.24 - 2,972.31	2109	12
F_B2	-34.3805	22.81015	118.7	10.23	24	142.7	123.4	12.31	24	147.4	B	122	853.85 - 2,072.88	1397	54
Ha_A1	-34.3568	25.67287	110.8	8.86	24	134.8	111.3	10.91	24	135.3	C	77	594.78 - 4,398.96	3213	28
Hb_G1	-34.1854	25.86094	123.1	18.18	24	147.1	123.8	20.68	24	147.8	D	19	792.92 - 1,736.96	1390	28
Hb_K1	-34.2838	25.90249	128.4	28.37	24	152.4	207.2	29.85	24	231.2	D	79	1,315.54 - 1,925.08	1543	15
Jc_B1	-29.5074	31.6243	136.6	4.94	20	156.6	130.2	6.51	20	150.2	D	13	2,893.08 - 3,948.18	3750	5
K_A1	-30.808	16.0157	147.9	4.34	22	169.9	147.4	4.46	22	169.4	C	38	2,129.2 - 4,818.36	2476	27
K_A2	-30.8346	16.00818	150.5	8.89	22	172.5	148.6	9.45	22	170.6	B	142	1,656.84 - 5,829.36	2520	63
K_D1	-31.7316	16.33634	146.8	8.89	22	168.8	150.6	8.09	22	172.6	B	145	1,574.25 - 4,710.79	4244	24
K_H1	-32.6894	17.23313	124.9	4.6	22	146.9	124.5	4.84	22	146.5	B	132	1,645.16 - 4,260.95	2897	68

Visualising breakout data

The first step in visualising data is to compile the borehole breakout logs derived from FACT analyses (see Figure 22 as an example). These provide a rose diagram of breakout picks indicating the overall breakout pattern for both length- and number-weighted results. They also provide the mean breakout azimuth (parallel to S_{hmin}) and standard deviation for the average picks. As described in borehole breakout theory, the mean S_{Hmax} azimuth is also displayed as it is defined as at 90° to the mean S_{hmin}.

Corrections for the magnetic declination at the time of drilling and logging are required to provide real azimuth values. As the calliper logs files possessed no time stamps, the magnetic declination values for the 12 year period in which the majority of the "Soekor" exploration wells were drilled was determined and averaged. Grid points were chosen across the basins of interest (Figure 26) and for each coordinate, the average magnetic declination was calculated from the results for the years 1980, 1984, 1988 and 1992. These values were obtained using the online "Magnetic Field Calculator" tool provided by the National Geophysical Data Centre [http://www.ngdc.noaa.gov/ - last accessed 15/02/2015], which are based in the International Geomagnetic Reference Field dataset (IGRF-12) and covers the period of drilling and logging.

These averages values were then again averaged across the whole basin as the total variation did not exceed 2° over the 12-year period indicating a constant drift direction. A single value was then used to correct S_{hmax} orientations for each basin (Table 4). All basins displayed positive (westward) magnetic declination resulting in an eastward shift of S_{hmax} values when corrected. S_{hmax} orientations were shifted by 22° E for the Orange Basin, 24° E for the Outeniqua Basin, and 20° E for the Durban Basin. The breakout orientations derived from the FACT tool are presented below for each basin and sub-basin with the calculated S_{hmax} orientation corrected for magnetic deviation.

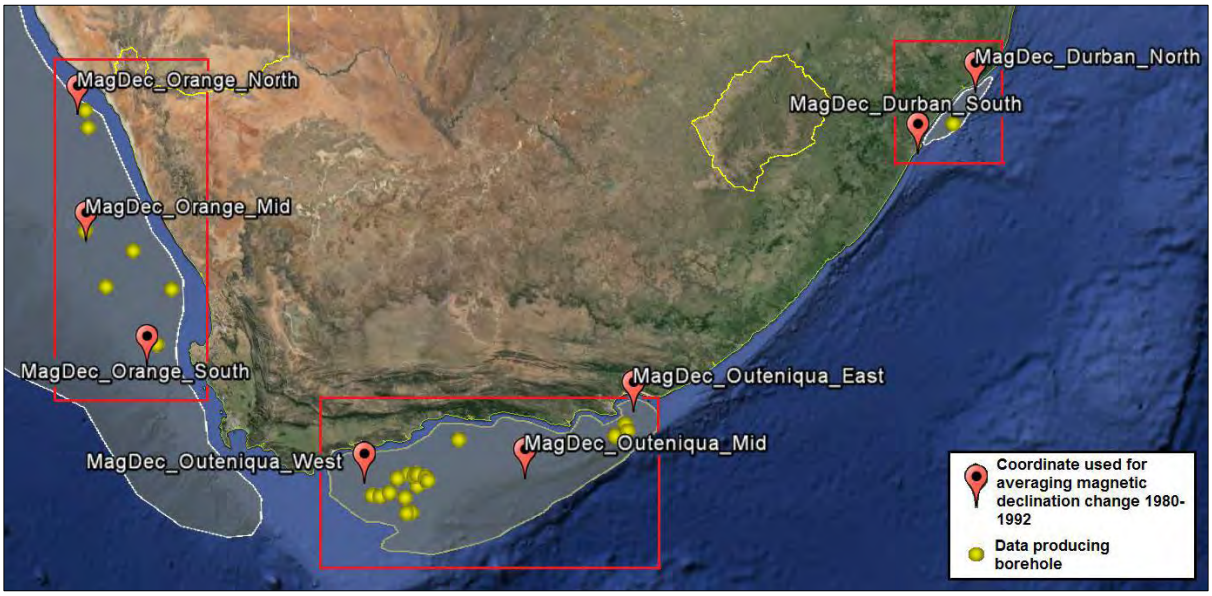

Figure 26: Coordinates chosen for averaging magnetic declination corrections for each major sedimentary basin. Values and calculation are found in Table 3 below.

Table 4: Magnetic declination corrections for each sedimentary basin. Reference points taken from Figure 25.

BASIN	REFERENCE POINT	1980	1984	1988	1992	AVERAGE	
Orange	North	21.11	20.55	20.29	20.04	20.50	
	Mid	22.26	21.76	21.57	21.42	21.75	
	South	23.1	22.69	22.61	22.59	22.75	
						21.67	**Basin Average**
						22	**Rounded Correction**
Outeniqua	West	23.86	23.66	23.81	24.09	23.86	
	Mid	24.04	23.96	24.25	24.68	24.23	
	East	23.56	23.52	23.86	24.36	23.83	
						23.97	**Basin Average**
						24	**Rounded Correction**
Durban	North	20.07	20.69	21.06	21.6	20.86	
	South	19.82	19.81	20.17	20.71	20.13	
						20.49	**Basin Average**
						20	**Rounded Correction**

Breakout results for the Orange Basin

Analysis of 20 boreholes from the Orange Basin produced 9 calliper logs with usable breakout data. This breakout orientation data includes of 4 "B", 3 "C" and 2 "D" quality results using the WSM guidelines seen in Table 2. The final S_{Hmax} orientation presented below has been corrected for the magnetic declination and does not appear perpendicular to the average breakout data. The magnetic declination correction for the Orange Basin is 22° eastwards (Table 4).

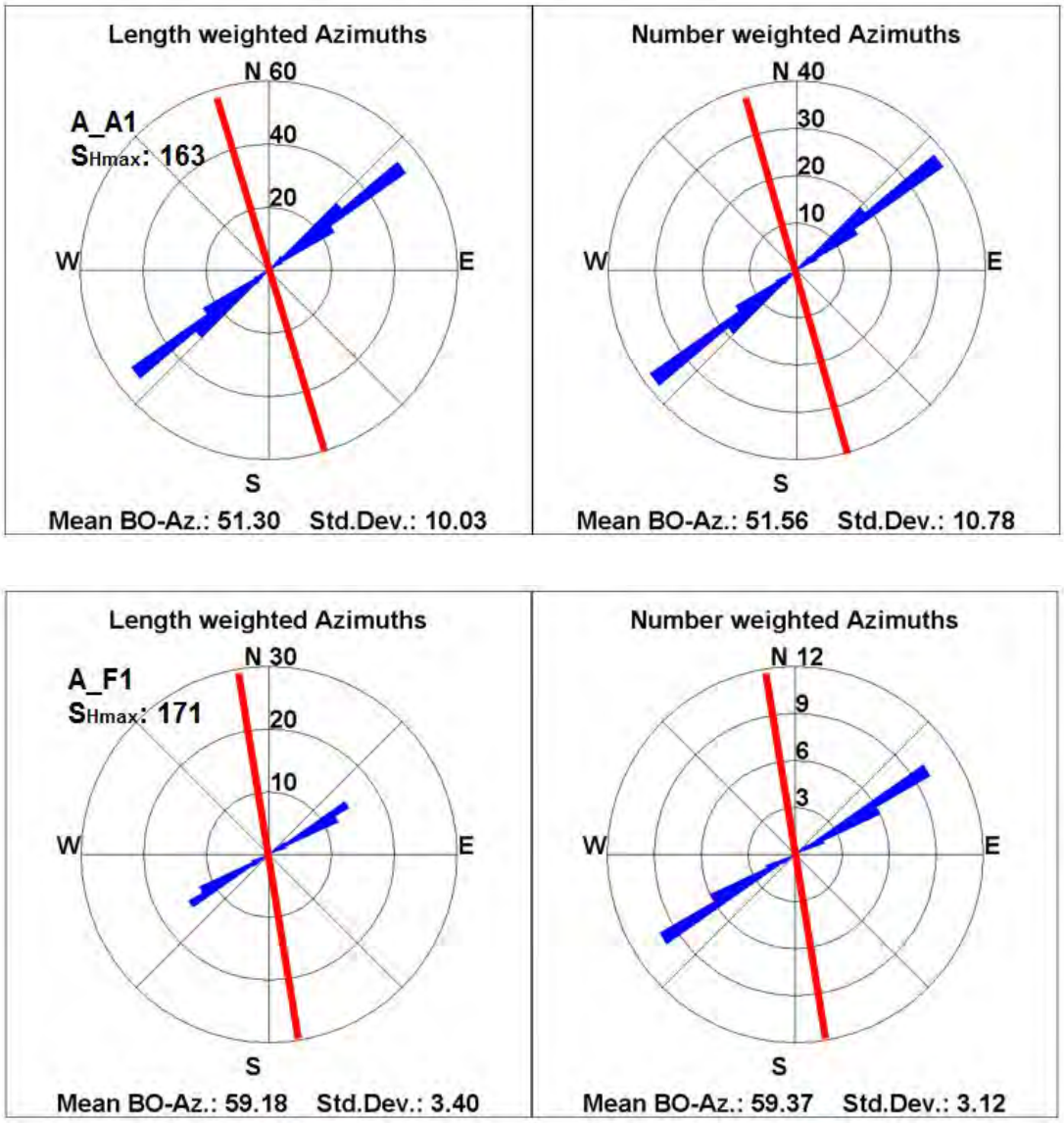

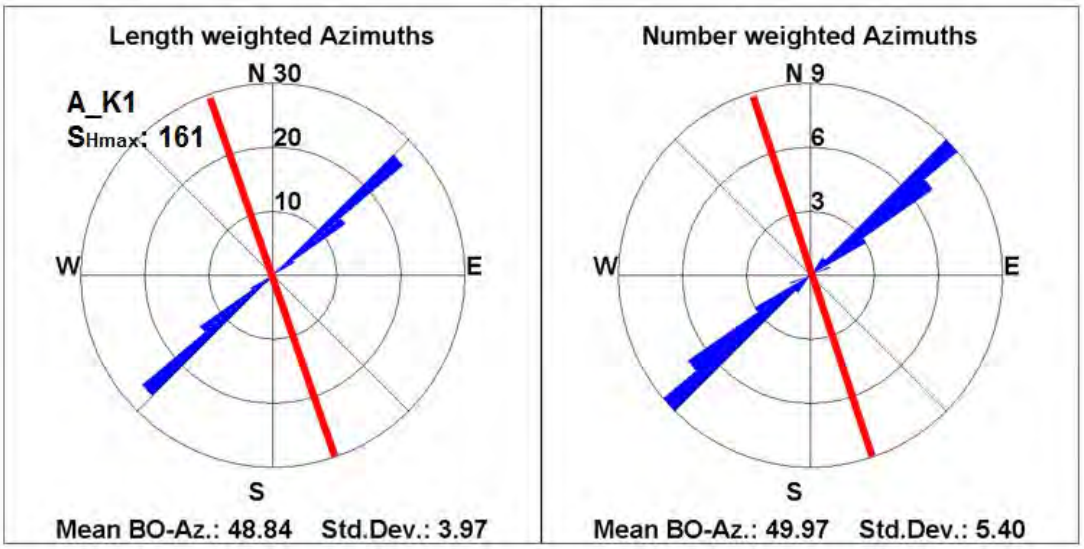
Length weighted Azimuths
A_K1
SHmax: 161
N 30
20
10
W
E
S
Mean BO-Az.: 48.84 Std.Dev.: 3.97
Number weighted Azimuths
N 9
6
3
W
E
S
Mean BO-Az.: 49.97 Std.Dev.: 5.40

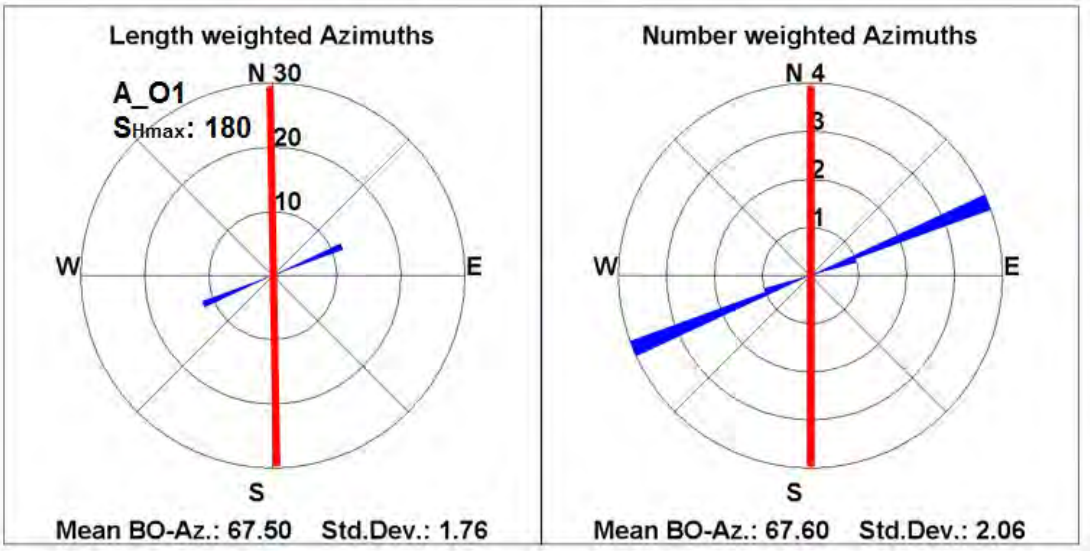
Length weighted Azimuths
A_O1
SHmax: 180
N 30
20
10
W
E
S
Mean BO-Az.: 67.50 Std.Dev.: 1.76
Number weighted Azimuths
N 4
3
2
1
W
E
S
Mean BO-Az.: 67.60 Std.Dev.: 2.06

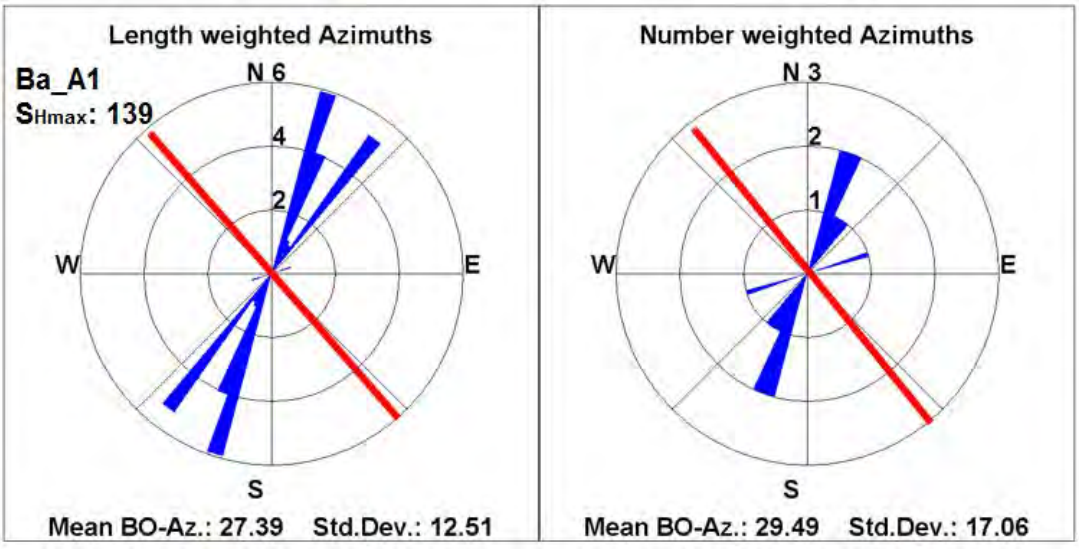
Length weighted Azimuths
Ba_A1
SHmax: 139
N 6
4
2
W
E
S
Mean BO-Az.: 27.39 Std.Dev.: 12.51
Number weighted Azimuths
N 3
2
1
W
E
S
Mean BO-Az.: 29.49 Std.Dev.: 17.06

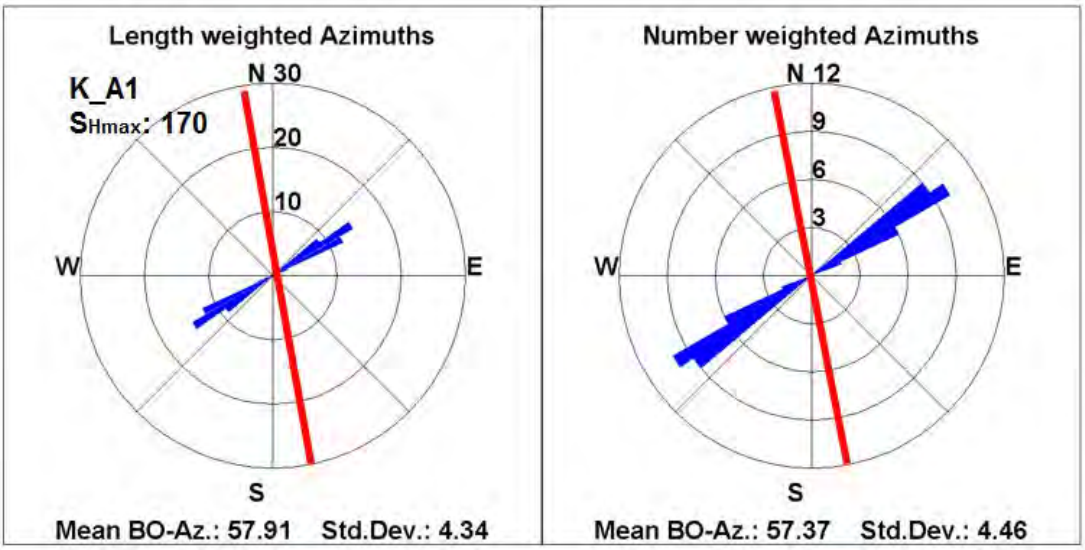
Length weighted Azimuths
K_A1
SHmax: 170
N 30
20
10
W
E
S
Mean BO-Az.: 57.91 Std.Dev.: 4.34
Number weighted Azimuths
N 12
9
6
3
W
E
S
Mean BO-Az.: 57.37 Std.Dev.: 4.46

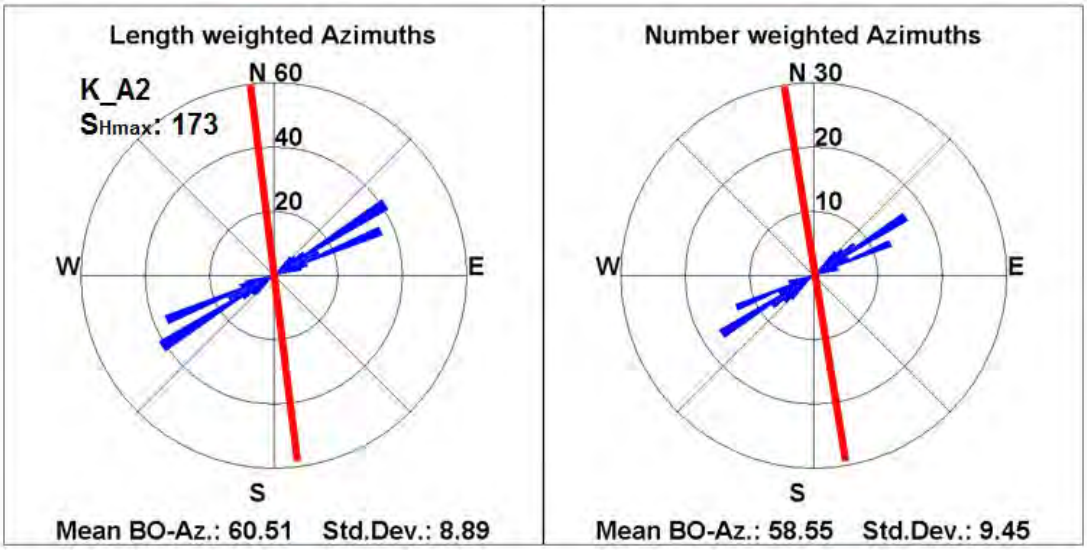
Length weighted Azimuths
K_A2
SHmax: 173
N 60
40
20
W
E
S
Mean BO-Az.: 60.51 Std.Dev.: 8.89
Number weighted Azimuths
N 30
20
10
W
E
S
Mean BO-Az.: 58.55 Std.Dev.: 9.45

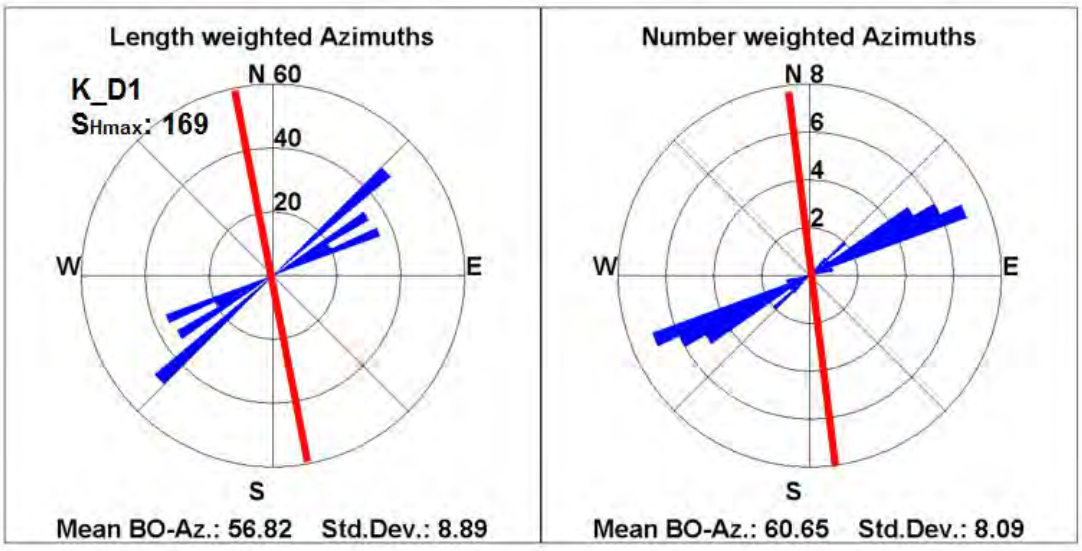
Length weighted Azimuths
K_D1
SHmax: 169
N 60
40
20
W
E
S
Mean BO-Az.: 56.82 Std.Dev.: 8.89
Number weighted Azimuths
N 8
6
4
2
W
E
S
Mean BO-Az.: 60.65 Std.Dev.: 8.09

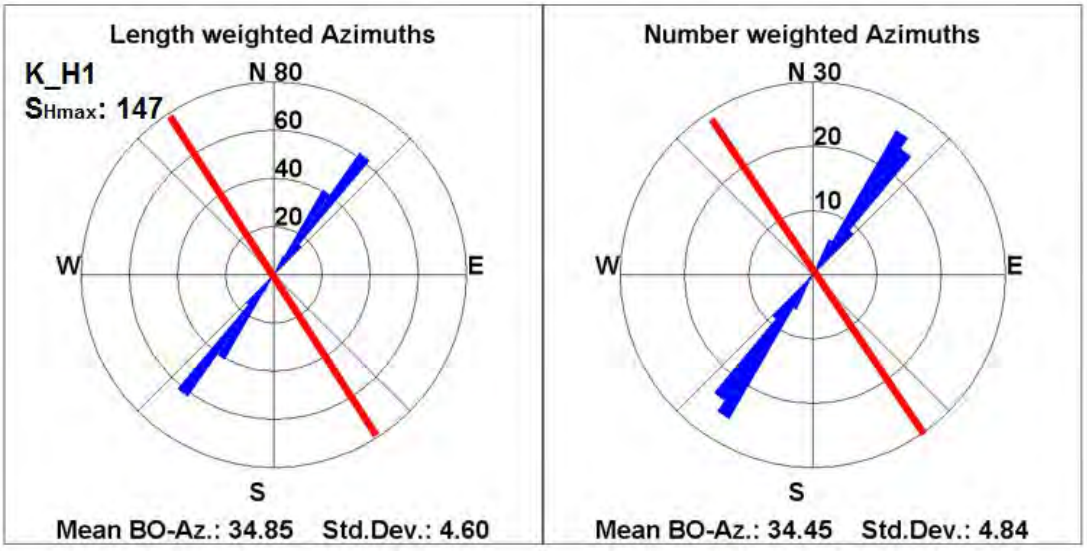

Breakout results for the Bredasdorp sub-basin

This sub-basin displayed the highest degree of hydrocarbon exploration and a total 74 boreholes were available analysed. Analysis of these calliper logs produced 15 breakout orientations which includes 1 "B", 10 "C" and 4 "D" quality data. The results from this basin show the greatest variation of S_{Hmax} orientations contrasting with the consistency seen in other basins. The magnetic declination correction for the Outeniqua Basin is 24° eastwards (Table 4).

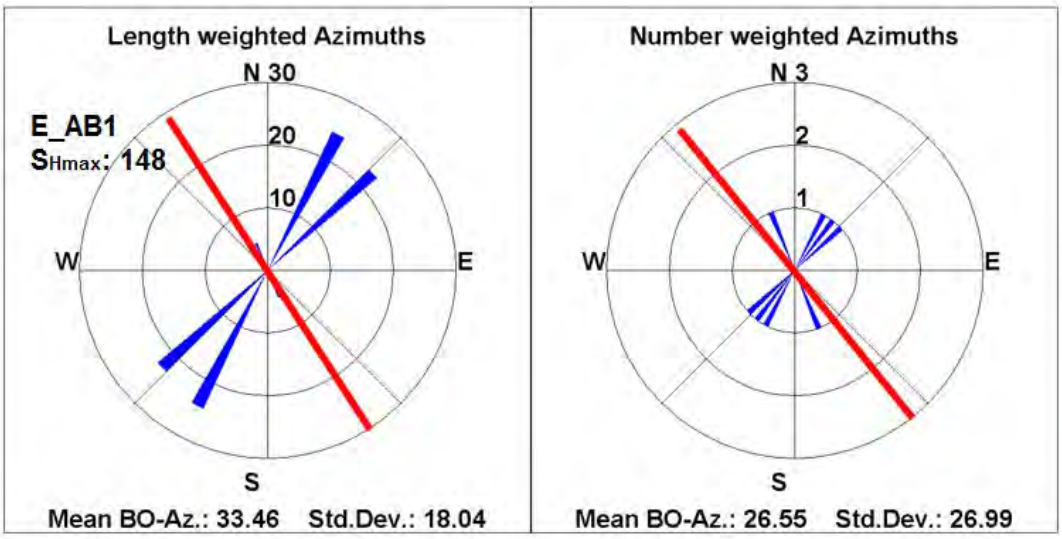

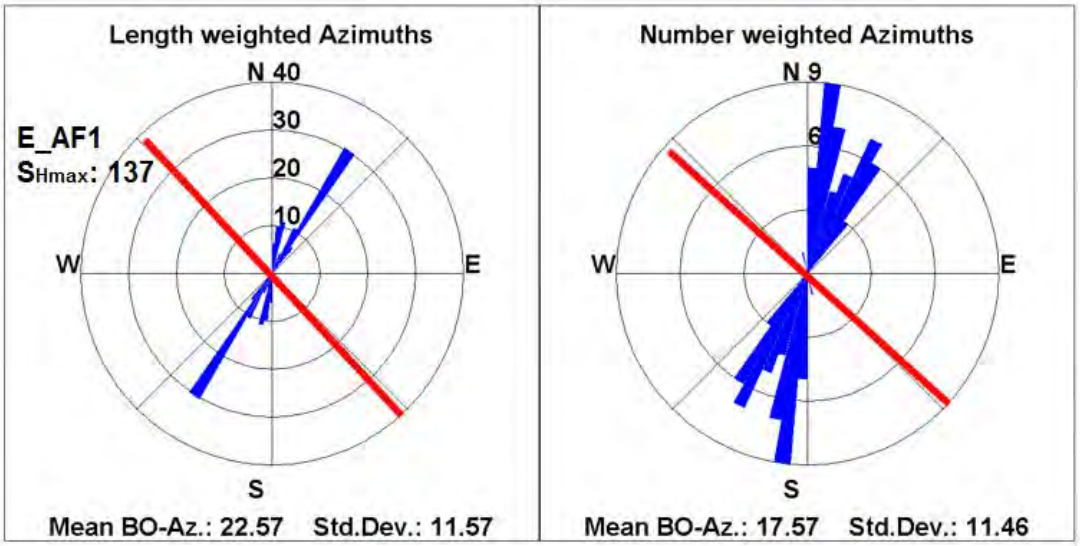
Length weighted Azimuths
N 40
30
20
10
E_AF1
SHmax: 137
W
E
S
Mean BO-Az.: 22.57 Std.Dev.: 11.57
Number weighted Azimuths
N 9
6
W
E
S
Mean BO-Az.: 17.57 Std.Dev.: 11.46

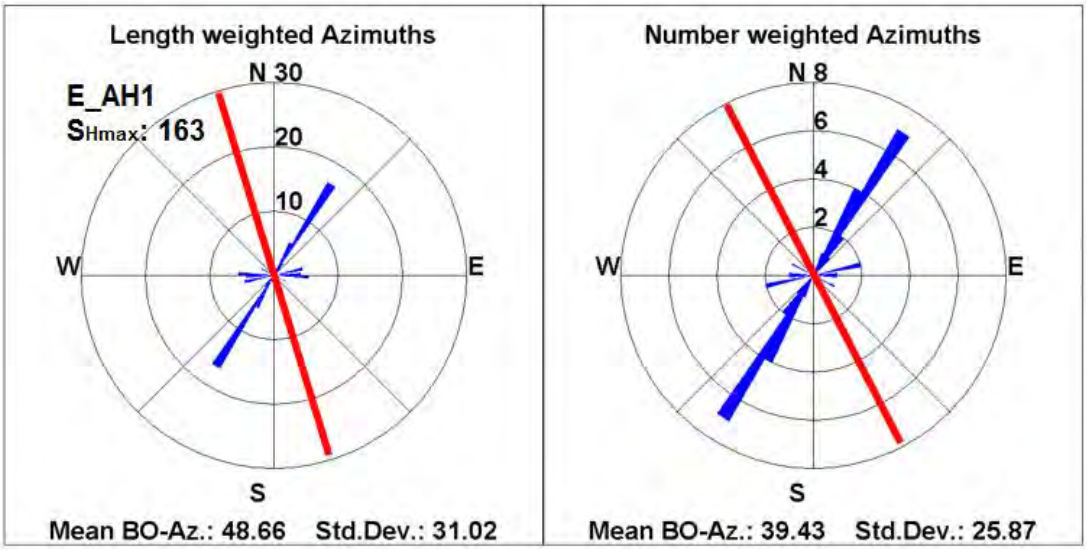
Length weighted Azimuths
N 30
20
10
E_AH1
SHmax: 163
W
E
S
Mean BO-Az.: 48.66 Std.Dev.: 31.02
Number weighted Azimuths
N 8
6
4
2
W
E
S
Mean BO-Az.: 39.43 Std.Dev.: 25.87

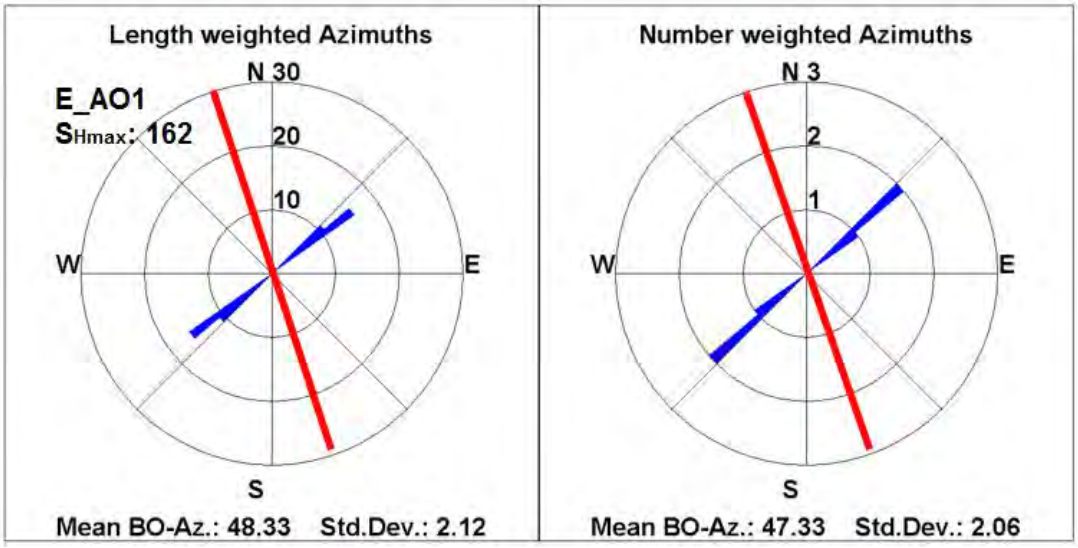
Length weighted Azimuths
N 30
20
10
E_AO1
SHmax: 162
W
E
S
Mean BO-Az.: 48.33 Std.Dev.: 2.12
Number weighted Azimuths
N 3
2
1
W
E
S
Mean BO-Az.: 47.33 Std.Dev.: 2.06

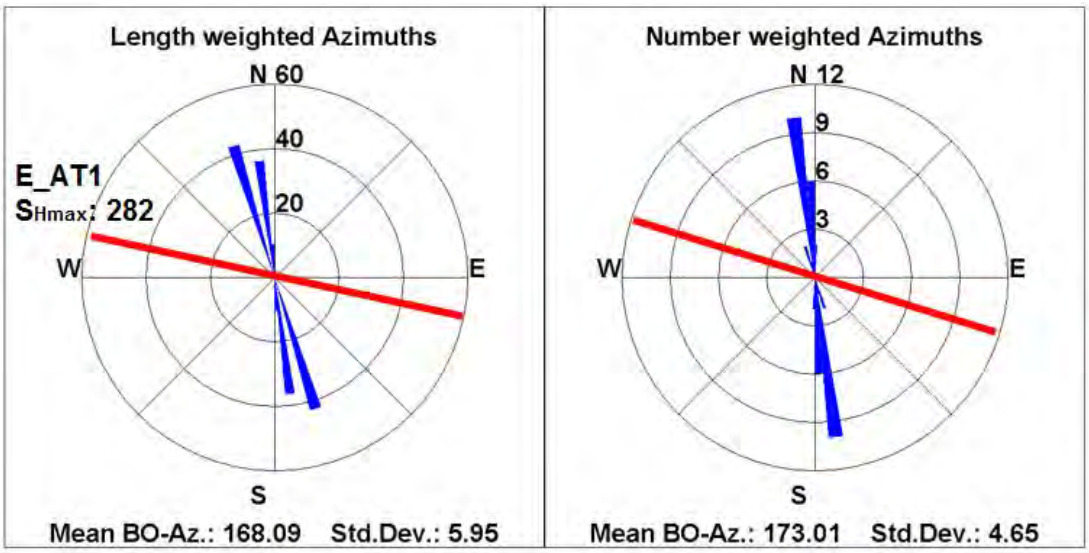
Length weighted Azimuths
N 60
40
20
E_AT1
SHmax: 282
W
E
S
Mean BO-Az.: 168.09 Std.Dev.: 5.95
Number weighted Azimuths
N 12
9
6
3
W
E
S
Mean BO-Az.: 173.01 Std.Dev.: 4.65

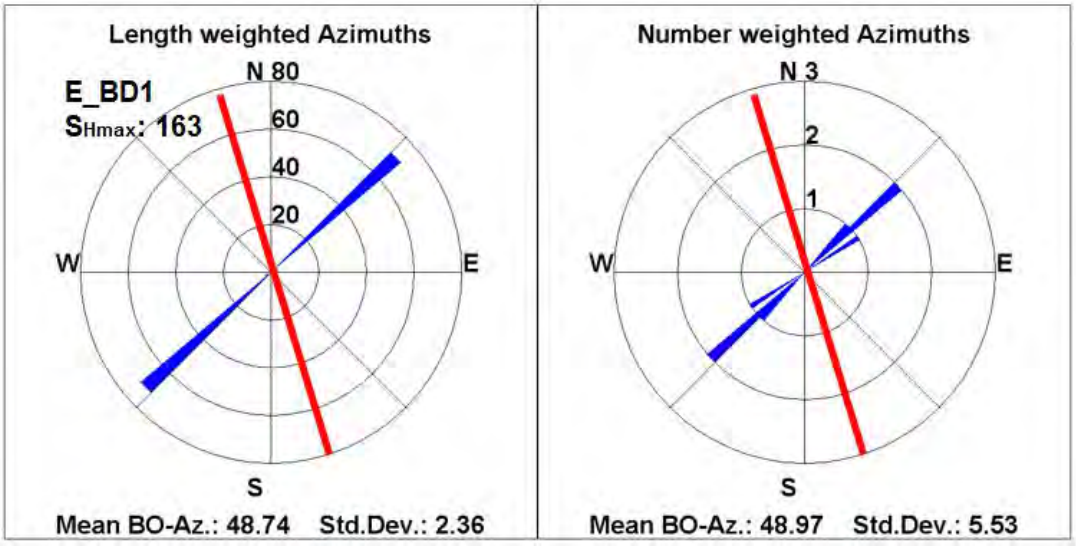
Length weighted Azimuths
N 80
60
40
20
E_BD1
SHmax: 163
W
E
S
Mean BO-Az.: 48.74 Std.Dev.: 2.36
Number weighted Azimuths
N 3
2
1
W
E
S
Mean BO-Az.: 48.97 Std.Dev.: 5.53

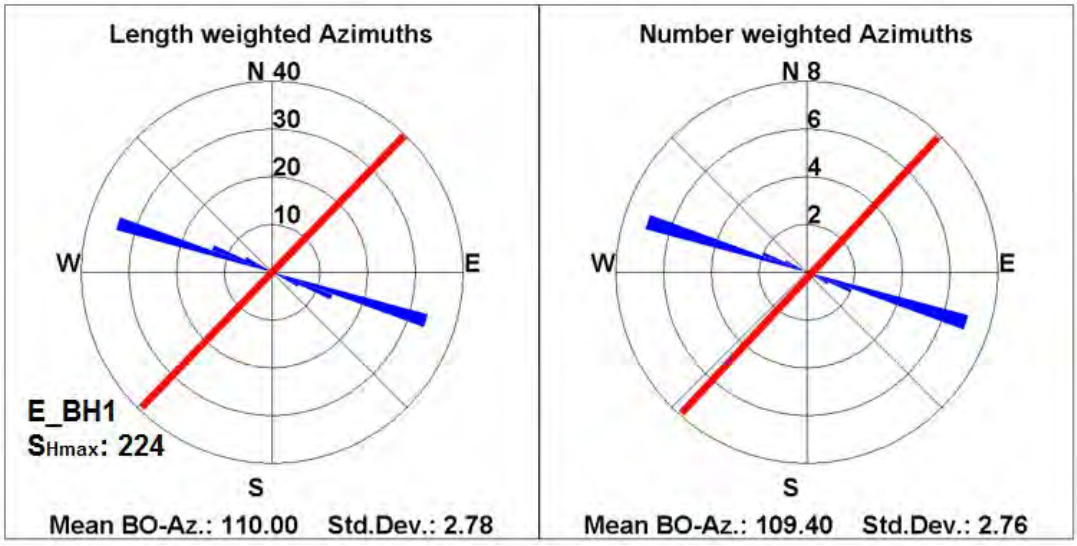
Length weighted Azimuths
N 40
30
20
10
W
E
E_BH1
SHmax: 224
S
Mean BO-Az.: 110.00 Std.Dev.: 2.78
Number weighted Azimuths
N 8
6
4
2
W
E
S
Mean BO-Az.: 109.40 Std.Dev.: 2.76

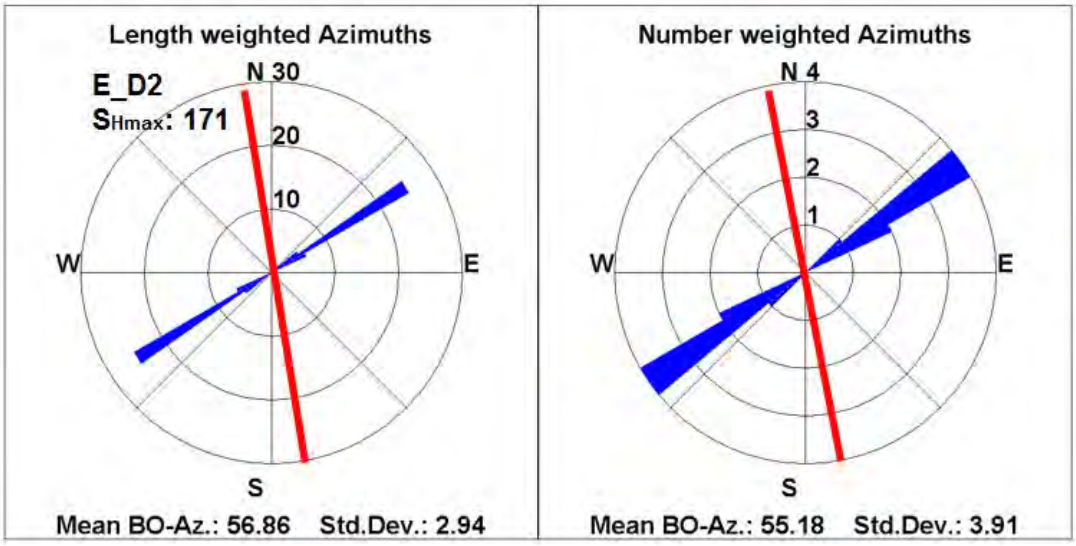
Length weighted Azimuths
E_D2
SHmax: 171
N 30
20
10
W
E
S
Mean BO-Az.: 56.86 Std.Dev.: 2.94
Number weighted Azimuths
N 4
3
2
1
W
E
S
Mean BO-Az.: 55.18 Std.Dev.: 3.91

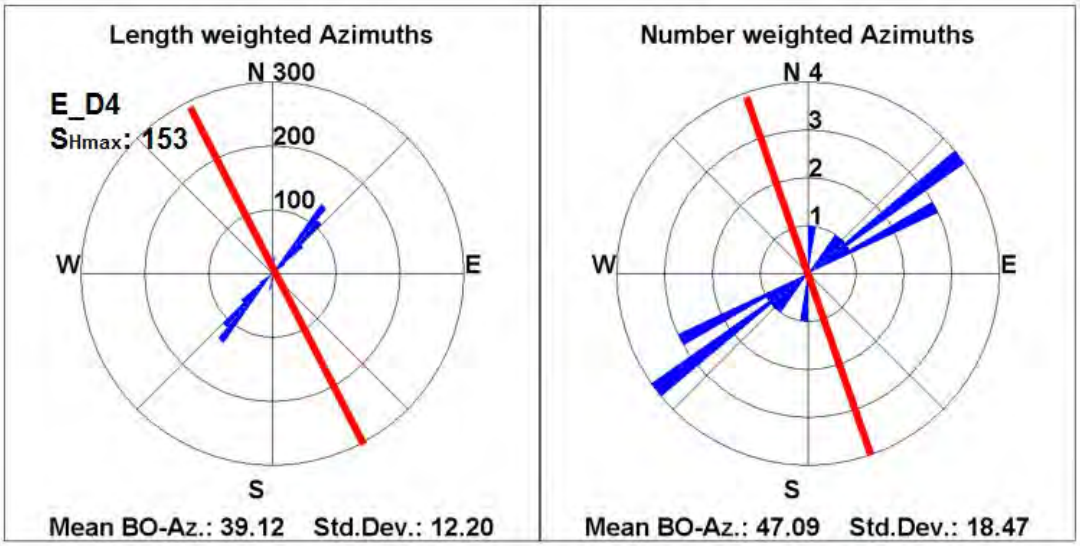
Length weighted Azimuths
E_D4
SHmax: 153
N 300
200
100
W
E
S
Mean BO-Az.: 39.12 Std.Dev.: 12.20
Number weighted Azimuths
N 4
3
2
1
W
E
S
Mean BO-Az.: 47.09 Std.Dev.: 18.47

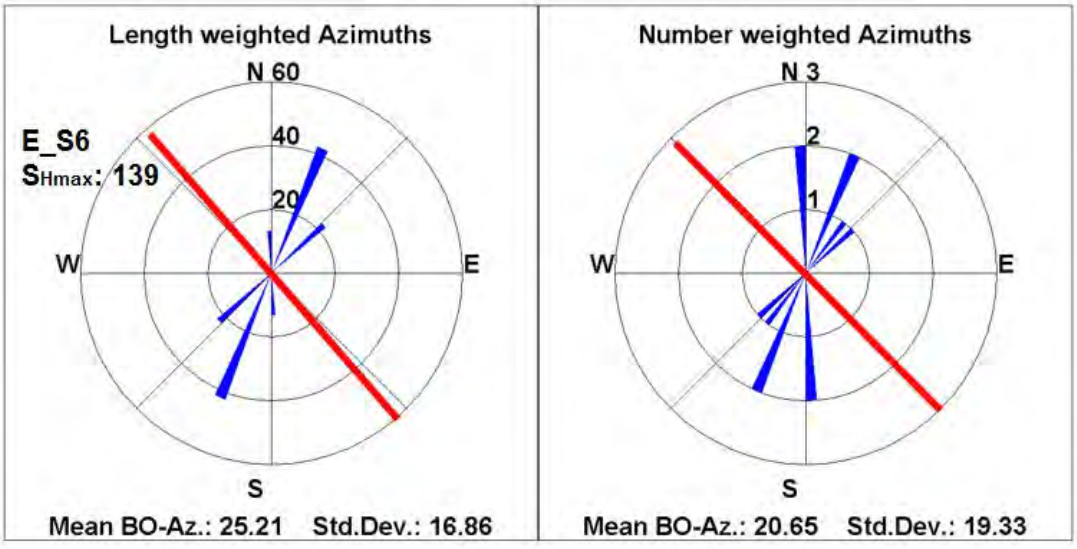
Length weighted Azimuths
E_S6
SHmax: 139
N 60
40
20
W
E
S
Mean BO-Az.: 25.21 Std.Dev.: 16.86
Number weighted Azimuths
N 3
2
1
W
E
S
Mean BO-Az.: 20.65 Std.Dev.: 19.33

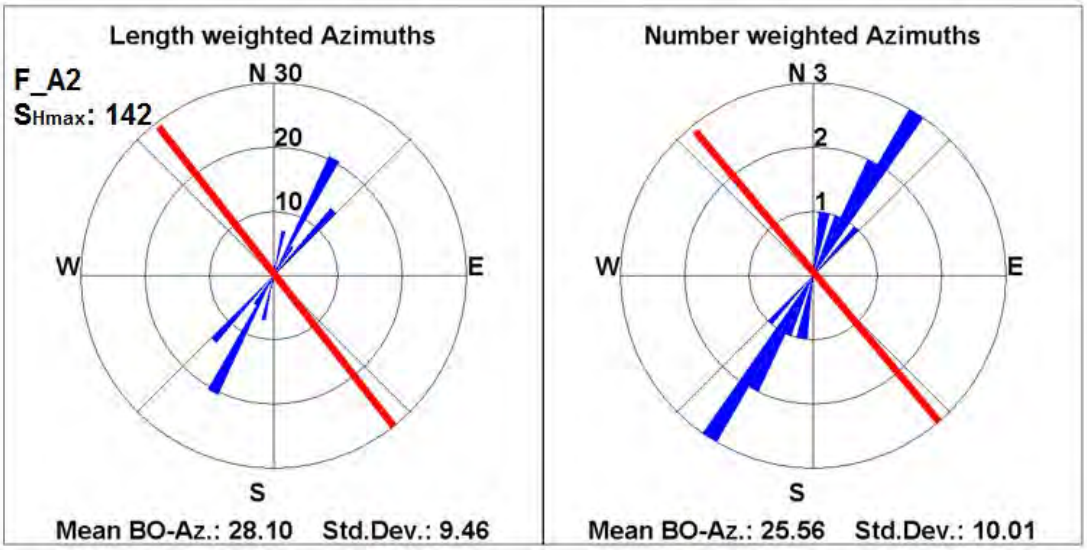
Length weighted Azimuths
F_A2
SHmax: 142
N 30
20
10
W
E
S
Mean BO-Az.: 28.10 Std.Dev.: 9.46
Number weighted Azimuths
N 3
2
1
W
E
S
Mean BO-Az.: 25.56 Std.Dev.: 10.01

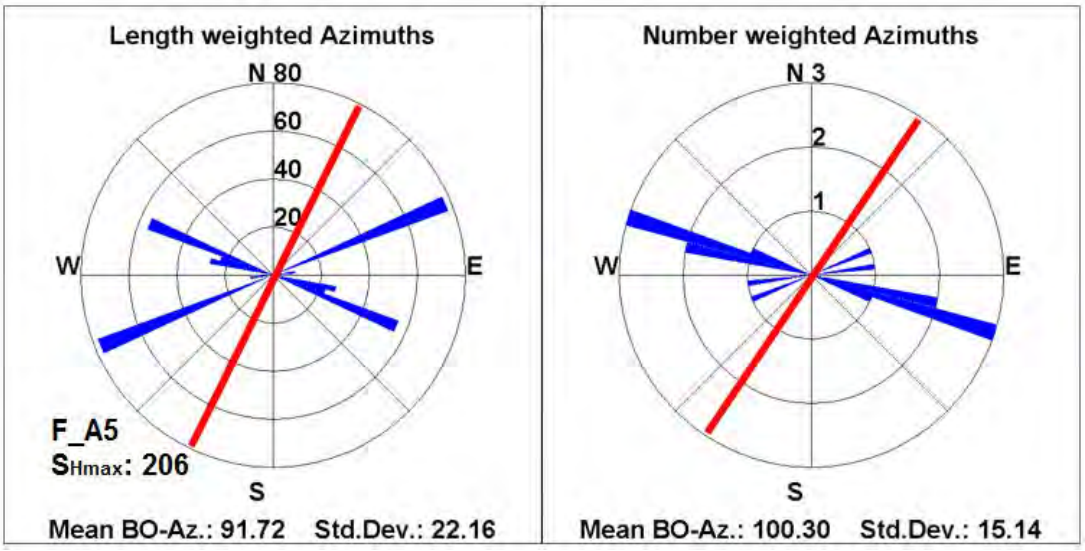
Length weighted Azimuths
N 80
60
40
20
W
E
F_A5
SHmax: 206
S
Mean BO-Az.: 91.72 Std.Dev.: 22.16
Number weighted Azimuths
N 3
2
1
W
E
S
Mean BO-Az.: 100.30 Std.Dev.: 15.14

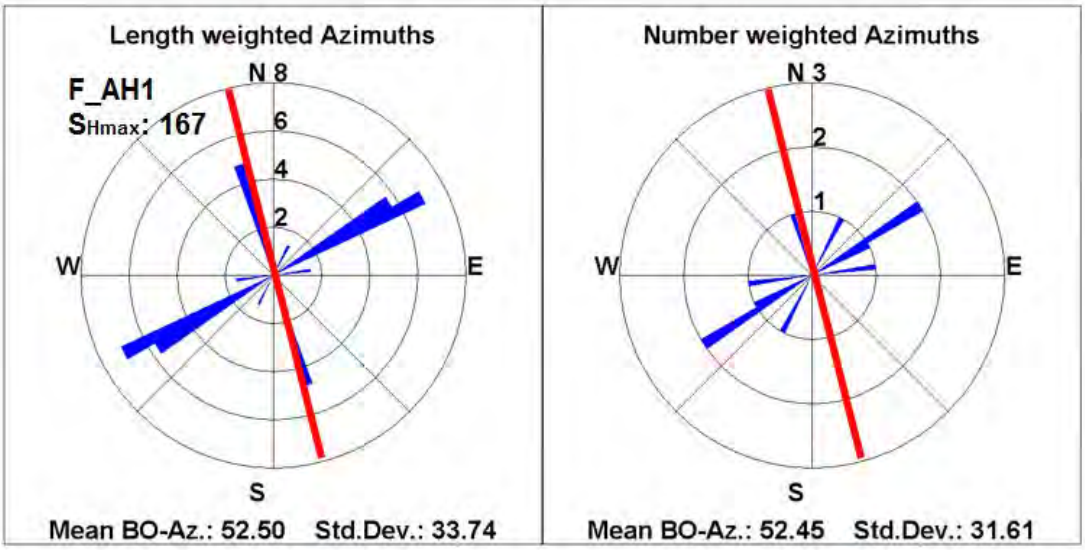
Length weighted Azimuths
F_AH1
SHmax: 167
N 8
6
4
2
W
E
S
Mean BO-Az.: 52.50 Std.Dev.: 33.74
Number weighted Azimuths
N 3
2
1
W
E
S
Mean BO-Az.: 52.45 Std.Dev.: 31.61

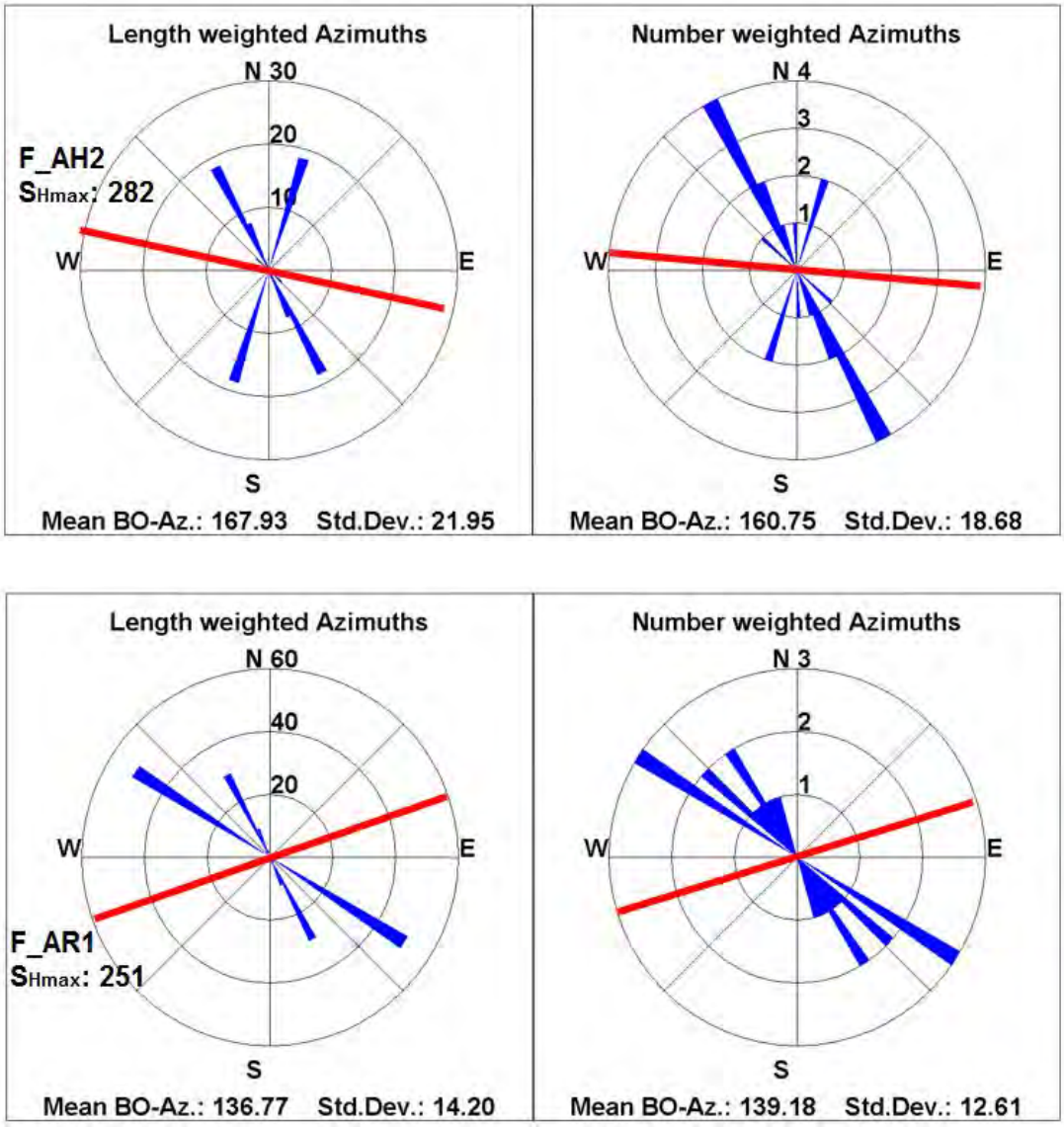

Breakout results for the Pletmos sub-basin

The Pletmos sub-basin produced only one usable log from 15 calliper logs provided. It is the least represented sub-basin given the total area of the sub-basin. The single result was of "B" quality and suitable for incorporation into the WSM records and usable with the smoothing scripts.

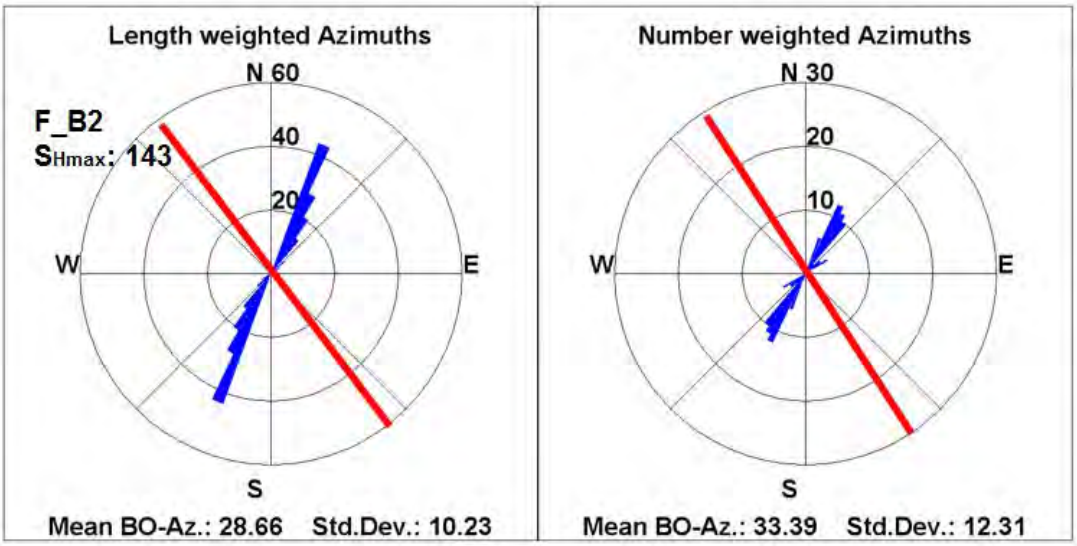

Breakout results for the Gamtoos sub-basin

The Gamtoos sub-basin produced only 1 calliper log with a usable breakout orientation from 4 available boreholes. This result was of "C" quality so is suitable for inclusion in the WSM database and is used in the smoothing scripts.

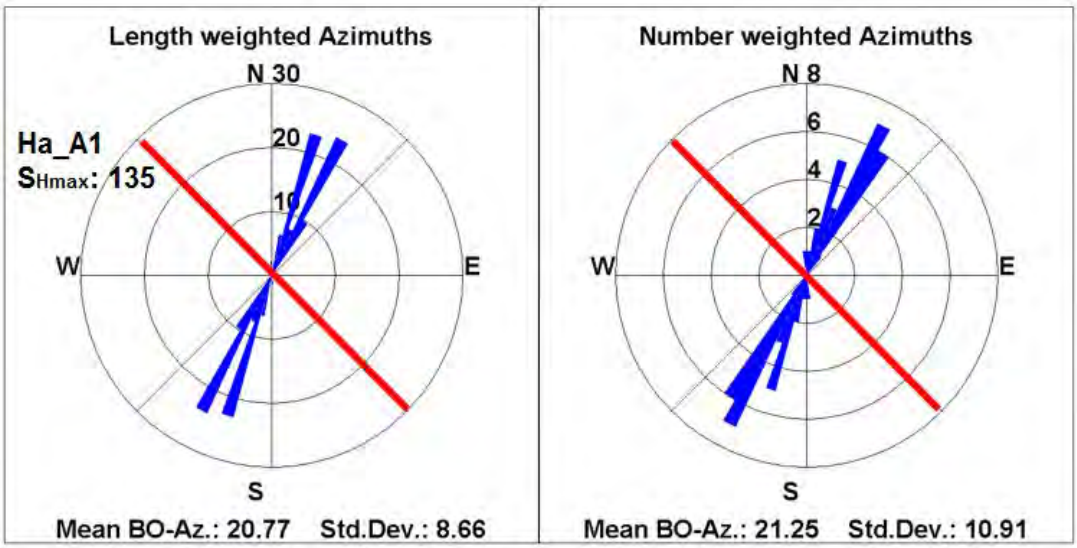

Breakout results for the Algoa sub-basin

The Algoa sub-basin produced 2 calliper logs with usable breakout orientations from 10 available boreholes. Both results are of "D" quality and support the general trend seen across all basins but are not of sufficient quality to be included in the WSM database, nor for use in the smoothing scripts.

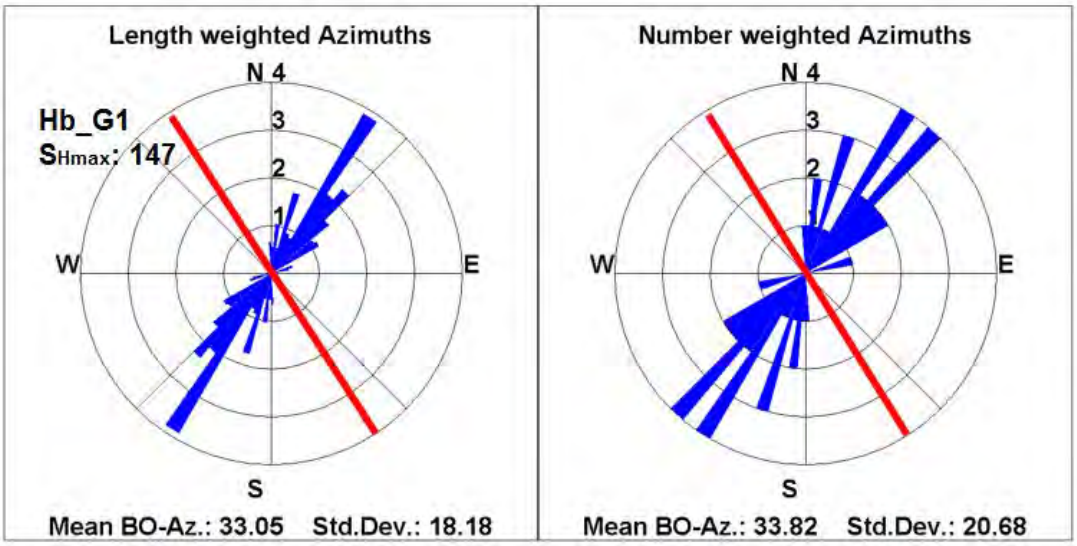

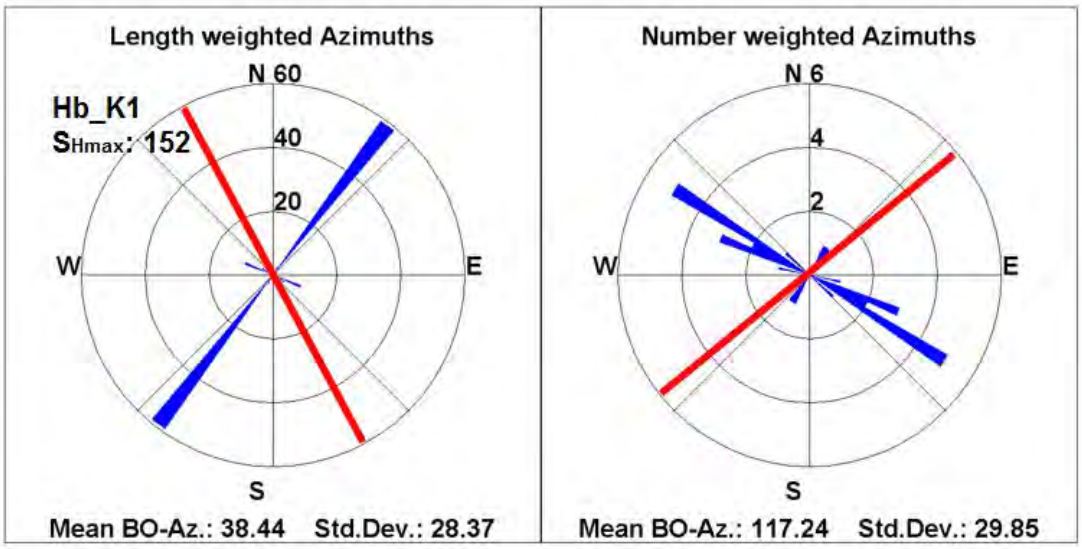

Breakout results for the Durban Basin

Only two boreholes were provided for the relatively small Durban Basin, one of which had provided breakout orientation data of "D" quality. This isolated data is not usable in the WSM database or for smoothing scripts but is presented as it conforms to the general trend seen across all basins. The magnetic declination correction for the Durban Basin is 20° eastwards (Table 4).

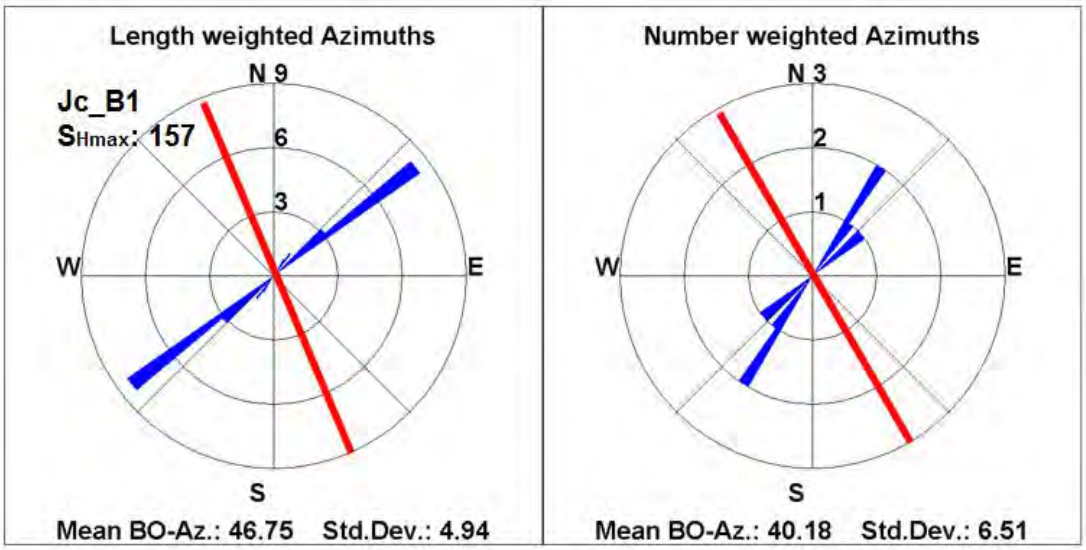

Boreholes producing no usable data

Calliper logs with no usable breakout data typically appeared to be washed out with both calliper diameters far exceeding the maximum specified bit-size and many calliper logs revealed poor calliper rotation, with the tool often failing to fully rotate over 100's of meters and showing no clear pattern of entering or exiting potential breakout zones. A full log of all boreholes analysed and descriptions for accepted and rejected logs is presented in the appendix.

The complete table of data for all 29 data-producing boreholes with comments can also be found in the Appendix and contains both the length-weighted S_{Hmax} orientations and the required parameters for quality ranking (overall breakout length, standard deviation of the breakout orientation and the number of breakout zones/picks). These data are suitable for submission to the WSM catalogue and use smoothing scripts to generate a regional stress field map.

CHAPTER 5: DISCUSSION

Usefulness of the borehole breakout technique

FACT analysis of 131 borehole calliper logs produced 29 with usable breakout data, a 22% recovery rate for extracting usable data. Of these, only 20 were of sufficient quality (A - C) to contribute to the WSM database and for use in the smoothing scripts to generate gridded regional stress field maps which represents a 15% recovery rate. The overall success rate is low for identifying usable breakout orientations and determining S_{Hmax}, but given the infrequent seismicity in the region and currently limited catalogue of reliable stress indicators, borehole breakouts still provide the best indicators of the horizontal compressive stress orientation given South Africa's extensive offshore basins and available boreholes related to previous and current hydrocarbon exploration. The other alternative sources of stress information which are currently represented in the WSM catalogue (see Figure 2) are *in situ* measurements, such as over-coring data and hydraulic fracturing, taken during mining and excavation operations (Stacey and Wesseloo, 1998). This data is generally considered less reliable as it is more sensitive to local conditions such as excavation damage to the material, high porosity rocks and anisotropic strength changes layered geological strata (Zang and Stephansson, 2010).

In this project, lithology and structural data was not provided and had to be inferred by projecting study boreholes to the closest available profile line as seen in Figures 8, 10 and 12. Amadei and Stephansson (1997) note variation in the orientation of S_{Hmax} over depth has been observed in previous studies. This "stress decoupling" has been observed in structurally complex regions (such as major faults and shears zones), regions of densely-layered geology (volcanic flows) and across evaporite layers. On the other hand, numerous studies have also shown great consistency from depths near surface to 5000 m such as in Jurassic- to Miocene-age sediments in eastern Canada (Amadei & Stephansson, 1997). In this project, rotation was only seen in regions of poor calliper rotation, consistant with the direction of rotation, and excluded. S_{Hmax} results were generally consistent over large depths in the boreholes analysed, including those which displayed orientation inconsistent with the average trend. Deviation from the average trend was almost always perpendicular to the S_{hmin} and appeared as narrow features, most likely drilling induced fractures which would be expected to be parallel to the S_{Hmax}.

Many of the boreholes analysed display washed-out conditions, mechanical failure of the calliper tool and output errors from the logging software. Obtaining both numerous and high quality borehole breakout results requires a large sample size, most common in regions of extensive hydrocarbon exploration, unless the drilling project is specifically designed for the purpose of generating calliper logs for breakout analysis. Boreholes need to be vertical to sub-vertical, which is not always possible when targeting hydrocarbon reservoirs and at least 4-arm calliper log data is needed. Additionally a large total sample size is needed to ensure a good spatial distribution of results and the ability to regions in which local changes in S_{Hmax} results can be observed. The technique used in this project has shown the potential to provide a spread of good-quality data but when utilising exploration industry logs, it is not guaranteed to provide data for each borehole.

When the new data is data plotted with the WSM 2008 catalogue using the CASMO tool, it indicates a considerable improvement on both data quality and density when contrasted with the original database, presented in Figure 3. The data also appears relatively consistent with the current catalogue (Figure 27).

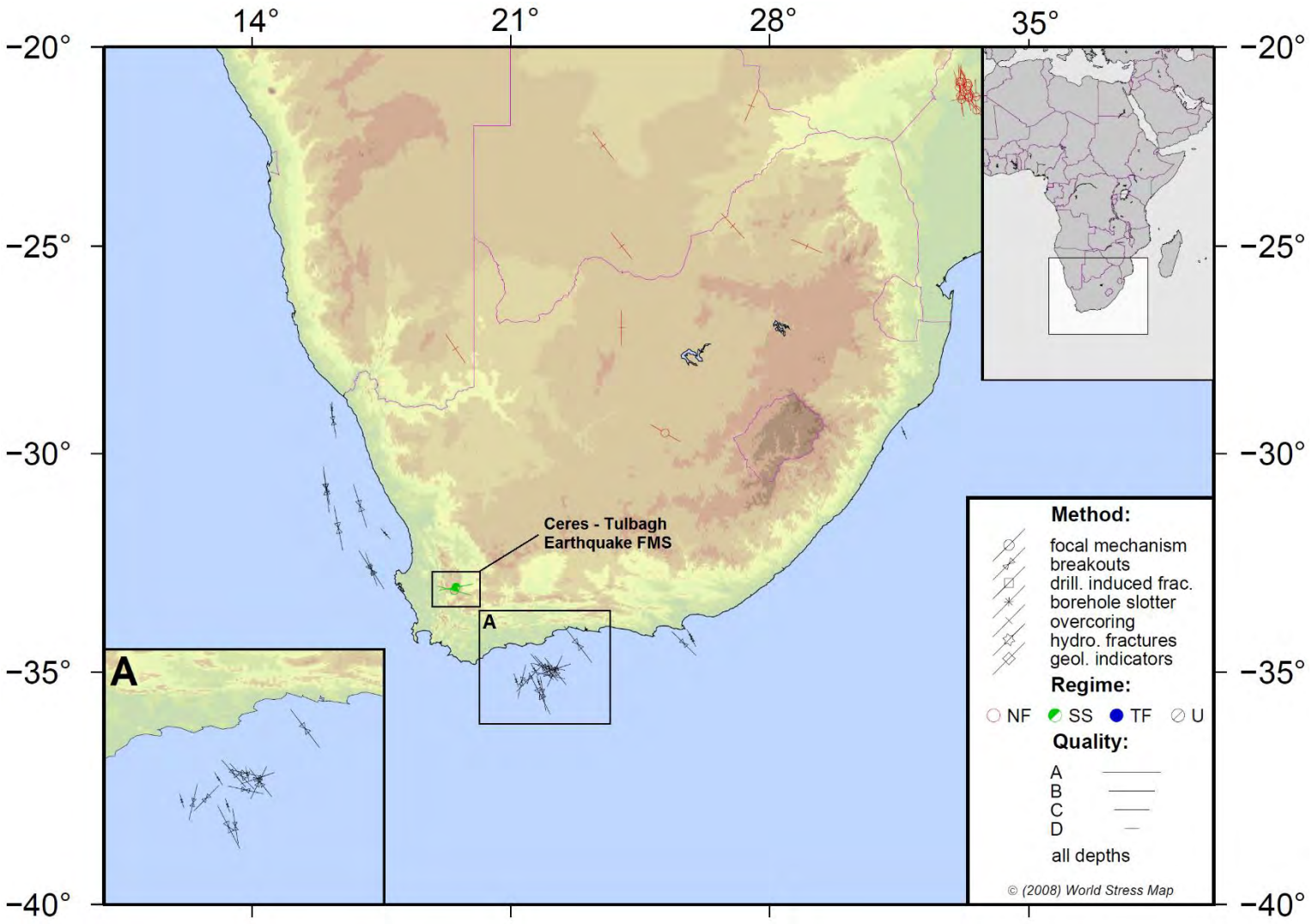

Figure 27: M.Sc. project data combined the WSM 2008 release, displayed using the CASMO tool. The data provides a spread of B , C and D-quality, length-weighted S_{Hmax} orienatations for the Orange and Outeniqua Basins, the majority of which show a NNW-SSE S_{Hmax} however data for the Outeniqua sub-basin is highly variable.

Distribution of data and regional trends

Compiling all the available data from both the FACT analysis and existing WSM 2008 release into Google Earths indicate the overall S_{Hmax} orientation for South Africa ranges from E-W to N-S but most consistently trends NNE (Figure 28).

The spatial distribution of the new data provides good cover of the Orange Basin and Outeniqua sub-basins with a range of data quality whereas only a single "D"-quality orientation was determined for the Durban Basin which still leaves the eastern half of the country with extremely limited stress orientation data. However, the western and southern coastlines which are of most interest as they currently host South Africa's only NPP and proposed nuclear sites, are partially represented in this study. Nevertheless, the data may provide an approximation of the contemporary stress field which may be of value to future safety case studies for these sites. Furthermore, the high variability in some regions (Figure 28 Inset A) indicate the need for further studies to provide reliable, onshore stress indicators for each site.

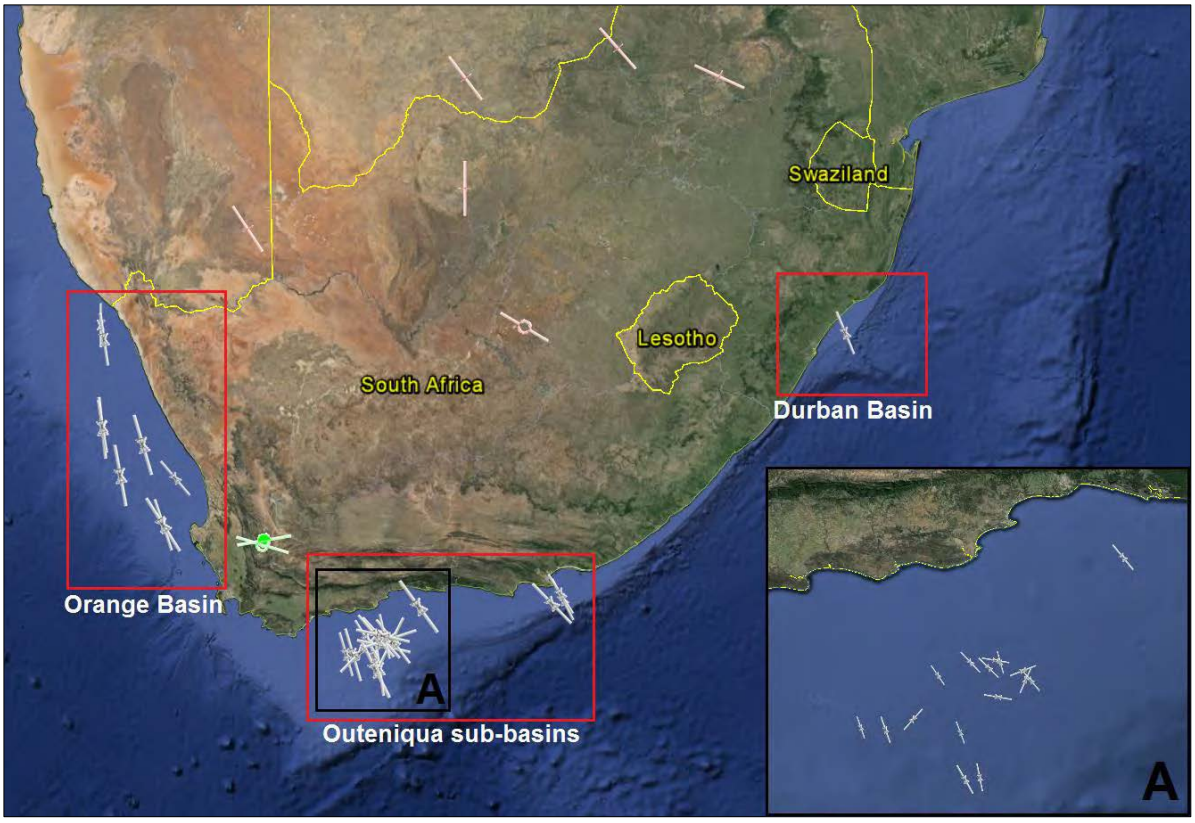

Figure 28: An overview of the updated stress data for South Africa. Excluding the cluster of highly variable oreinatations in the Bredasdorp sub-basin (subset A), the general trend is NW-SE to NNW-SSE.

Stress orientation trends in the Orange Basin

When plotted, the individual S_{Hmax} orientation data for the Orange Basin show a clear and consistent NNW-orientated pattern of S_{Hmax}. Breakout orientation rose diagrams (S_{hmin}), generated from FACT analysis, and the determined S_{Hmax} orientations, show little variation across the entire basin, coupled with low standard deviation (Figure 29). "D"-quality data, presented as smaller stress orientation symbols, are also shown as these further support the presence of this regional trend and may even suggest the average S_{Hmax} orientation shifts from a NW to N-S trend moving from the southern to northern parts of the basin. These results are however less reliable and not used in the smoothing scripts.

Using all calculated orientation values from "B"- to "D"-quality (Table 5), the average S_{Hmax} orientation across the Orange Basin is **163.6°** with a standard deviation of **12.15**. These results are supported by both previous studies and existing records in WSM 2008 release. A "C"-quality FMS orientation of **167°** was derived from an earthquake along the Walvis Ridge off the Namibian coastline to the northwest of the Basin (see Figure 3) and work by Avraham *et al.* (2002) and Viola *et al.* (2005) identified the preferential NNW-alignment of offshore mud volcanoes, considered as a high-quality young geological indicator of S_{Hmax} orientation. Mapping of fault slip patterns observed in both onshore Namibia and the Namaqualand region of South Africa also produce conjugate sets suggestive of NNW-aligned sigma-1, typically parallel to the S_{Hmax} orientation determined in borehole breakout analysis (Figure 30) (Viola *et al.*, 2005).

Table 5: S_{Hmax} orientation data for the Orange Basin

Borehole ID	Location (Decimal Deg)		S_{Hmax} (length-weighted)	Standard Deviation	WSM Quality	Total breakout length (m)	Depth Range	Avg. Breakout Depth (m)
	Latitude	Longitude						
ORANGE BASIN								
A_A1	-31.21954	16.92035	163.3	10.03	B	129	2,578.35 - 3,806.97	2904
A_F1	-29.22436	16.19956	171.2	3.4	C	33	2,231.61 - 2,846.74	2415
A_K1	-32.68941	17.23313	160.8	3.97	C	47	2,090.61 - 3,121.87	3348
A_O1	-28.9485	16.16566	179.5	1.76	D	13	1,808.23 - 4,569.52	4291
Ba_A1	-31.86711	17.60955	139.4	12.51	D	18	217.68 - 1,374.94	660
K_A1	-30.80798	16.0157	169.9	4.34	C	38	2,129.2 - 4,818.36	2476
K_A2	-30.83457	16.00818	172.5	8.89	B	142	1,656.84 - 5,829.36	2520
K_D1	-31.7316	16.33634	168.8	8.89	B	145	1,574.25 - 4,710.79	4244
K_H1	-32.68941	17.23313	146.9	4.6	B	132	1,645.16 - 4,260.95	2897
			163.6	**12.15**				

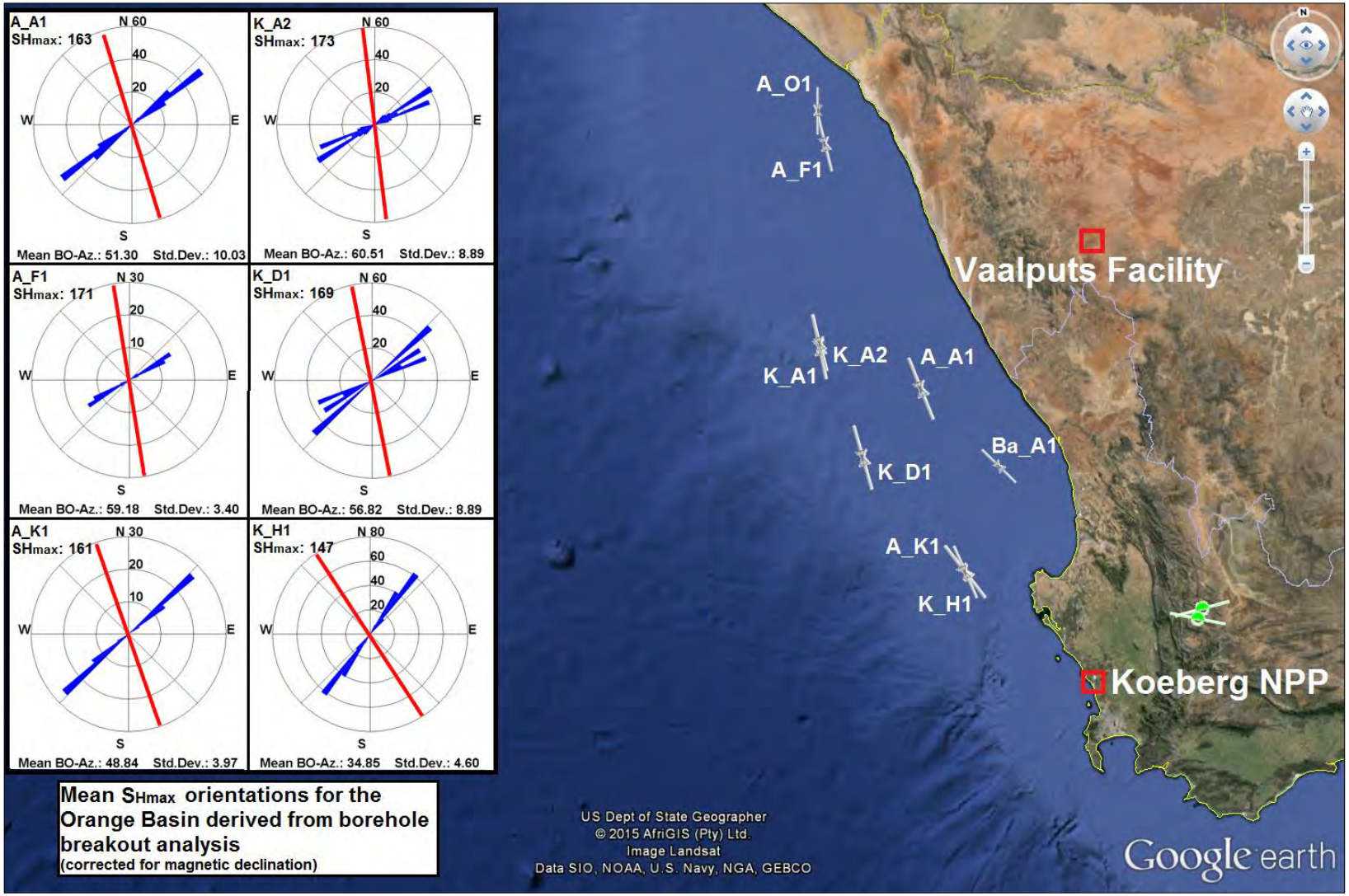

Figure 29: Breakout data for the Orange Basin reveals consistent NNW-SSE S_{Hmax} orientations for B- and C-quality data with low standard deviation. D-quality data (indicated by shorter symbols) are also displayed as it supports the trend.

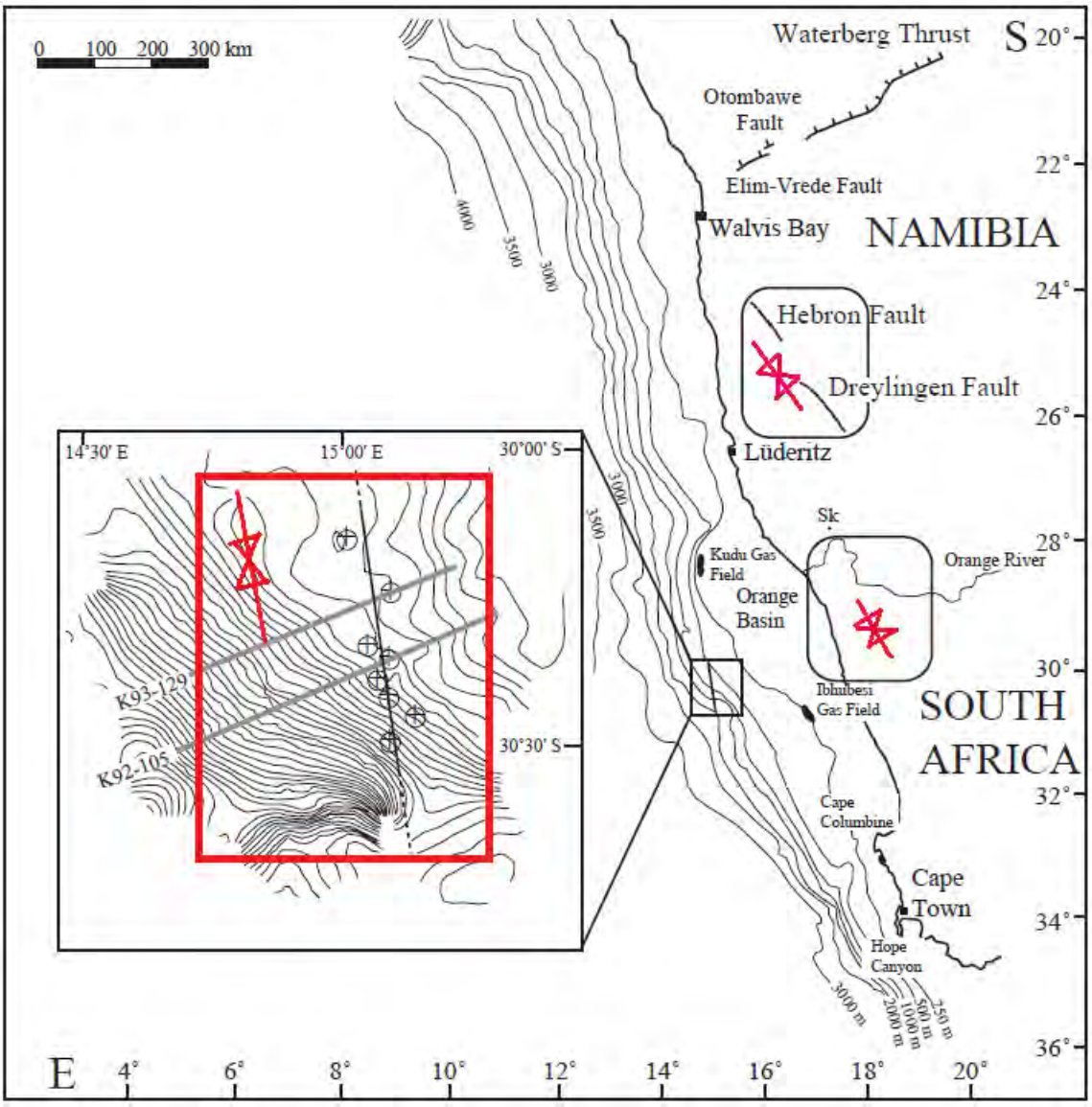

Figure 30: Mud volcano alignment seen in the Orange Basin is regarded a good indicator of a NNW-SSE maximum horizontal stress orientation. The red convergent arrows indicate the proposed compressive stresses from geological indicators (Viola et al., 2005).

Looking at the Orange Basin structure described under Chapter 2, exploration boreholes analysed from both the thinnest and thickest regions of the basin show a consistent NNW-SSE trend (Figure 9) and breakouts analysed at all depths (ranging from ~1,650 – 5,800 m across all boreholes) suggests the stress field is consistent with depth (Figure 10).

Proximity of boreholes to the transform faults which structural highs, the Kudu Arch in the north and Cape Transform Zone in the south of the basin, show little impact on the overall S_{Hmax}. If the pattern of slight rotation of the S_{Hmax} orientations from south to north is correct

(suggested by "D"-quality data), boreholes K_H1 and A_K1 near the E-W-aligned CTZ may be slightly rotated westward suggesting the possible influence of a 3rd order stress driver. The overall NNW-trend observed in the basin sediments does not conform to the expected 1st order stress driver impacting the region; namely the tectonic forces related to the overall NE drift of the African plate, the ridge-push effect of the South Atlantic ridge at >2,500 km to the west, nor the E-W push expected by the continued extension of the EARs southward. The closest 1st order stress drivers which would supports the observed S_{Hmax} orientation are the ridge-push forces generated from the South Indian ridge at ~2,000 km to the south or the extremely distant African-Eurasian convergent boundary (Figure 3).

Stress orientation trends in the Outeniqua sub-basins

Looking at individual S_{Hmax} orientation data in the Outeniqua sub-basins (B-, C- and D-quality results), it at first appears a broad NNW-trending S_{Hmax} pattern may persists across the entire basin (Figure 31). However a cluster of data from the eastern Bredasdorp sub-basin show a range of S_{Hmax} orientations from WSW to ENE across a relatively short distance of 100 km. This cluster includes 4 "C"-quality breakouts suggesting the data is reliable and indicates a real feature (Figure 31 - Inset A). Breakout orientations and the resultant S_{Hmax} show low variation across the Pletmos, Gamtoos, Algoa sub-basins, as well as the western part of the Bredasdorp sub-basin (Figure 29). "D"-quality data, presented as shorter stress orientation symbols, are also shown as these further support the presence of this regional NNW- trend.

Using all calculated orientation values from "B" to "D"-quality, the average S_{Hmax} orientation across the Bredasdorp sub-basin is **185.9°**, N-S overall compared to the regional trend, but with a high standard deviation **48.89** due to the cluster of variable orientations in the eastern Bredasdorp sub-basin (Table 9). As the data has such a high standard deviation, the data must be taken with great caution as local variations may exist. The higher quality data from the basin does however, For the Pletmos sub-basin, the S_{Hmax} orientation is **142.7° (s.d. 10.23),** the Gamtoos **134.8° (s.d. 8.86)** and Algoa **149.8° (s.d. 2.65)** (Table 9). These orientations for the remaining sub-basins are more in line with the regional trend, however the total number of available data is lower than that for the Bredasdorp sub-basin and Orange Basin.

Looking at the basin structure in Figure 6, exploration boreholes on, or near the fault bounded basin margins show little evidence of deviation due to local structural features except for the eastern margin of the Bredasdorp sub-basin adjacent to Infanta embayment. Excluding this cluster of data, the breakout logs show a consistent NNW- trend at all depths (~500 – 4,400 m), suggesting the stress field is consistent with depth (Table 6). Boreholes located closest to the available cross-section in Figure 7 show the average breakout depth is within drift sediments and suggests no obvious structural control over the perpendicular S_{Hmax} orientations calculated for the two adjacent boreholes E_BD1 and E_BH1 suggesting the possible impact of differing lithology (Figure 8).

Boreholes with S_{Hmax} orientations not conforming to the regional trend also show consistency over a range of depths suggesting this is not the cause of the local variation. While borehole E_BH1 lies on no obvious structural feature, the densely-faulted Infanta Embayment which forms the local high may account for local 3rd order stress driver affecting the regional pattern. Excluding the highly variable data from the eastern Bredasdorp sub-basin, the overall NNW-trend would conform to the expected impact of the ridge-push effect from the South Indian ridge, the closest tectonic boundary at >1,500 km to the south and closest 1st order stress driver. The high variability of S_{Hmax} orientations derived for the Bredasdorp sub-basin is further reinforced by the recent study of Hodge (2013), who looked at faults, folds, fracture-sets and soft-sediment deformation features in Plio-Pleistocene aeolian deposits in the Agulhas Peninsula region of the Western Cape Province. While not indicative of the contemporary stress field, these results suggest a similar variation of S_{Hmax} orientations were experienced in the region at <5 Ma as seen in the western Bredasdorp sub-basin. A total of 6 sites were assessed and lineament orientations compiled which gave a range of S_{Hmax} orientations which ranged from 99° – 174°. (Figure 32). Sites to the east of Cape Agulhas suggest an E-W to ENE-WSW orientation whereas sites to the west indicate a range of orientations from E-W to N-S over a distance of ~25 km (Figure 32).

Stress orientation in the Durban Basin

Only a single "D" quality breakout was obtained from the two borehole calliper logs provided for the region. The "S_{Hmax} orientation suggests the basin shares the NNW-trend seen

in other basins (Table 7, Figure 33). However as the data is isolated, of low-quality, and the nearest adjacent orientation data are > 500 km away in the Free State and Mpumalanga provinces (which do support a NW-SE S_{Hmax}), this data is not reliable but nonetheless presented for completeness.

Table 6: S_{Hmax} orientation data for the Outeniqua sub-basins.

Borehole ID	Location (Decimal Deg)		S_{Hmax} (length-weighted)	Standard Deviation	WSM Quality	Total breakout length (m)	Depth Range	Avg. Breakout Depth (m)
	Latitude	Longitude						
BREDASDORP SUB-BASIN								
E_AB1	-34.94141	21.63773	147.5	18.04	D	53	1,846.27 - 2,957.37	2493
E_AF1	-34.91608	21.95487	136.6	11.57	C	83	1,392.02 - 2,883.1	1770
E_AH1	-35.18706	21.14363	162.7	31.02	D	44	2,706.3 - 3,728.92	3309
E_AO1	-35.23768	21.76164	162.3	2.12	D	27	1,394.61 - 3,356.61	3133
E_AT1	-35.06614	22.00594	282.1	5.95	C	94	1,498.4 - 3,381.91	1867
E_BD1	-35.20568	21.29701	162.7	2.36	C	76	1,494.28 - 3,247.03	1640
E_BH1	-35.15824	21.47533	224	2.78	C	53	1,291.44 - 3,357.68	1442
E_D2	-35.46962	21.86854	170.9	2.94	C	37	1,521.74 - 3,370.9	1706
E_D4	-35.47696	21.77673	153.1	12.2	B	380	1,766.9 - 3,630.86	2329
E_S6	-34.88366	21.84366	139.2	16.86	C	80	1,694.6 - 2,901.86	2129
F_A2	-34.98732	22.21024	142.1	9.46	C	50	356.91 - 2,903.8	1800
F_A5	-34.98376	22.18312	205.7	22.16	C	192	427.65 - 2,989.91	1932
F_AH1	-34.89121	22.02797	166.5	33.74	D	20	1,588.78 - 2,688.33	2158
F_AH2	-34.87936	22.001	281.9	21.95	C	51	1,578.05 - 2,673.46	1825
F_AR1	-34.93675	22.16896	250.8	14.2	C	97	1,899.24 - 2,972.31	2109
			185.9	**48.89**				
PLETMOS SUB-BASIN								
F_B2	-34.38052	22.81015	**142.7**	**10.23**	B	122	853.85 - 2,072.88	1397
GAMTOOS SUB-BASIN								
Ha_A1	-34.35678	25.67287	**134.8**	**8.86**	C	77	594.78 - 4,398.96	3213
ALGOA SUB-BASIN								
Hb_G1	-34.18536	25.86094	147.1	18.18	D	19	792.92 - 1,736.96	1390
Hb_K1	-34.28379	25.90249	152.4	28.37	D	79	1,315.54 - 1,925.08	1543
			149.8	**23.23**				

Table 7: The details for the single SHmax orinetation determined for the Durban Basin.

Borehole ID	Location (Decimal Deg)		S_{Hmax} (length-weighted)	Standard Deviation	WSM Quality	Total breakout length (m)	Depth Range	Avg. Breakout Depth (m)
	Latitude	Longitude						
DURBAN BASIN								
Jc_B1	-29.5074	31.6243	**156.6**	**4.94**	D	13	2,893.08 - 3,948.18	3750

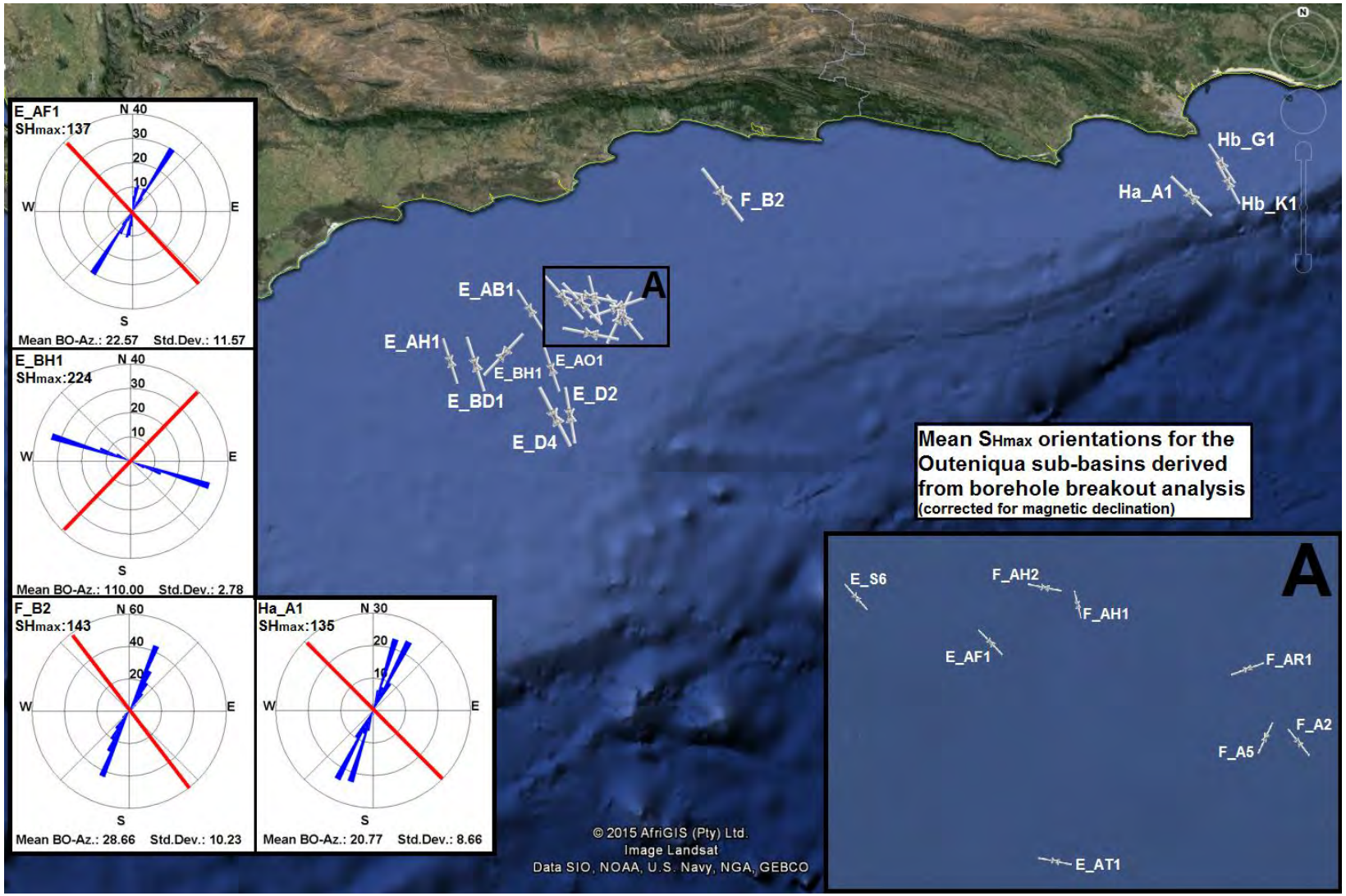

Figure 31: Breakout data for the Outeniqua sub-basins reveal a relatively consistent NW-SE S_{Hmax} for thePletmos, Gamtoos, Algoa and western part of the Bredasdorp sub-basins. Breakout logs for the eastern margin of the Bredasdorp sub-basin high variability show a range of orientations from N-S to E-W.

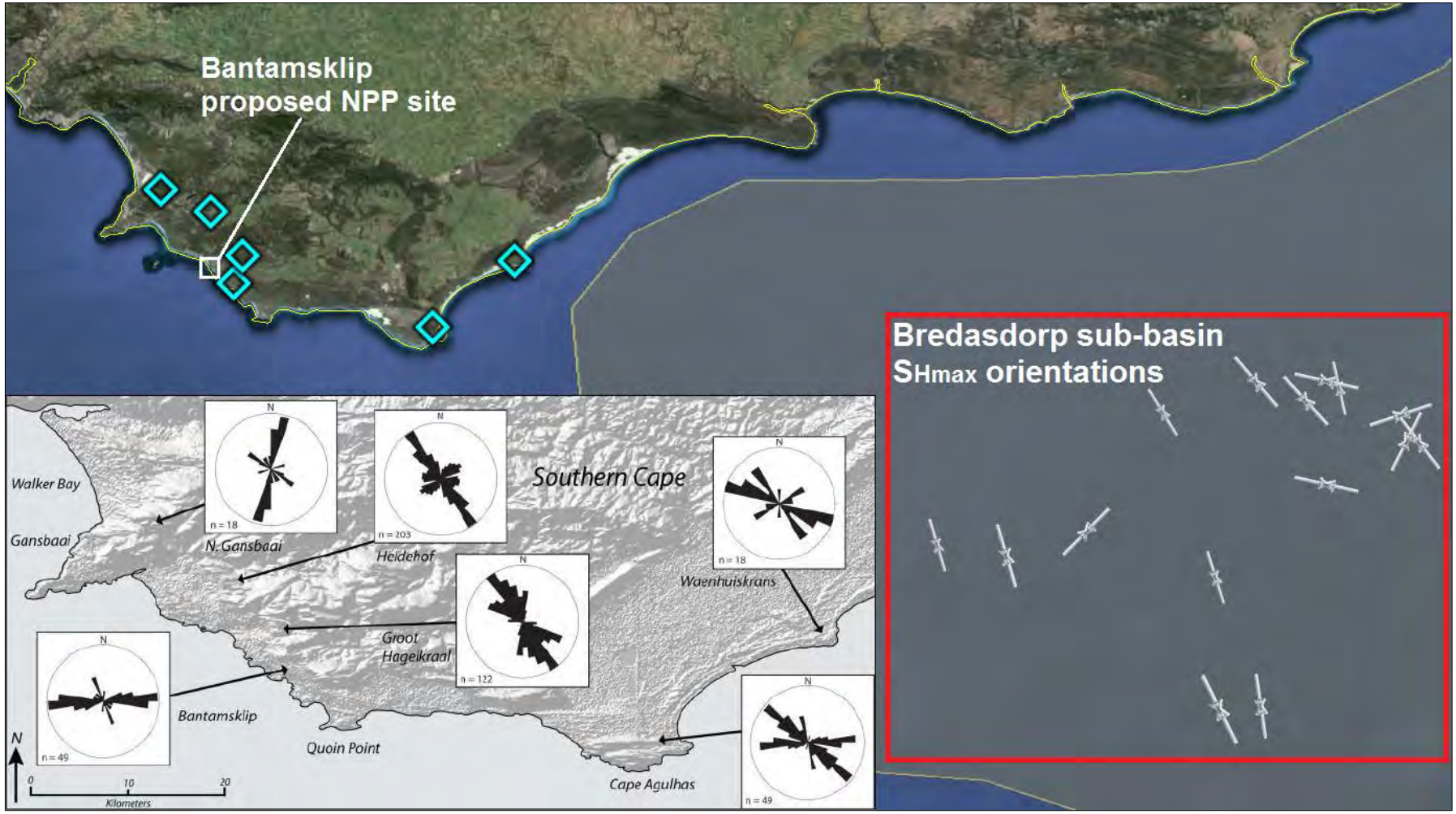

Figure 32: The S_{Hmax} orientation for the southern Cape determined from joint orientation by Hodge (2013). As with the Bredasdorp sub-basin, the orientations show high variability, ranging from E-W to N-S.

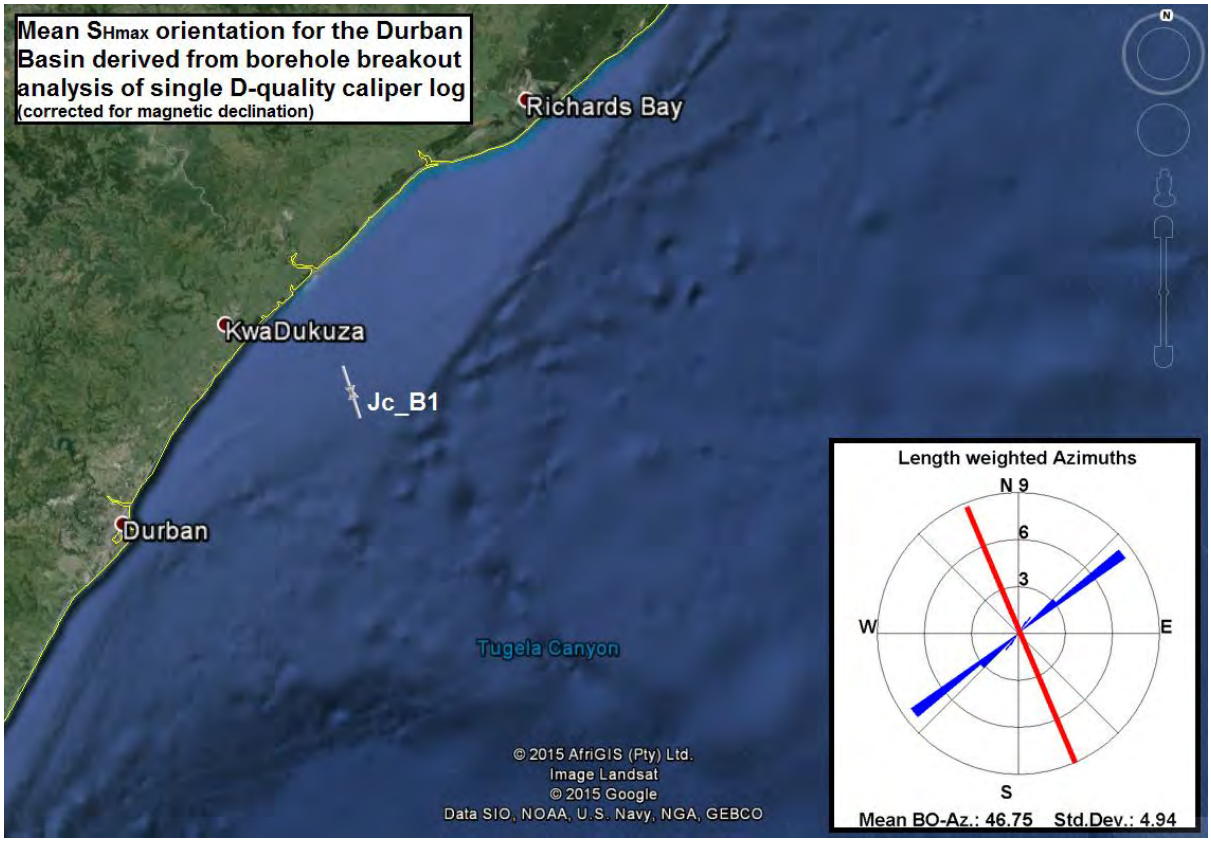

Figure 33: The single "D"-quality S_{Hmax} orientation calculated for the Durban Basin.

Generating a regional stress map

In order to produce an updated regional stress map, B- and C-quality data from this study was combined with the existing WSM database. This data was then processed using the WSM smoothing script described in Chapter 3. The resultant grid data (including mean S_{Hmax} azimuth and variance for each gridded point) was plotted within the QGIS software to display a gridded map of mean S_{Hmax} orientations for regions of interest and provide a regional approximation of the contemporary stress field.

The first script allows the user to adjust a number of parameters to iterate on the process of generating a representative stress field map:

Grid size was adjusted between **1°**, **0.5°** and **0.25°** in an attempt to accurately account for tightly clustered data, particularly results from the heavily explored Bredasdorp sub-basin. For larger grid sizes, clusters of data are averaged and the overall variance for the gridded point makes the average appear unreliable, even as part of a regional trend. For the regional map of South Africa, a **0.5°** grid size was chosen based on the WSM goals for their catalogue, however

this still results in the averaging of good-quality but tightly clustered data. For the individual basins and sub-basins, a **0.25°** grid was used to better account for closely spaced good-quality orientation data. This results in distant gridded data in the interior having a higher overall variation but the overall trend still fits the existing real data.

Search radius was kept consistent in all analyses and set 50 km to 1,000 km (in the intervals 50, 100, 200, 300, 400, 500, 600, 700, 800, 900, 1,000) to ensure tightly clustered sufficient overage for the interior of the country and that distant grid points data would have sufficient surrounding S_{Hmax} values to generate a transitional value between clusters of data. The choice of 1,000 km also excludes the script using orientation data from distant plate boundaries (which are often excluded by default). This was done so the new offshore basin S_{Hmax} results could be used as a boundary condition for the interior of the country. Within the search radius, any gridded data required at least two real S_{Hmax} data to fall diagonal within the search quadrants.

Quality Range and **Quality Weighting** and **Distance-Weigh Threshold** was kept consistent with the WSM standards: Only "A" to "C" quality data was used in the script with the weighting of 1./15, 1./20 and 1./25 respectively. The **Distance-Weigh Threshold** was left at 10, given the dense clusters of data in some sub-basins.

The second script processes the results of the gridded data produced by the first which include: the mean S_{Hmax} orientation, the variance of the mean S_{Hmax} orientation, the number of data records within the search radius, and the mean distance of these data records to the grid point. The second script then allows the user to filter the results:

Number-threshold was set to 5, filtering results to remove any gridded data point generated with less than 5 real data in the maximum search radius defined in the first script. Although the individual basins possess regions of clustered data and the bulk of the interior very little data and a threshold of 5 results in more distant S_{Hmax} data being used when calculating averages. Given the regional trend of data is consistant, this was decided a preferable to using less data per average.

Variance was set between **25** (as used in official WSM releases) and **45** (to increase coverage at the expense of reliability). At a maximum variance of 25, S_{Hmax} orientations fall reliably into a cardinal direction for S_{Hmax}. At a variance of 45, full coverage of the areas of interest are generated but at the expense of reliability. As these averages still conformed to real data, these maps were retained for discussion.

Smoothed stress data for the Orange Basin

As described above, a 0.25° grid was chosen for the Orange Basin in order to utilise the spread of good-quality data produced for the breakout analyses. Setting the variance threshold at 25, the basin displays a reasonably consistent NNW to N-orientated S_{Hmax}. Not using the plate boundary data limits the westward extent of the smoothed data but suggests the modelled data is a more accurate representation of the current stress field. The data indicates the Orange Basin is most likely dominated by a NNW-orientated S_{Hmax}, (Figure 34). The south-western grid point indicates a low-variation outlier that appears unreliable given its distant position relative to available data.

When the maximum allowed variance is raised to 45, a much larger region is covered with again suggests NNW-orientated S_{Hmax} is the regional trend, however less reliable, and the presence of the Ceres FMS data possibly suggests an E-W rotation of the stress field in place across the western Cape Fold belt, rotating progressively towards the regional NNW-trend away from this geological domain (Figure 35). The north-west part of Figure 35 shows the impact of the heavily-weighted Walvis Ridge FMS data on the model and produces a braod region of low-variance smoothed data.

Both real and smoothed data provide a first approximation of the contemporary S_{Hmax} for the offshore region near South Africa's Koeberg NPP which may in future be expanded to house new reactors (IRP 2010-2030). The modelled data also suggests the presence of a shifting S_{Hmax} orientation from E-W across the western Cape Fold belt to a more NW-SE trend seen in the offshore basin. Local data for the Koeberg site would therefore be required to obtain and accurate orientation for the contemporary stress field. Modelled data for the westernin interior, in which the Vaalputs radiaoctive waste disposal site is located, suggest a persistant NW-SE trend however, the region is sparsely represented by real data (Figure 35).

Smoothed stress data for the Outeniqua sub-basins

Again a 0.25° grid was chosen for the Outeniqua sub-basins in order to utilise the spread of good-quality data produced for the breakout analyses and try minimise the impact of the clustered data in the Bredasdorp sub-basin. Setting the variance threshold at 25, the basin displays a general NW to NNW-orientated S_{Hmax} but the high variance limits to total number of available gridded data. Additionally the averages generated by clustered data from the Bredasdorp sub-basin results in unreliable averages with high extremely variance (Figure 36). An extremely low grid size would be required to accurately represent changes in the stress pattern at such a low scale, the individual data is more representative.

When the maximum allowed variance is raised to 45, a much larger region is covered with again suggests NW to NNW-orientated S_{Hmax} is the regional trend. However the presence of the highly variable data in the eastern Bredasdorp again creates regions of high variance in the model which makes the data unreliable. As with the Orange Basin, no plate boundary data is considered and this limits the southward extent of the smoothed data. The impact of FMS data from the Ceres event again suggests there may be an E-W stress field is operating across the western Cape Fold belt, rotating progressively towards the regional NNW-trend away south into the offshore basins (Figure 37).

Again the distribution of both individual data and the smoothed data are reasonably close to the Thyspunt and Bantamsklip sites which have been proposed as possible nuclear developments. However the high variability requires additional indicators of stress to be considered for accurate modelling. The overall regional trend near the Bantamsklip site is best represented by the S_{Hmax} orientations determined in the study of Hodge (2013) assuming no major variations in stress orientation have taken place during the Plio-Pleistocene (< 5 Ma).

Smoothed stress map for South Africa

To create a smoothed stress map for South Africa, a 0.5° grid was chosen based on WSM goals, however the limited stress data for the interior results in high variation away from data clusters. Given the scarce quantity of smoothed data with a variation of less than 25, the averaged stress data is presented allowing a maximum variation of 45 (Figure 38).

While the average variation is high for the bulk of the interior (typically 30-35), the modelled trend still supports the individual breakout data and existing data in the WSM catalogue (Figure 27). A broad NW to NNW-orientated S_{Hmax} appears to dominate the western half of the country with the most notable feature again being the more E-W orientated field for the western part of the Cape Fold belt, influenced by the FMS data from the 1969 Ceres earthquake. The average orientation data for the offshore basins less displays lower variance at the 0.5 grid size in the Orange Basin whereas tightly clustered and highly-variable data in the Bredasdrop sub-basin still results in high variance averages.

When the gridded stress orientation data is presented with the regional geology of the offshore basins, it can be seen the contemporary stress field is typically sub-parallel (Orange Basin) to oblique (Outeniqua Basin) with many of the major structural features which define the geometry of the offshore basins (Figure 39).

Figure 34: Smoothed stress data for the Orange Basin. Grid size = 0.25, Variance = 25

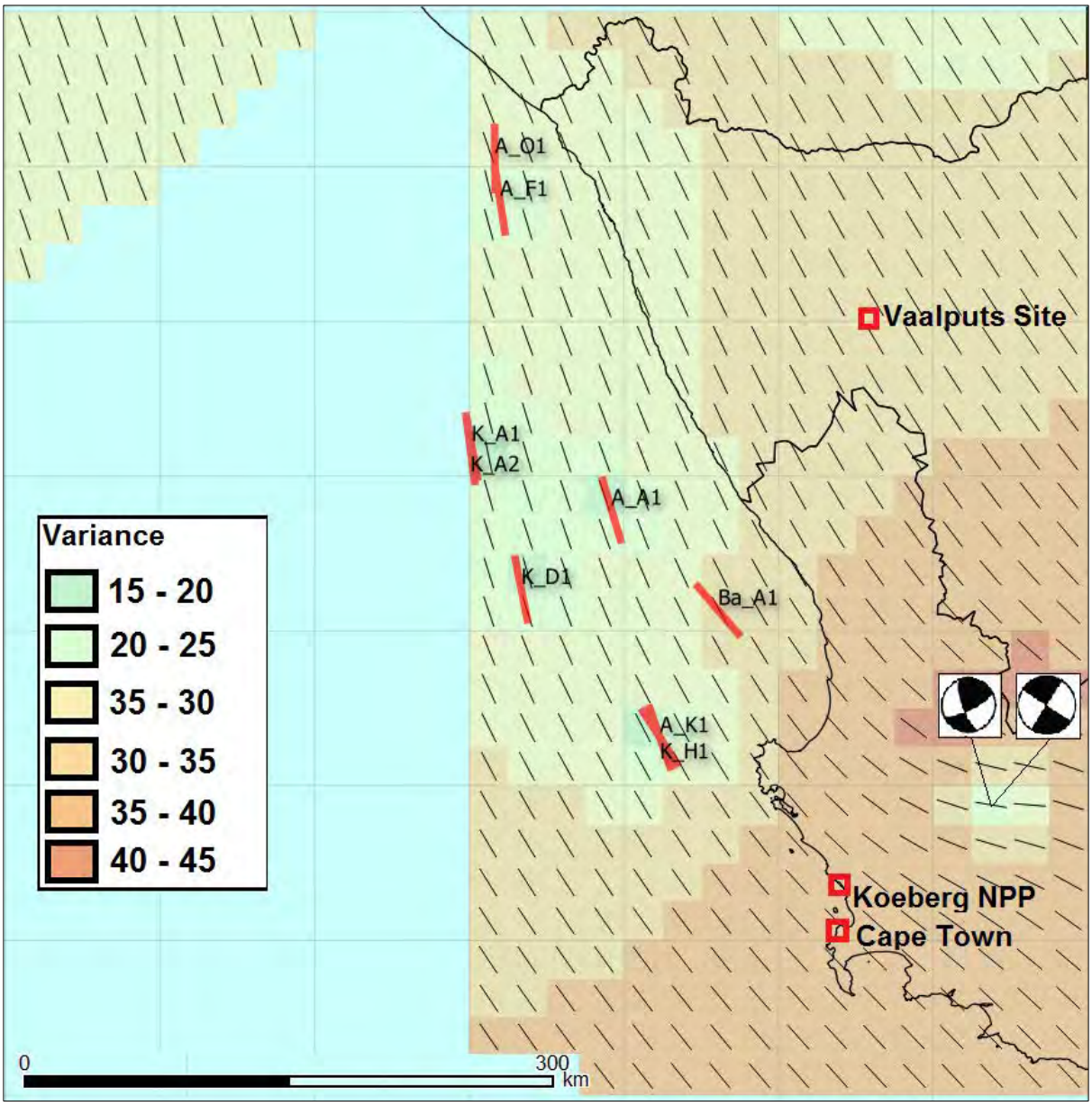

Figure 35: Smoothed stress data for the Orange Basin. Grid size = 0.25, Variance = 45. The impact on the Walvis Ridge FMS data on the model is seen in the north-west of the map.

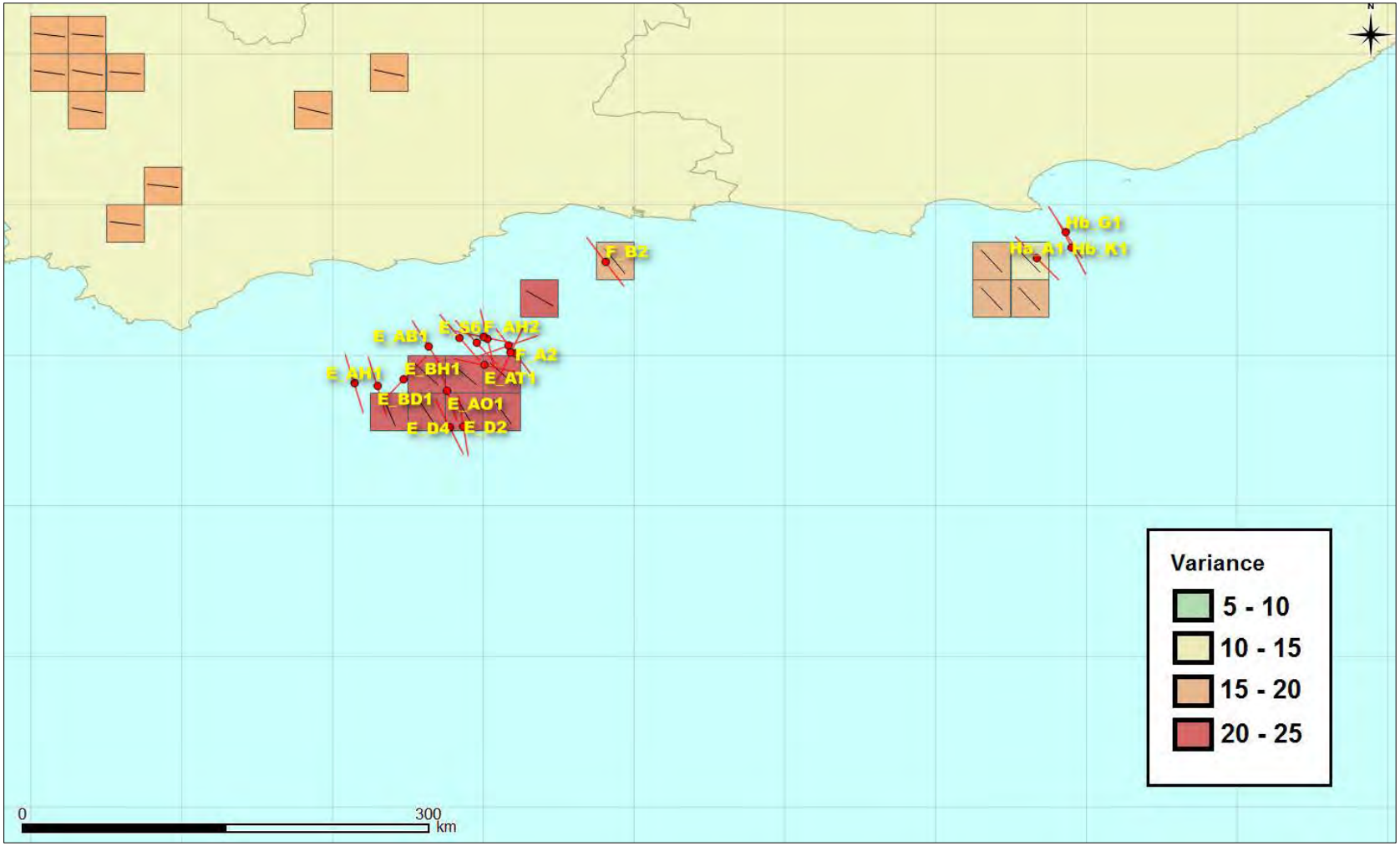

Figure 36: Smoothed stress data for the Outeniqua sub-basins. Grid size = 0.25, Variance = 25. The dense clustering of orineatation data makes it difficult to created a smoothed map event at a 0.25° spacing. This results in scattered high-variance averages.

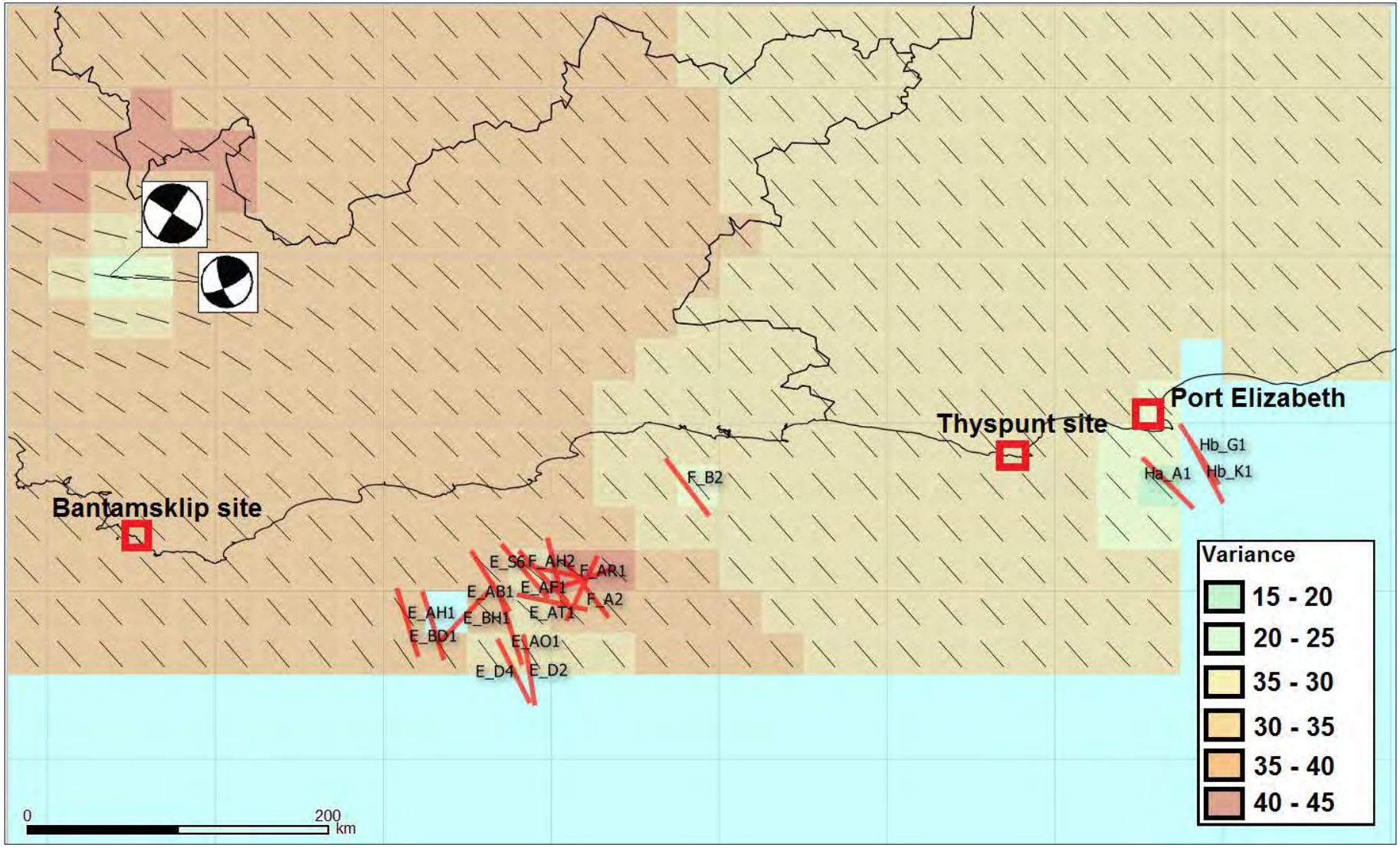

Figure 37: Smoothed stress data for the Outeniqua sub-basins. Grid size = 0.25, Variance = 45

Figure 38: Smoothed stress data for the South African offshore basins and interior. Grid size = 0.5, Max. Allowered variance = 45.

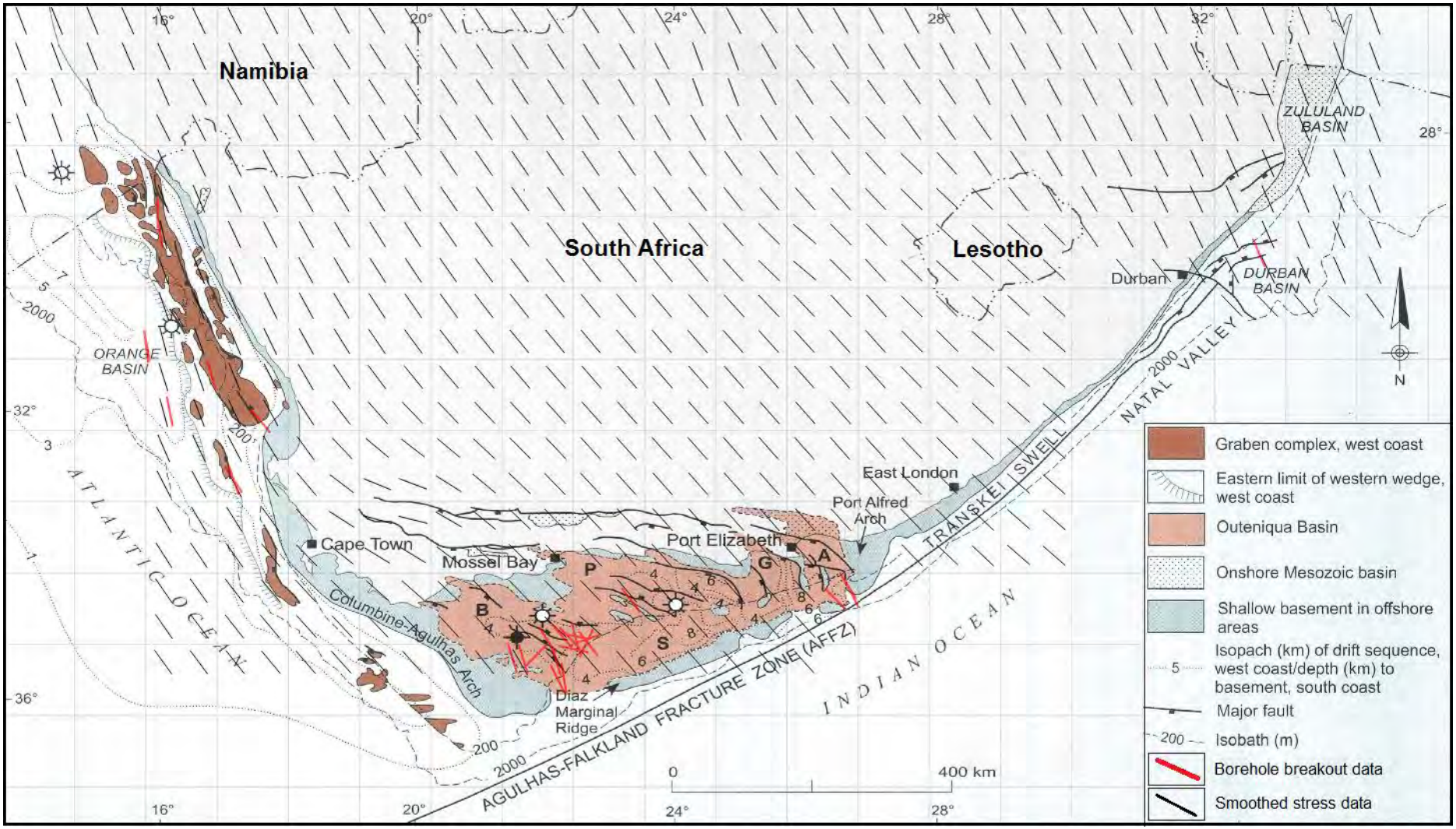

Figure 39: The geology of the offshore basins overlain with the regional stress map for South Africa and breakout data.

Comparison to previous studies

While not capable of quantifying stress forces, the regional stress map generated using both new data and the existing WSM catalogue compares favourably with previous compilations and models for South Africa. The work by Stacey and Wesseloo (1998) which compiled primarily onshore *in situ* stress data for South Africa (of which some results are part of the WSM catalogue), rely on stress data obtained within the mining and civil engineering projects (Figure 40). The high quality data from this study includes limited borehole breakout observations but is primarily from *in situ* mining techniques such as over-coring, rock slotter and hydrofracturing measurements. Observations suggest that the S_{Hmax} orientations trend approximately NW–SE exist across the central to western parts of South Africa, with S_{Hmax} often equal to, or greater than S_V at depth (Stacey and Wesseloo, 1998).

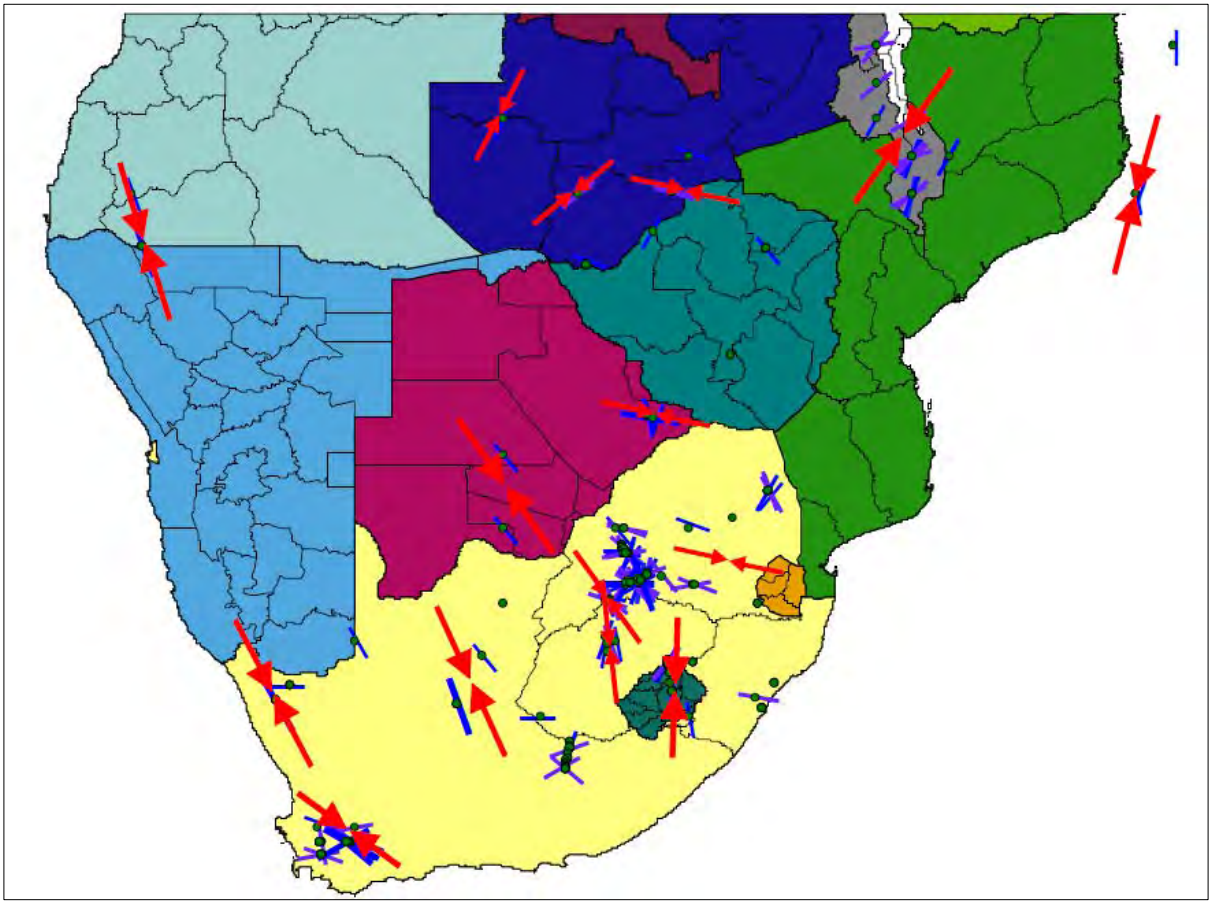

Figure 40: Compilation of compressive stress orientation data from industry measurements in southern Africa (Stacey and Wesseloo, 1998)

The resultant stress field map presented in Figure 39 also reinforces the earliest proposed stress orientation by Andreoli *et al.* (1996) who attempted to map all major geological structures and fabrics in South Africa and incorporate available indicators of stress-driven movement at the time. This work was expanded upon in the paper by Viola *et* al. (2005) as seen in Figure 41. These observations again suggest the presence of a persistent NNW-orientated compressive stress field acting on the western portion of Southern Africa which was contrary to the expected orientation of the maximum compressive stress, based on plate boundary forces (ridge push forces from the south Atlantic, south Indian ridges and the continued propagation of the EARs) and the general motion of the apparent north-eastwards motion of the African plate (Nocquet *et al*., 2006). This orientation was characterised by a horizontal compressive stress exceeding the vertical stress S1 > SV > S3, as seen in underground mining operation in and around Springbok in the Northern Cape Province (Andreoli *et al.*, 1996). This regional feature was named the "Wegener Stress Anomaly" by Andreoli *et al.* (1996) and was thought to represent a narrow band of NNW-trending compressive stress operating along the western coastline of southern Africa.

This work was expanded upon and again by the work of Bird *et al.* (2006) who used an earlier release of the WSM catalogue as part of a finite-element model for the principle horizontal stress directions affecting southern Africa. Their model used both WSM data for the crust but also considered the stress generated along the boundaries of the African Plate (which are not considered in this study). Using the limited onshore and offshore data, they produced a stress map indicating the compressive horizontal stress orientation and the expected faulting regime (Figure 42). The data produced in this project supports overall patterns modelled for the Outeniqua Basin and interior of South Africa. However the broad offshore region of E-W aligned S_{Hmax} is not apparent in borehole breakout data suggesting the NNW-trend is continuous, at least into the offshore sedimentary basins.

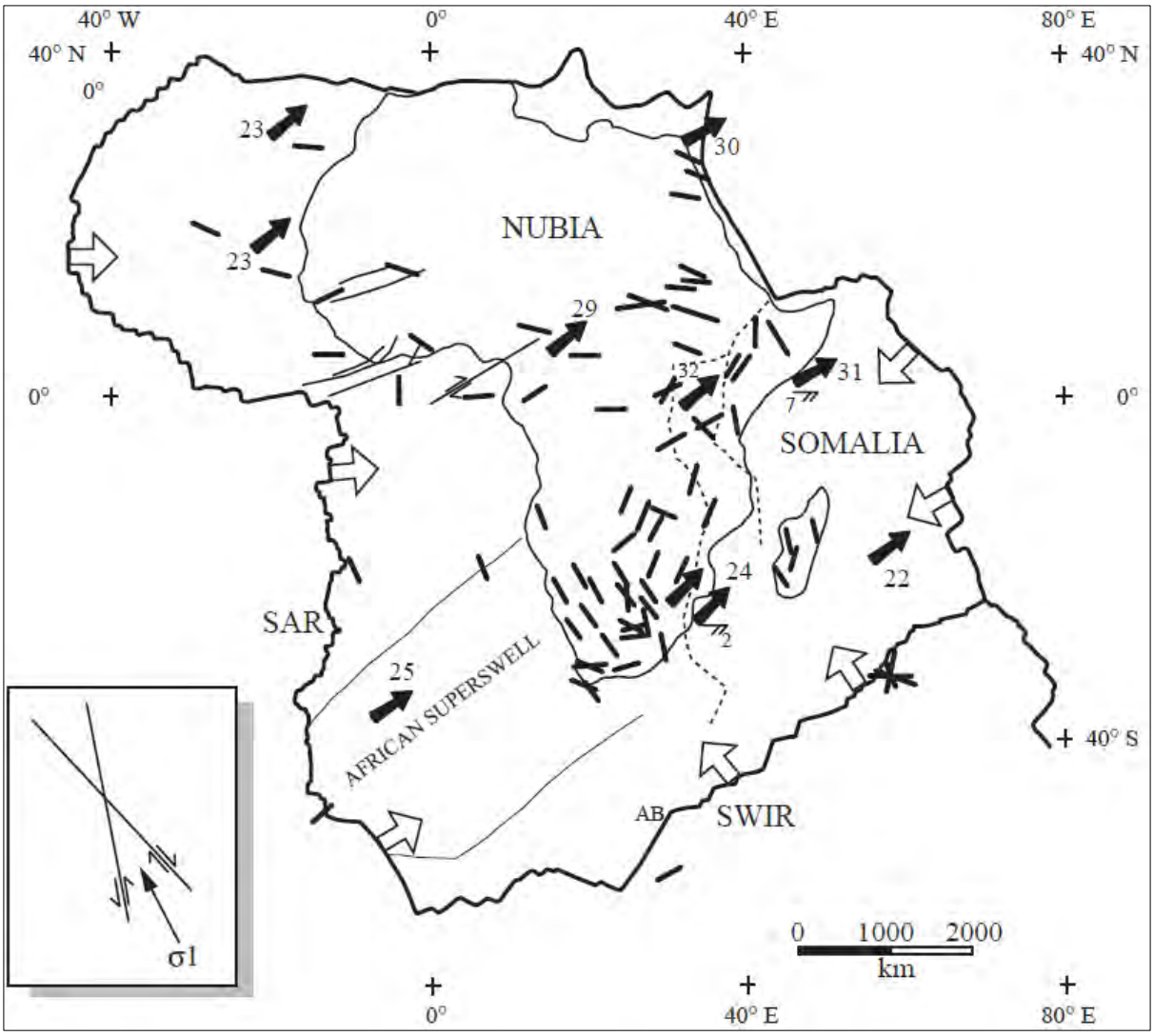

Figure 41: Compilation of stress orientation data for southern Africa by Viol *et al.* (2005) which expands on the work started by Andreoli *et al.* (1996).

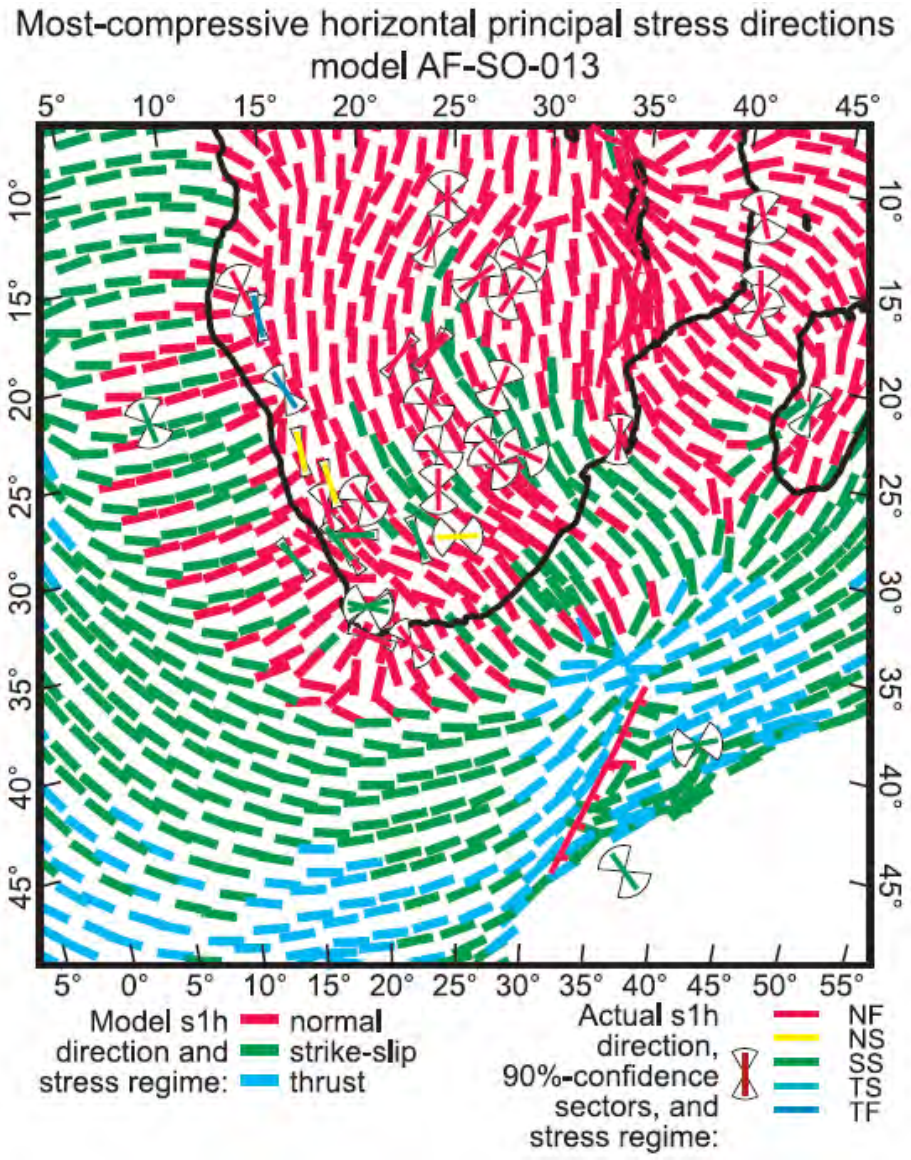

Figure 42: The finite element model produced by Bird et al. (2006) agrees with the data from this project however the new data indicates the broad NW-SE S_{Hmax} pattern extends into the Orange Basin.

Stress data and recent seismicity

Data determined by the borehole breakout technique used in this study is not capable of determining the ratio of forces for S_V, S_{Hmax} and S_{hmin}. However in light of previous studies suggesting a strong compressive horizontal force in the western half of the country (Andreoli *et al.*, 1996, Stacey and Wesseloo, 1998) and the possibility of strike-slip conditions (Bird *et al.*, 2006), the regional stress field was considered with regard to recent seismicity and historical earthquakes.

Recent seismic data for southern Africa was obtained from the Incorporated Research Institutions for Seismology (IRIS) catalogue [www.iris.edu] which hosts data generated by the Africa Array network [www.africaarray.psu.edu]. Public-domain event data for the period of 2005 – 2015 for southern Africa was filtered to only events from the Africa Array (AF) network which has good coverage of South Africa with an established network of permanent stations. This data was then combined with averaged stress field results in an attempt to assess any impact of the regional stress field on the major geological structures of the Orange and Outeniqua Basins (Figure 43). The resultant image reveals very few events recorded for the offshore basins with the notable exception of the 1932 St. Lucia event which was estimated between M 6.3 and M 6.8, but falls within an area of little reliable real stress data (Midzi *et al*., 2013).

The combination of stress and seismic data does reveal numerous clusters of seismicity in the western and central parts of the country, distant from the major mining areas. The major clusters are located in the Augrabies region (Figure 43 - A), associated with a recent swarm in 2010; the Bushmanland Plateau (Figure 43 - B), associated with a broad region of low-magnitude seismicity; and the western part of the Cape Fold Belt (Figure 43 - C) which display a dense cluster of recent seismicity and is the site of the 1969 Tulbagh-Ceres earthquake M6.3 (Midzi *et al*., 2013). More distant from the new data is the site of the Koffiefontein event determined to be M6.2 (Midzi *et al*., 2013).

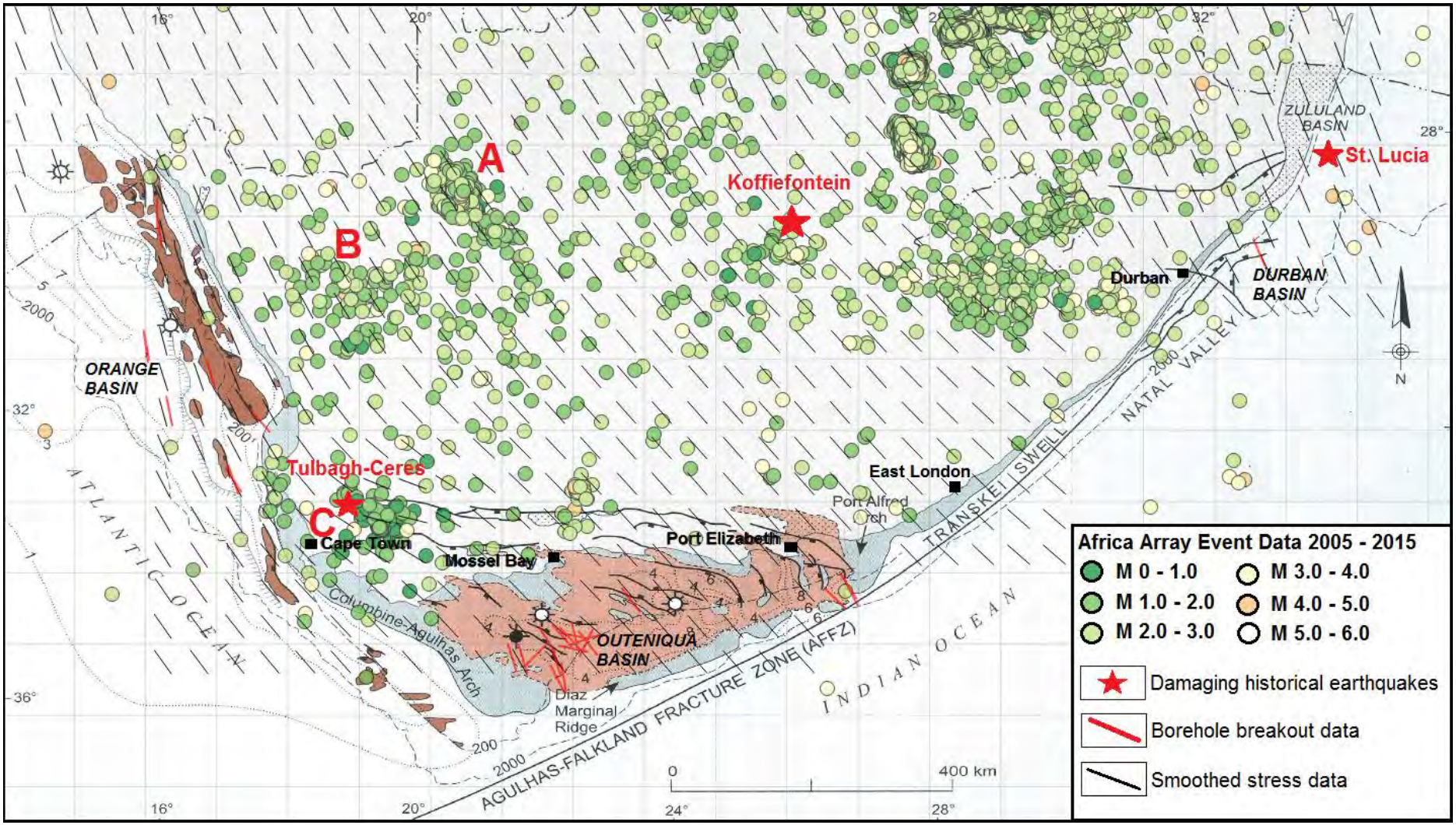

Figure 43: Africa Array event data for the period 2005 - 2015 reveals little data for the offshore basins but does indicate 3 major clusters of interest in the western half of the country.

The Augrabies cluster (Figure 43 - A) is located in a heavily sheared region at the boundary of the Kaapvaal Craton, the Kheis orogenic belt and the Namaqua-Natal metamorphic belt (Figure 44 – A) (Cornell *et al.*, 2006; Eglinton, 2006). The shear zones and other structural lineaments in the region are typically trending NW, sub-parallel to the predicted stress field orientation in the region. These structural lineaments are also on strike with the Hebron fault (Figure 30) which provided NW-orientated S_{Hmax} result in the study of Viola *et al.* (2005).

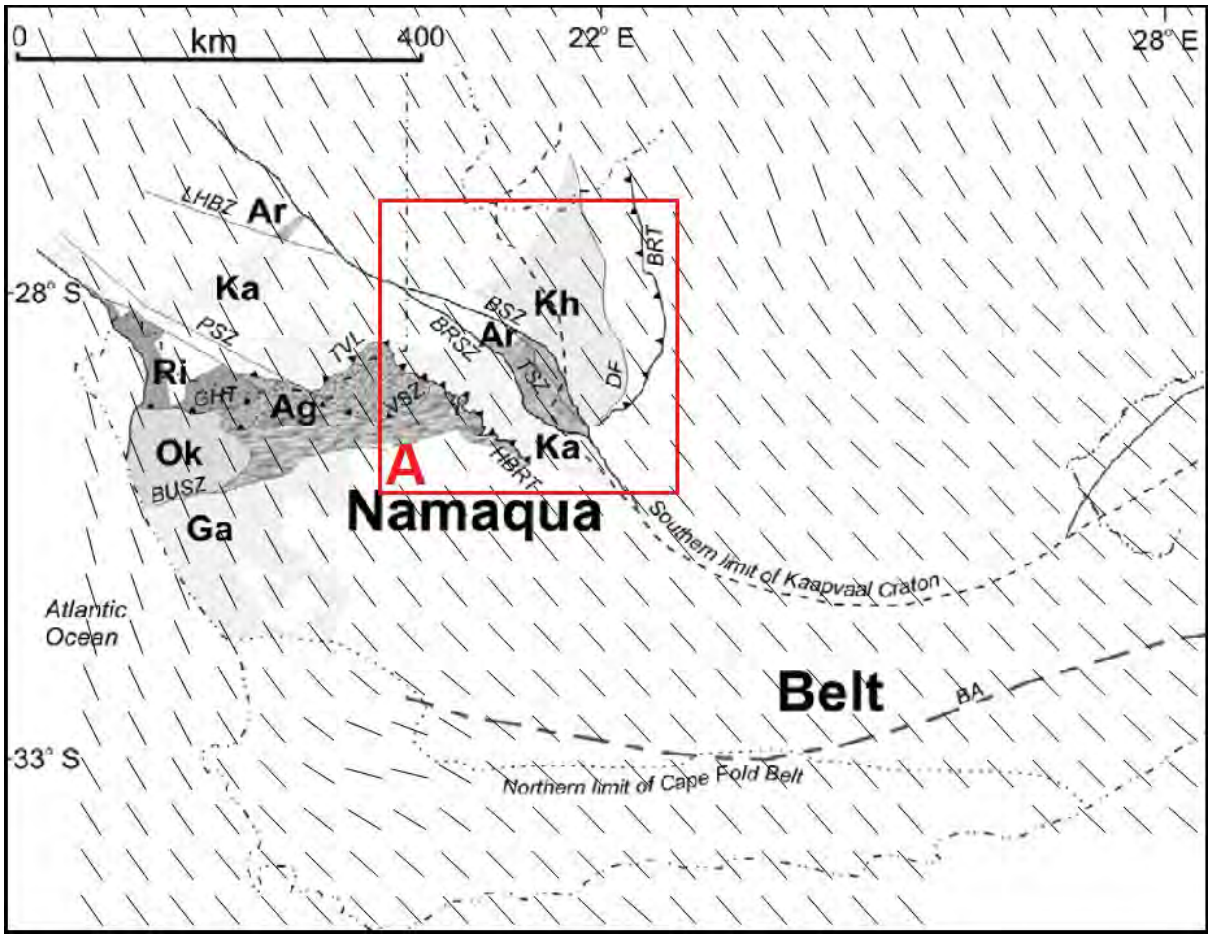

Figure 44: Structure of the Namaqua-Natal belt, the Kheis orogenic belt and Kaapvaal craton overlain with the modelled regional stress field (modified after Eglington, 2006). **Ag** – Aggeneys terrane, **Ar** – Areachap terrane, **Ga** – Garies terrane, **Ka** – Kakamas terrane, **Kh** – Kheis sub-province, **Ok** – Okiep terrane, **Ri** – Richtersveld sub-province, **BRSZ** – Bovenrugzeer shear zone, **BRT** – Blackridge thrust, **BSZ** – Brakbosch shear zone, **BUSZ** – Buffels River shear zone, **DF** – Dabep fault, **GHT** – Groothoek thrust, **HBRT** – Hartbees River thrust, **LHBZ** – Lord Hill Boundary Zone, **PSZ** – Pofadder shear zone, **TSZ** – Trooilapspan shear zone, **TVL** – Tantalite Valley line, **VSZ** – Vogelstruislaagte shear zone

The Bushmanland Plateau cluster (Figure 43 - B) lies within the Namaqua-Natal metamorphic belt however the basement geology and structure is typically obscured by Karoo Supergroup sediments and Tertiary cover (Cornell *et al.*, 2006). Uplift associated with the Great Escarpment along the western margin of this region reveals heavily-faulted basement with structural lineaments typically orientated NNW, parallel to the escarpment edge and, as a result, parallel to the contemporary stress field presented in this project.

The ongoing seismicity in the western part of the Cape Fold Belt (Figure 43 - C) falls within the same region as the 1969 Ceres earthquake and after-shocks. Uncertainty still exists as to the exact location of the event however the earthquake occurs in a region of E-W orientated lineaments, parallel to the escarpment. Based on both the available FMS data (Figure 43) for the Tulbagh-Ceres earthquake and the smoothed stress field based (Figure 39), structural lineaments in this region would again lie sub-parallel to the contemporary stress field.

The above observations suggest a correlation between the regional stress field and pre-existing sub-vertical geological structures. Looking at the Anderson's classification scheme for relative stress magnitudes in the crust (Figure 45), possible reactivation along these sub-vertical to vertical structures is most likely in a strike-slip environment in which $S_{Hmax} > S_V > S_{hmin}$ (Zoback, 2010).

Recent work by Brandt and Saunders (2011), compiled previous regional motion tensor data (most notably the Ceres event) with new data for the central and north-east of the country (Figure 46). The "beach ball" data for the Ceres events indicate a strong horizontal compression consistent suggestive of a strike-slip environment as presented in Figure 45. In addition, 2 new events ("2" and "3" in Figure 46) from the central and north-eastern part of the country indicated a component of horizontal compression component, orientated roughly NW.

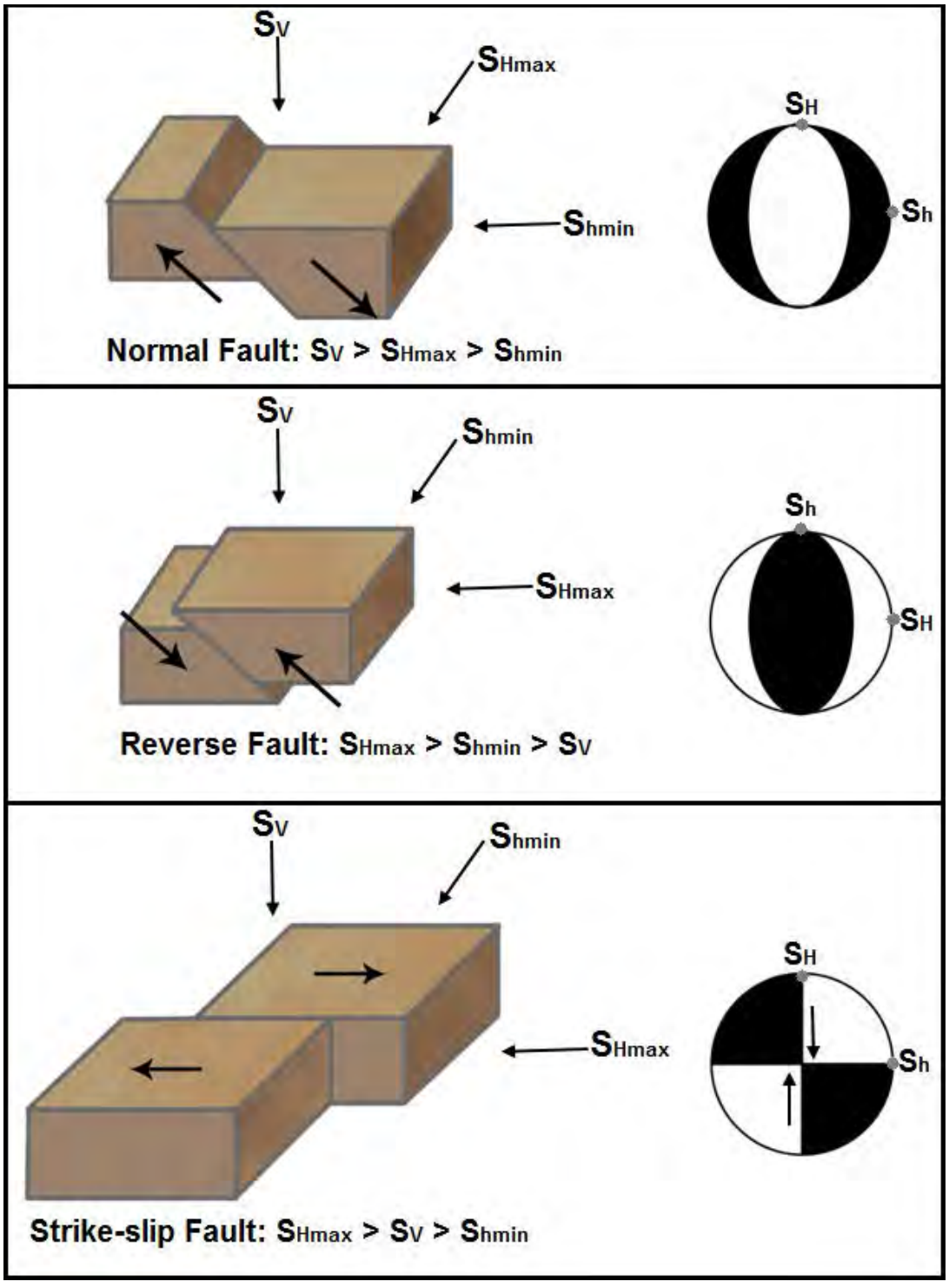

Figure 45: E. M. Anderson's classification scheme for relative stress magnitudes.

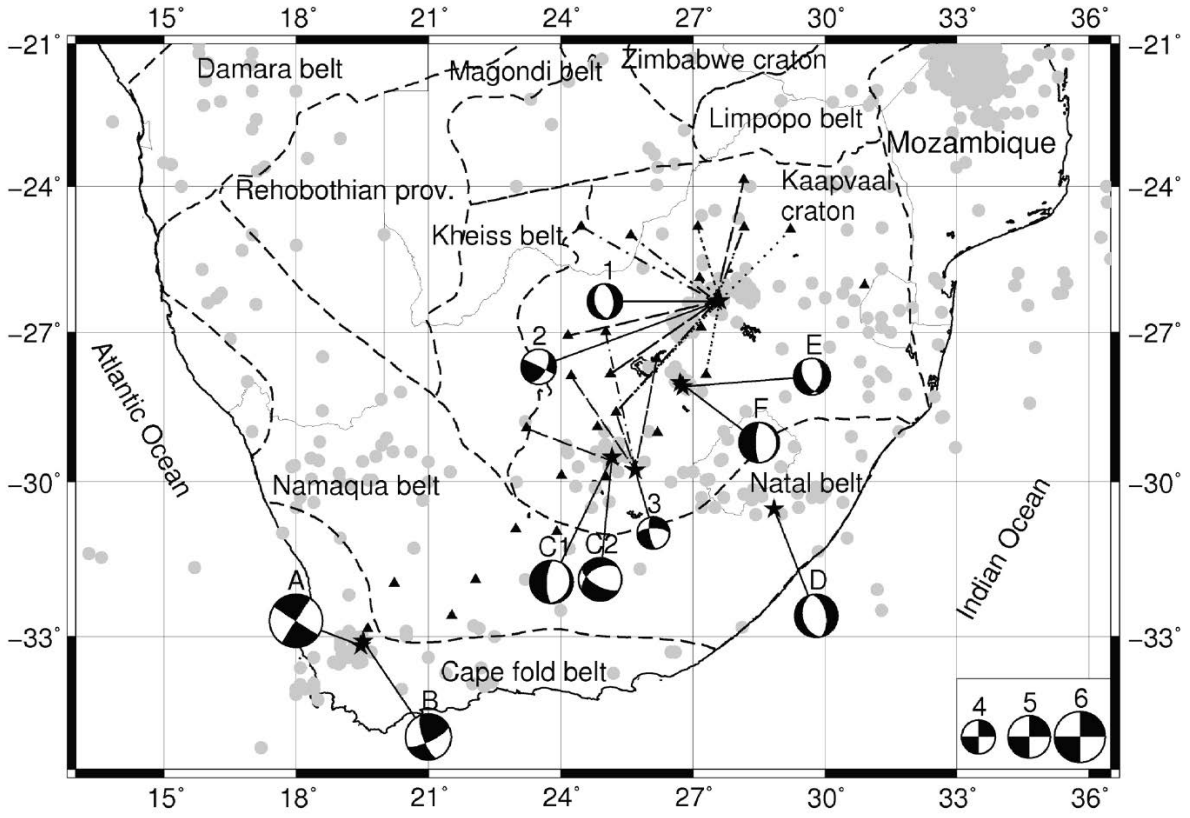

Figure 46: A compilation of previous and regional movement tensors for major events in South Africa (Brandt & Saunders, 2011). The Ceres event indicates a clear strike-slip component orientated with the maximum compressive stress axis between W and NW. New data by Brandt & Saunders (2011), "2" and "3" both indicate a strike slip component.

CHAPTER 6: CONCLUSIONS

The borehole breakout technique has proved a reliable method for determining stress orientation data in a relatively aseismic region, with few other high-quality indicators of stress available, such as focal mechanism solutions. The success rate in recovering usable breakout data was however low and attempting an analysis on a small sample of boreholes may not necessarily provide any data. The continued exploration drilling, primarily related to hydrocarbon exploration in South Africa could provide a continuous source of new stress data going forward, however collaboration would be required to ensure emphasis is placed on collecting quality logging data.

With an initial sample size of 131 boreholes, only 29 usable breakouts were obtained (an overall success rate of 22%). A total of 20 breakouts were of A-C quality (15%), based on the WSM quality ranking criteria data, and suitable for input to the WSM catalogue and for use in creating a smoothed stress field map. A total of 102 borehole logs yielded no usable data due to missing/erroneous log parameters, too short lengths of breakout, borehole washout and calliper tool problems.

Of the 29 boreholes with usable breakout data, the overall breakout orientation were extremely consistent with all but 5 logs displaying a NNW-trending S_{Hmax}. This trend appears continuous from the western limit of the Orange Basin dataset, through the Outeniqua Basin. A single breakout result for the Durban Basin also gives this orientation however the low-quality short breakout does not make the S_{Hmax} orientation reliable. All results are consistent with the sparse onshore and offshore data currently available for South Africa.

The average S_{Hmax} orientation (based on B, C and D-quality data) were determined as 163.6° (s.d. 12.15) for the Orange Basin, 185.9° (s.d. 48.89) for the Bredadorp sub-basin, 142.7° (s.d. 10.23) for the Pletmos sub-basin, 134.8° (s.d. 8.86) for the Gamtoos sub-basin and 149.8° (s.d. 2.65) for the Algoa sub-basin. The single D-quality orientation for the Durban Basin gives the S_{Hmax} orientation of 156.6 (s.d. 4.94). The high variability in the Bredasdorp sub-basin occurs within a cluster of data on the eastern margin with the Infanta Embayment, suggesting local structural features (3rd order stress drivers) may have a significant impact on the local stress field across very short distances (~100 km).

The S_{Hmax} orientation data determined from the borehole breakouts technique for the offshore basins is supported by stress data generated from recent studies (including stress orientations derived from focal mechanism solutions, mud-volcano vent alignment, fault-slip indicators, and lineament fracture patterns). This suggests that the orientation data derived from the offshore basins is part of a real trend that can be extrapolated into the interior of the country (primarily the western half) and good coupling is likely present between the basin deposits and underlying continental and oceanic crust.

Attempts to create a regional stress map for region indicate challenges still remain with limited stress data from the interior and clustered data for the offshore basins and EARs to the northeast of the country. This results in the over-representation of data in some areas (which can lead to high variance), and heavily extrapolated, high variance data in other areas. At the local basin scale, individual data is likely to provide a more reliable indication of the stress pattern whereas smoothing of this data may result in unreliable results. Overall, both the smoothed local stress maps for the Orange and Outeniqua Basins (at a 0.25° and 0.5° smoothed grid), indicate a persistent NNW-trend. The tight cluster of variable data in the Bredasdorp sub-basin is a feature that requires further investigation as 90° shifts in S_{Hmax} orientations are not always correlated with structural features and may have a lithological control.

The NNW-trend identified in both individual breakout data and the resultant smoothed stress map reinforce previous studies which suggested the presence of a NW to NNW S_{Hmax} stress field in the western half of South Africa. The findings of this study suggest the existence of the "Wegener Stress Anomaly" ($S_1 > S_V > S_3$), assumed to affect a narrow stretch of the western coastline of southern Africa, may instead be part of a broad region NNW-trending compressive stress. The breakout data itself cannot determine the magnitude of the horizontal compressive force but S_{Hmax} is expected to be sub-parallel to sigma 1.

When the new model is compared to the finite-element model created by Bird et al. (2006), it generally supports the presence of a NNW-trending stress field established in the Outeniqua Basin and western interior of the country. The new data (both real and modelled) however disagrees with the model and indicates this stress pattern persists into the offshore basins of the western coastline of the country which was expected to have an E-W orientated S_{Hmax}.

When comparing both the real data and 0.5° grid averaged regional stress field for South Africa to recent seismicity (2005 – 2015) and previous damaging earthquakes, there is little seismicity in the offshore basins themselves. The data does however indicate 3 distinct clusters of seismic events in the western interior of the country, namely the Augrabies cluster, the Bushmanland Plateau cluster and western Cape Fold Belt cluster (associated with the 1969 Tulbagh-Ceres event). All these regions display continuous seismicity and are associated with structural lineaments which typically lie sub-parallel to S_{Hmax} in the modelled stress field.

Considering the Anderson's classification scheme for relative stress magnitudes in the crust, the most likely environment in which these regions would experience reactivation of seismogenic structures is in a strike-slip setting where $S_{Hmax} > S_V > S_{hmin}$. The breakout technique in this project is not able to quantify forces, however the combination of new data, previous compilations of mining data, and the recent update of available regional motion tensors for South Africa suggest there is a strong component of NW-trending horizontal compression experienced in the South African crust.

REFERENCES:

Amadei, B. and Stephansson, O. (1997). *Rock Stress and Its Measurement*. Springer Publishing, Netherlands

Andreoli, M.A.G., Doucouré, M., Van Bever Donker, J., Brandt, D. and Andersen N.J.B. (1986). Neotectonics of southern Africa – a review. *Africa Geoscience Review*, **3**, 1-19

Ben-Avraham, Z. and Tibor, G. (1993). The northern edge of the Gulf of Elat. *Tectonophysics*, **226**, 319-331

Ben Avraham, Z., Smith, G., Reshef, M, and Jungslager, E. (2002). Gas hydrate and mud volcanoes on the southwest African continental margin off South Africa. *Geology*, **30**, 927-930

Behn, M.D., Conrad, C.P. and Silver, P.G. (2004). Detection of upper mantle flow associated with the African superplume. *Earth and Planetary Science Letters*, **224**, 259-274

Bell, J.S., Price, P.R. and Courel, R. (1993). How accurately can borehole breakouts record in-situ stress orientations? In: Haimson, B. (ed.), *Rock Mechanics in the 1990's*, Volume 1 – Pre-print proceedings of the 34th US Symposium on Rock Mechanics, 121-124

Bell, J.S., Price, P.R. and McLellan, P.J. (1994). In-situ stress in the Western Canada Sedimentary Basins, In: Mossop, G.D. and Shetsen, I. (compilers), *Geological Atlas of western Canada Sedimentary Basins*, Canadian Society of Petroleum Geologists and Alberta Research Council, 439-446

Bird, P. (2003). An updated digital model for plate boundaries. *Geochemistry Geophysics and Geosystems*, **4** (3), 1027

Bird, P., Ben-Avraham, Z., Schubert, G., Andreoli, M. and Viola, G. (2006). Patterns of stress and strain-rate in southern Africa. *Journal of Geophysical Research*, **111**

Broad, D.S., Jungslager, E.H.A., McLachlan, I.R. and Roux, J. (2006). Offshore Mesozoic Basins. *In:* Johnson, M.R., Anhaeusser, C.R. and Thomas, R.J. (Eds.), *The Geology of South Africa*. Geological Society of South Africa, Johannesburg/Council for Geoscience, Pretoria, 553-571

Brandt, M.B.C. and Saunders, I. (2011). New Regional Moment Tensors in South Africa. *Seismological Research Letters*, **82**, 69-80

Brown, L.F. Jr., Benson, J.M., Brink, G.J., Doherty, S., Jollands, A., Jungslager, E.H.A., Keenan, J.H.G., Muntingh, A. and Van Wyk, N.J.S. (1996). Sequence stratigraphy in offshore South African divergent basins. An atlas on exploration for Cretaceous lowstand traps by SOEKOR (Pty) Ltd. *American Association of Petroleum Geologists Studies*, **41**, 184

Cornell, D.H, Thomas, R.J., Moen, H.F.G., Reid, D.L., Moore, J.M. and Gibson, R.L. (2006). The Namaqua-Natal Province. *In:* Johnson, M.R., Anhausser, C.R. and Thomas, R.J. (Eds.), *The Geology of South Africa*, Johannesburg/Council for Geoscience, Pretoria, 325-379

De Swardt, A.M.J. and McLachlan, I.R. (1982). Petroleum exploration in the South African offshore: the geological framework and hydrocarbon potential. *In:* Glen, H.W. (Ed.), *Proceedings, Twelfth Congress of the Council of Mining and Metallurgical Institutions 1*. South African Inst. Min. Metall./Geol. Soc. South Africa, 147-161

Eglington, B.M. (2006). Evolution of the Namaqua-Natal Belt, southern Africa – A geochronological and isotope geochemical review. *Journal of African Earth Sciences*, **46**, 93-111

England, P. and Jackson, J. (2011). Uncharted seismic risk. *Nature Geoscience*, **4**, 348-349.

Fenton, C.H., Adams, J. and Halchuk, S. (2006). Seismic hazards assessment for radioactive waste disposal sites in regions of low seismic activity. *Geotechnical and Geological Engineering*, **24**, 579-592

Gerrard, I. and Smith, G.C. (1982). The post-Palaeozoic succession and structure of the south-western African continental margin. *In:* J.S. and Drake, C.L. (Eds.). *Studies in Continental Margin Geology*. Mem. Am. Assoc. Petrol. Geol., **34**, 49-74

Heidbach, O., Reinecker, J., Tingay, M., Müller, B., Sperner, B., Fuchs, K. and Wenzel, F. (2007). Plate boundary forces are not enough: Second- and third-order stress patterns highlighted in the World Stress Map database. *Tectonics*, **26**, 1-19

Heidbach, O and Müller, B. (2008). *Report – Analysis of offshore borehole data in the Bredasdorp Basin, South Africa*. Report produced for the South African Nuclear Energy Corporation, December 2008

Heidbach, O., Tingay, M., Barth, A., Reinecker, J., Kurfeß, B. and Müller, B. (2008). *The 2008 release of the World Stress Map* (available online at www.world-stress-map.org)

Heidbach, O., Tingay, M., Barth, A., Reinecker, J., Kurfeß, B. and Müller, B. (2010). Global crustal stress pattern based on the World Stress Map database release 2008. *Tectonophysics*, **482**, 3-15

Hodge, M.S. (2013). "Neotectonic deformation features in Plio-Pleistocene coastal aeolianites: Palaeoseismology and earthquake hazard implications for the Southern Cape, South Africa". M.Sc. Thesis, University of Cape Town, Cape Town

Jaeger, J.C., Cook, N.G.W. and Zimmerman, R.W. (2007). *Fundamentals of Rock Mechanics (Forth Edition)*. Blackwell Publishing, USA

Johnson, M.R., Anhaeusser, C.R. and Thomas, R.J. (Eds.) (2006). *The Geology of South Africa*. Geological Society of South Africa, Johannesburg/Council for Geoscience, Pretoria

Lithgow-Bertelloni, C. and Silver, P.G. (1998). Dynamic topography, plate driving forces and the African superswell. *Nature*, **395**, 269-272

Mardia, K.V. (1972). *Statistics of directional data: probability and mathematical statistics*. Academic Press, London, 357pp

Midzi, V., Bommer, J.J., Strasser, F.O., Albini, P., Zulu, B.S., Prasad, K. and Flint, N.S. (2013). An intensity database for earthquakes in South Africa from 1912 to 2011. *Journal of Seismology*, **17**, 1183-1205

McCalpin, J.P. and Nelson, A.R. (2009). *Paleoseismology - International Geophysics Series Vol. 95*, Elsevier, 1-27

Nocquet, J.M., Willis, P. and Garcia, S. (2006). Plate kinematics of Nubia-Somalia using a combined DORIS and GPS solution. *Journal of Geodesy*, **80**, 591-607

Nyblade, A.A. and Robinson, S.W. (1994). The African Superswell. *Geophysical Research letters*, **21**, 765-768

Plumb, R.A. and Hickman, S.H. (1985). Stress-induced borehole enlargement: a comparison between the four-arm dipmeter and the borehole televiewer in the Auburn geothermal well. *Journal of Geophysical Research*, **90**, 5513-5521

Pusch, R. (2008). *Geological Storage of Radioactive Waste*. Springer

Saria, E., Calais, E., Stamps, D.S., Delvaux, D. and Hartnady, C.J.H. (2014). Present-day kinematics of the East African Rift. *Journal of Geophysical Research: Solid Earth*, **119**, 3584-3600

Smith, W.H.F. and Sandwell, D.T. (1997). Global Sea Floor Topography from Satellite Altimetry and Ship Depth Soundings. *Science*, **277**, 1956-1962

South African Department of Energy (2013). *Integrated Resource Plan for Electricity 2010-2030: Update Report 2013*. November 2013, Pretoria

Sperner, B., Müller, B.. Heidbach, O., Delvaux, D., Reinecker, J. and Fuchs, K. (2003). Tectonic Stress in the Earth's Crust: Advances in the World Stress Map Project. In: Nieuwland D. (ed.): New Insights into Structural Interpretation and Modelling. *Geological Society of London Special Publication*, **212**, 101-116.

Stacey, T.R. and Wesseloo, J. (1998). Evaluation and upgrading of records of stress measurement data in the mining industry. Safety in Mines Research Advisory Committee, GAP 511, June 1998, 1-53

Stover, C.W. and Coffman, J.L. (1993). Seismicity of the United States, 1568-989 (Revised). *U.S. Geological Survey Professional Paper*, **1527**

Viola, G., Andreoli, M., Ben-Avraham, Z., Stengel, I. and Reshef, M. (2005). Offshore mud volcanoes and onland faulting in southwestern Africa: neotectonic implication and constraints on the regional stress field. *Earth and Planetary Science Letters*, **231**, 147-160

Viola, G., Kounov, A., Andreoli, M.A.G. and Matilla, J. (2012). Brittle tectonic evolution along the western margin of South Africa: More than 500 Myr of continued reactivation. *Tectonophysics*, **514-517**, 93-114

Watkeys, M.K. (2006). Gondwana Break-Up: A South Africa Perspective. *In:* Johnson, M.R., Anhaeusser, C.R. and Thomas, R.J. (Eds.), *The Geology of South Africa*. Geological Society of South Africa, Johannesburg/Council for Geoscience, Pretoria, 531-539

White, S.H., Bretan, P.G. and Rutter, E.H. (1986). Fault-Zone Reactivation: Kinematics and Mechanisms. *Philosophical Transactions of the Royal Society of London. Series A, Mathematical and Physical Sciences*, **317**, 81-97

Zang, A. and Stephansson, O. (2010). *Stress Field of the Earth's Crust*. Springer

Zheng, Z., Kemeny, J. and Cook, N.G.W. (1989). Analysis of borehole breakouts. *Journal of Geophysical Research*, **94**, 7171-7178

Zoback, M.D., Moos, D.L., Mastin, L. and Anderson, R.N. (1985). Wellbore breakouts and in situ stress. *Journal of Geophysical Research*, **90**, 5523-5530

Zoback, M.L. and Zoback, M.D. (1989). Tectonic stress field of the conterminous United States. *Mem. Geol. Soc. Am.*, **172**, 523-539.

Zoback, M.D. and Zoback, M.L. (1991). Tectonic stress fields of North America and relative plate motions. *In:* Slemmons, D.B. *et al.* (Eds.), *Neotectonics of North America, Decade Map vol 1*. Geological Society of America, Boulder, Colorado, 339-366

Zoback, M.L. (1992). First and second order patterns of tectonic stress: The World Stress Map Project. *Journal of Geophysical Research*, **97**, 11,703-11,728

Zoback, M.D. (2010). *Reservoir Geomechanics (Paperback Edition)*. Cambridge University Press, UK

APPENDIX:

Table 8: Part 1 of the complete list of all borehole data analysed

Borehole ID	Latitude	Longitude	S_{Hmax}	Quality	Comment
A_A1	-31.21954167	16.92035	163.3	B	Clear NNW-SSE orientation, good total breakout length
A_C1	-32.50848333	16.89085833			Washed out well, poor calliper rotation
A_C2	-32.33234444	16.82288056			Washed out well, poor calliper rotation
A_C3	-32.54556944	16.79315556			Washed out well
A_E1	-29.88859167	16.29365833			Washed out well
A_F1	-29.22436111	16.19955556	171.2	C	Clear NNW-SSE orientation, short total breakout length
A_G1	-30.916175	16.385075			Washed out well
A_J1	-30.60212778	17.16735833			Washed out well, poor calliper rotation
A_J1Z1	-30.60212778	17.16735833			Washed out well
A_K1	-32.68941111	17.23313056	160.8	C	Clear NNW-SSE orientation, short total breakout length
A_O1	-28.94849722	16.16566389	179.5	D	Clear N-S orientation, very short total breakout length
A_U1	-31.64726111	16.50647222			Washed out well, poor calliper rotation
Ba_A1	-31.86711111	17.60955278	139.4	D	Clear NW-SE orientation, short total breakout length
Ba_A2	-31.90861667	17.68625278			No clear calliper rotation
E_AA1Z1	-35.18355556	21.59338611			Washed out well, poor calliper rotation
E_AB1	-34.94141389	21.63773056	147.5	D	Overall NW-SE orientation but high variability
E_AD1Z1	-35.19974444	21.64951389			Washed out well, poor calliper rotation
E_AE1	-35.27515278	21.35173611			Washed out well, poor calliper rotation
E_AF1	-34.91608333	21.95486667	136.6	C	NW-SE to E-W orientation, good total breakout length
E_AG1	-34.88793333	21.77933611			Washed out well
E_AH1	-35.18705556	21.14363056	162.7	D	Overall NNW-SSE orientation but high variability
E_AO1	-35.23768417	21.76163833	162.3	D	Clear NNW-SSE orientation, few and short-length breakout zones
E_AI1	-35.30472222	21.23611111			Insufficient parameters
E_AJ1Z1	-35.335875	21.97706944			Washed out well, poor calliper rotation
E_AK1	-34.96879167	21.17531111			Washed out well, poor calliper rotation
E_AL1	-35.10750833	21.83638333			Washed out well
E_AM1	-35.11634722	21.75981944			Insufficient parameters
E_AO2	-35.33389444	21.46209444			Washed out well, poor calliper rotation
E_AP1	-34.96879167	21.17531167			Washed out well, poor calliper rotation
E_AR1	-35.20354444	21.54504722			Washed out well, poor calliper rotation
E_AR2	-35.19256111	21.53813611			Washed out well, poor calliper rotation
E_AS1	-35.00899444	21.88096667			Washed out well, poor calliper rotation
E_AT1	-35.06613611	22.00594444	282.1	C	Clear NE-SW to E-W orientation
E_AV1	-35.086325	21.50014444			No breakouts
E_AY1	-35.20497222	21.73845			Washed out well
E_B1	-34.7368	21.16634444			Washed out well
E_BD1	-35.20567778	21.29700833	162.7	C	Clear NNW-SSE orientation, good total breakout length but few breakout zones
E_BH1	-35.15824444	21.475325	224	C	Clear NE-SW but few breakout zones
E_BI1	-35.33389444	21.46209444			No breakouts
E_BJ1	-35.28191389	21.66551667			No clear calliper rotation
E_BO1	-35.085	22.03361111			No clear calliper rotation
E_BP1	-35.08840278	21.58506389			No clear calliper rotation
E_BT1	-35.23295556	21.49902222			No breakouts
E_C1	-34.88803889	21.42481111			Insufficient parameters
E_D1	-35.45343333	21.84223611			Insufficient parameters
E_D2	-35.46962222	21.86853889	170.9	C	Clear NNW-SSE orientation but short total breakout length
E_D3	-35.47951944	21.93728611			Washed out well, poor calliper rotation
E_D4	-35.47696389	21.77673333	153.1	B	Clear NNW-SSE orientation, some variation but excellent total breakout length
E_E1	-34.93787778	21.84394167			Washed out well, poor calliper rotation
E_F1	-35.52210278	21.76503889			Washed out well, poor calliper rotation
E_G1	-35.28012222	21.46065278			No clear calliper rotation
E_H1	-34.89555556	21.72090278			No clear calliper rotation
E_J1	-34.86195833	21.61316944			No clear calliper rotation
E_K1	-34.77977778	21.60411111			No clear calliper rotation
E_L1	-35.10227778	21.19540556			Washed out, BO orientations rotate continously with caliper depth
E_M6	-34.92033333	21.65391667			No calliper rotation
E_N1	-35.16979722	21.29786389			WSM E-Quality - discarded
E_P2	-35.36404722	21.39644722			No breakouts
E_S6	-34.88366389	21.84366111	139.2	C	Variable NW-SE to N-S orientation, good total breakout length
E_V1	-35.94677778	21.42475			Poor calliper rotation, no breakouts
E_W2	-34.98496111	21.78633611			No breakouts
E_Z1	-35.12708556	21.38734944			No breakouts
ES_5	-34.87543333	21.85121389			Washed out well, poor calliper rotation
EY_1	-34.85691667	21.90683333			No breakouts

Table 9: Part 2 of the complete list of all borehole data analysed

Borehole ID	Latitude	Longitude	S_{Hmax}	Quality	Comment
F_A2	-34.98732222	22.21023889	142.1	C	Clear NW-SE orientation, breakouts predominantly at shallow depth
F_A3	-35.02918611	22.27685833			No clear calliper rotation
F_A5	-34.98375833	22.18311667	205.7	C	Two large zones, 1 NW-SE, 1 NE-SW orientation
F_A6	-34.98400278	22.24774722			Washed out, BO orientations rotate continously with caliper depth
F_A7	-35.00674167	22.199775			No clear calliper rotation
F_A8	-35.01709444	22.30171389			No breakouts
F_A9	-35.00938333	22.23808056			No clear calliper rotation
F_AG1	-35.04	22.2325			Insufficient parameters
F_AH1	-34.89120833	22.02796944	166.5	D	Overall NNW-SSE orientation but high variability
F_AH2	-34.87935833	22.00100278	281.9	C	Shallow depth - NE-SW, greater depth - N-S to NW-SE
F_AH3	-34.88631667	21.94838889			WSM E-Quality - discarded
F_AR1	-34.93674722	22.16896389	250.8	C	Two large breakout zones, consistant E-W orientation
F_AR3	-34.91194722	22.05628333			Error in depth values
F_AV1	-34.94060556	22.32097222			No breakouts
F_AZ2					No coordinates were obtained so this borehole could not be plotted
F_B2	-34.38051944	22.81014722	142.7	B	Clear NW-SE orientation with good total breakout length
F_E2	-34.94007778	22.34430556			No clear calliper rotation
F_F2	-35.32738611	22.2967			No clear calliper rotation
F_I1	-34.62251667	22.69923056			No breakouts
F_J1	-35.06369444	22.41536111			No breakouts
F_K1	-34.92020278	22.81382222			Washed out, BO orientations rotate continously with caliper depth
F_L1	-35.57165278	22.22129444			Washed out, BO orientations rotate continously with caliper depth
F_O1	-35.14834722	22.530125			Washed out well, poor calliper rotation
F_P1	-35.47261667	22.18213333			Washed out well, poor calliper rotation
F_P2	-35.43375556	22.07078611			No clear calliper rotation
F_R1	-35.15711389	22.600025			No clear calliper rotation
F_T1Z1	-34.89303611	22.461325			No clear calliper rotation
FAR_5	-34.91166667	22.11463889			Washed out well, poor calliper rotation
Ga_AA1	-34.65886111	23.31583333			Insufficient parameters
Ga_D1	-34.34740833	23.43085833			No clear calliper rotation
Ga_E1	-34.70096389	23.8319			No clear calliper rotation
Ga_E2	-34.6872	23.76803056			No clear calliper rotation
Ga_F1	-34.28661111	23.85836111			Error in P1AZ values
Ga_G1a	-34.57801667	23.44971667			No clear calliper rotation
Ga_J1	-34.69230278	23.57635278			Washed out well, poor calliper rotation
Ga_M1	-34.62749444	23.476725			Washed out well, poor calliper rotation
Ga_Q1	-34.62000556	23.78085556			Calliper failure
Ga_X1	-34.41396111	23.43684167			No clear calliper rotation
Gb_C1	-34.41049167	24.39978889			No clear calliper rotation
Gb_K1	-34.53271333	24.67066194			No breakouts
Gb_Spr	-34.82061111	24.42683056			No clear calliper rotation
Ha_A1	-34.356775	25.67286667	134.8	C	Clear NW-SE orientation, good total breakout length
Ha_B2	-34.40588056	25.60912778			Washed out well, poor calliper rotation
Ha_I1	-34.25611111	25.70880556			No clear calliper rotation
Ha_J1	-34.50518056	25.15211389			WSM E-Quality - discarded
Ha_K1	-34.3958	25.687275			No clear calliper rotation
Hb_B1	-34.124425	26.19145			WSM E-Quality - discarded
Hb_C1	-34.28083333	26.20146389			Insufficient parameters
Hb_D1	-34.01394444	26.18791667			Insufficient parameters
Hb_G1	-34.18535833	25.86094167	147.1	D	Clear NW-SE orientation but short total breakout length
Hb_H1a	-34.2315	25.85582222			WSM E-Quality - discarded
Hb_Hart	-34.27746389	25.92170556			No clear calliper rotation
Hb_I1	-34.20304444	26.21016389			Washed out well, poor calliper rotation
Hb_K1	-34.28379167	25.90249167	152.4	D	Alternating NW-SE/NE-SW orientation at differing depths
Hb_P1	-34.02653889	26.08768889			Washed out well, poor calliper rotation
Jc_B1	-29.50740278	31.6243	156.6	D	Very short breakout zone but clear NW-SE orientation
Jc_C1	-34.87858333	21.83227778			Insufficient parameters
K_A1	-30.80798056	16.01570278	169.9	C	Consistant NNW-SSE orientation, short total breakout length
K_A2	-30.83457222	16.008175	172.5	B	Large breakout zones with clear NNW-SSE orientation
K_A3	-30.80272222	16.06316944			WSM E-Quality - discarded
K_B1	-30.71109722	15.44685833			Washed out well, poor calliper rotation
K_D1	-31.7316	16.33634444	168.8	B	Clear NNW-SSE orientation in deep breakout zones
K_E1	-30.63252778	15.43319722			Washed out well, poor calliper rotation
K_H1	-31.03956389	15.92325833	146.9	B	Clear NW-SE orientation throughout borehole log
P_A1	-32.68941111	17.23313056			Insufficient parameters

Table 10: Final length-weighted S_{Hmax} orientations data derived from FACT analysis of the 29 usable boreholes. All values have been corrected for the average magnetic declination at the time of logging.

Borehole ID	Location (Decimal Degrees)		S_{Hmax} (length-weighted) - Corrected	Standard Deviation	WSM Quality	Total breakout length (m)	Depth Range	Avg. Breakout Depth (m)	Picks	Comments
	Latitude	Longitude								
A_A1	-31.2195	16.92035	163.3	10.03	B	129	2,578.35 - 3,806.97	2904	89	Clear NNW-SSE orientation, good total breakout length
A_F1	-29.2244	16.1995556	171.2	3.4	C	33	2,231.61 - 2,846.74	2415	20	Clear NNW-SSE orientation, short total breakout length
A_K1	-32.6894	17.2331306	160.8	3.97	C	47	2,090.61 - 3,121.87	3348	22	Clear NNW-SSE orientation, short total breakout length
A_O1	-28.9485	16.1656639	179.5	1.76	D	13	1,808.23 - 4,569.52	4291	5	Clear N-S orientation, very short total breakout length
Ba_A1	-31.8671	17.6095528	139.4	12.51	D	18	217.68 - 1,374.94	660	8	Clear NW-SE orientation, short total breakout length
E_AB1	-34.9414	21.6377306	147.5	18.04	D	53	1,846.27 - 2,957.37	2493	4	Overall NW-SE orientation but high variability
E_AF1	-34.9161	21.9548667	136.6	11.57	C	83	1,392.02 - 2,883.1	1770	24	NW-SE to E-W orientation, good total breakout length
E_AH1	-35.1871	21.1436306	162.7	31.02	D	44	2,706.3 - 3,728.92	3309	20	Overall NNW-SSE orientation but high variability
E_AO1	-35.2377	21.7616383	162.3	2.12	D	27	1,394.61 - 3,356.61	3133	3	Clear NNW-SSE orientation, few and short-length breakout zones
E_AT1	-35.0661	22.0059444	282.1	5.95	C	94	1,498.4 - 3,381.91	1867	21	Clear NE-SW to E-W orientation
E_BD1	-35.2057	21.2970083	162.7	2.36	C	76	1,494.28 - 3,247.03	1640	4	Clear NNW-SSE orientation, good total breakout length but few breakout zones
E_BH1	-35.1582	21.475325	224	2.78	C	53	1,291.44 - 3,357.68	1442	10	Clear NE-SW but few breakout zones
E_D2	-35.4696	21.8685389	170.9	2.94	C	37	1,521.74 - 3,370.9	1706	11	Clear NNW-SSE orientation but short total breakout length
E_D4	-35.477	21.7767333	153.1	12.2	B	380	1,766.9 - 3,630.86	2329	13	Clear NNW-SSE orientation, some variation but excellent total breakout length
E_S6	-34.8837	21.8436611	139.2	16.86	C	80	1,694.6 - 2,901.86	2129	6	Variable NW-SE to N-S orientation, good total breakout length
F_A2	-34.9873	22.2102389	142.1	9.46	C	50	356.91 - 2,903.8	1800	9	Clear NW-SE orientation, breakouts predominantly at shallow depth
F_A5	-34.9838	22.1831167	205.7	22.16	C	192	427.65 - 2,989.91	1932	8	Two large zones, 1 NW-SE, 1 NE-SW orientation
F_AH1	-34.8912	22.0279694	166.5	33.74	D	20	1,588.78 - 2,688.33	2158	6	Overall NNW-SSE orientation but high variability
F_AH2	-34.8794	22.0010028	281.9	21.95	C	51	1,578.05 - 2,673.46	1825	11	Shallow depth - NE-SW, greater depth - N-S to NW-SE
F_AR1	-34.9367	22.1689639	250.8	14.2	C	97	1,899.24 - 2,972.31	2109	12	Two large breakout zones, consistant E-W orientation
F_B2	-34.3805	22.8101472	142.7	10.23	B	122	853.85 - 2,072.88	1397	54	Clear NW-SE orientation with good total breakout length
Ha_A1	-34.3568	25.6728667	134.8	8.86	C	77	594.78 - 4,398.96	3213	28	Clear NW-SE orientation, good total breakout length
Hb_G1	-34.1854	25.8609417	147.1	18.18	D	19	792.92 - 1,736.96	1390	28	Clear NW-SE orientation but short total breakout length
Hb_K1	-34.2838	25.9024917	152.4	28.37	D	79	1,315.54 - 1,925.08	1543	15	Alternating NW-SE/NE-SW orientation at differing depths
Jc_B1	-29.5074	31.6243	156.6	4.94	D	13	2,893.08 - 3,948.18	3750	5	Very short breakout zone but clear NW-SE orientation
K_A1	-30.808	16.0157028	169.9	4.34	C	38	2,129.2 - 4,818.36	2476	27	Consistant NNW-SSE orientation, short total breakout length
K_A2	-30.8346	16.008175	172.5	8.89	B	142	1,656.84 - 5,829.36	2520	63	Large breakout zones with clear NNW-SSE orientation
K_D1	-31.7316	16.3363444	168.8	8.89	B	145	1,574.25 - 4,710.79	4244	24	Clear NNW-SSE orientation in deep breakout zones
K_H1	-32.6894	17.2331306	146.9	4.6	B	132	1,645.16 - 4,260.95	2897	68	Clear NW-SE orientation throughout borehole log